PANJAB UNIVERSITY
RESEARCH JOURNAL (SCIENCE)

VOL. 71 2021

PANJAB UNIVERSITY RESEARCH JOURNAL (SCIENCE)

VOLUME 71, 2021

The subscription of the journal may be sent in the form of a Bank Draft payable to ***The Registrar***, ***Panjab University, Chandigarh*** and addressed to The Editor-in-Chief on the following address:

Research Journal (Science)
Old Corresponding Building,
Panjab University, Chandigarh -160 014, (India)

The manuscripts for publication or any other enquiry is also to be addressed to the Editor-in-Chief

Subscription fee:

	Inland	**Foreign**
Annual Subscription	Rs.400/-	US$ 50
Life Membership	Rs. 3000/-	US$ 250

Printed in 2022

CONTENTS

3D DIGITIZATION OF A HUMAN CRANIUM USING LASER SCANNER FOR FORENSIC DOCUMENTATION

Abhinav Sood[a*], Varsha Dogra[b], Gayatri Pathmanathan[a]

[a]*Department of Anthropology, Panjab University, Chandigarh*

[b]*Department of Environment Studies, Panjab University, Chandigarh*

ABSTRACT

Anthropologists usually employ the use of photography for documentation of specimens such as bones that lack morphological details due to the limitation of 2D images. But with the advancement in technology, a 3D representation of specimen bones is possible by the use of surface scanners. Like in every field including anthropology it is important to check the reliability of new techniques so that they can be used for future reference. Currently, there are no published standards for 3D scanning a human cranium. The paper is divided into two half, the first half involves the scanner specifications and previous studies conducted for 3D documentation of various specimens, the setting utilized for the creation of a 3D cranium model using NextEngine laser scanner, and post-processing of the resulting 3D data in dedicated software for further cleaning of any unwanted noise. The second half discusses the intra method reliability of the scanner with that to manual measurements based on ten different inter-landmark distances.

Keywords: Laser scanning; Cranium; Morphology; Triangulation; NextEngine.

INTRODUCTION

Laser scanning has proved to be relevant for the virtual creation of 3D models especially in the preservation of delicate materials. There have been rapid developments in laser scanning technology in terms of cost and time taken to digitize the specimen. A variety of laser scanners are currently available online starting from 1 lack onwards and can be rented out for a given time frame at a reasonable price. The complex morphology of the cranium makes it the most challenging bone in the human skeleton to document even with a laser scanner. To create a 3D model of a cranium NextEngine laser scanner was used. It is a desktop 3D scanner that uses an array of four solid-state lasers to scan objects at a resolution of 0.12 mm. The scanner has macro, wide and extended modes for scanning which are selected depending on the size of the object that can fit in the field of view of the scanner. The scanner has a flash that illuminates the object using the white lights and shows a live onscreen image so that the user can adjust the model on the scanning platform and twin 3.0 Megapixel CMOS color image sensors as well, so it collects 2D images to texture the 3D models it generates. This device uses a motorized turntable that rotates the specimen in supplement divisions to complete a 360° rotation. The only limiting factor includes its small scan volume which can be overcome by doing multiple scans of large objects with the use of specific software. Several researchers created great outcomes from the information gathered with the NextEngine scanner in comparison to other scanners in which they pointed out noticeable differences in the mesh quality and mesh degradations of the scanned models (Fries, 2012; Slizewski and Semal, 2009). Though the inter-observer error tested was found to change with the device (Slizewski and Semal, 2009; Slizewski *et al*., 2010). A couple of studies have contrasted NextEngine as one of the most widely used Surface scanners in several fields including anthropology because of its low cost in comparison to other scanners with similar results, easy to understand interface, and overall precision and compared the results with those of better quality scanners and found that for most purposes, the NextEngine scanner gives a sufficiently high resolution and showed no qualitative difference between the scans in highest and normal resolution (Chacón *et al*., 2016; Sholts *et al*., 2010; Garvin and Stock, 2016).

MATERIAL AND METHOD

Specimen: Ten unidentified cranium were obtained from the Department of Anthropology, Panjab University, Chandigarh.

Measurement: Ten different Inter-landmark distances were selected to compare the manual measurements with that to 3D digitized cranium models highlighted in table 1 with their acronyms. For manual measurements spreading and sliding caliper were used. The 3D measurements were carried out using Autodesk recap 2020 software.

Method for creating a 3D model: The 3D scan of the cranium was created by placing the cranium on the stage. The laser beam scanned the surface of the cranium and the detectors measured the distance to the cranium. The setting utilized was set with 360-

*Corresponding author: Abhinav Sood
E-mail: abhinavsood17@gmail.com
Received: March, 2021, Accepted: September, 2021

degree positioning and the number of points per square inch was set to 7000. A total of 12 divisions were used as it controls the degree of rotations rendered to 30 degrees between each scan which are grouped later into one complete scan. As the specimen in question was cranium so light mode was used rather than the dark mode as a target due to its light color. The range was set to wide mode placing the cranium 22 inches away from the scanner. The time taken to complete the scanning from all angles was approximately 1 hour. The cranium was oriented in different positions. The scans were taken from each perspective. The final 360-degree scan resulted in scan data shown in figure 1. The 3D scanned file can be output to .stl, .obj, .vmrl, .xyz, and .ply file formats. Once the scan data was acquired and exported as a 3D file the file was opened using software Autodesk remake pro-2020 software edition and Meshlab as shown in figure 2. The 3D model was opened and any sort of unwanted noise was removed. The final 3D model was oriented and aligned.

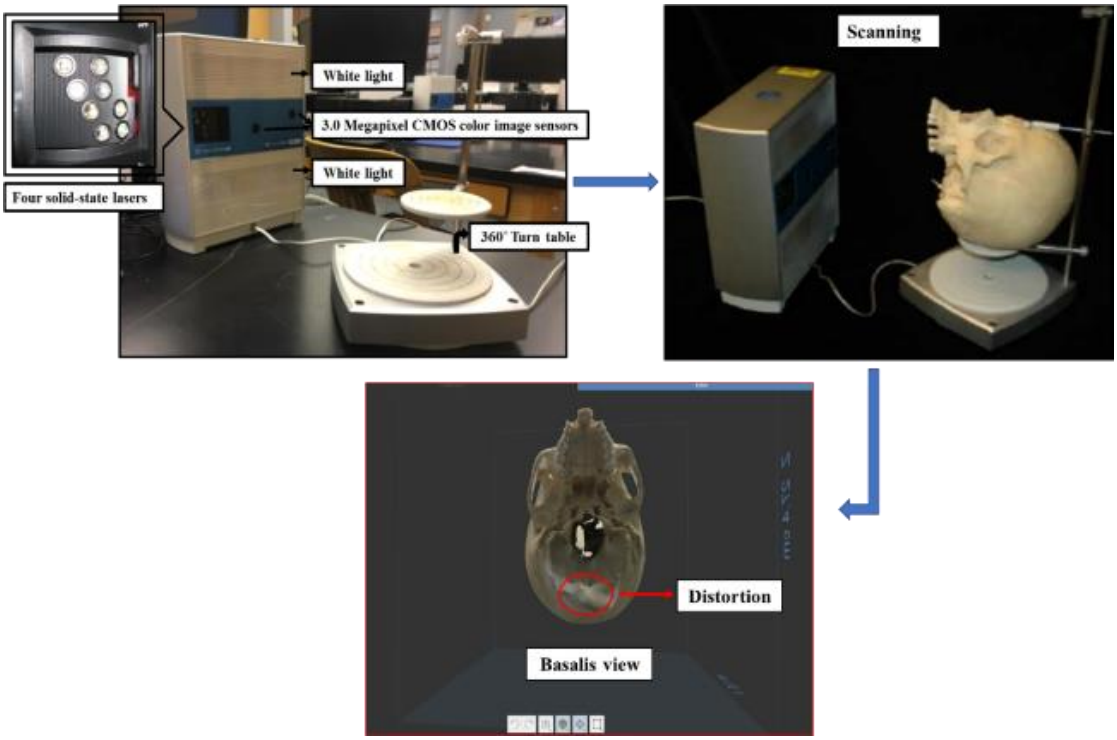

Figure 1: NextEngine 3D laser scanner with turntable highlighted on top left image followed by 3D digitization of base of cranium shown in the top right image and exported 3D file opened in Autodesk remake 2020 in basalis view with little distortion highlighted in a red circle.

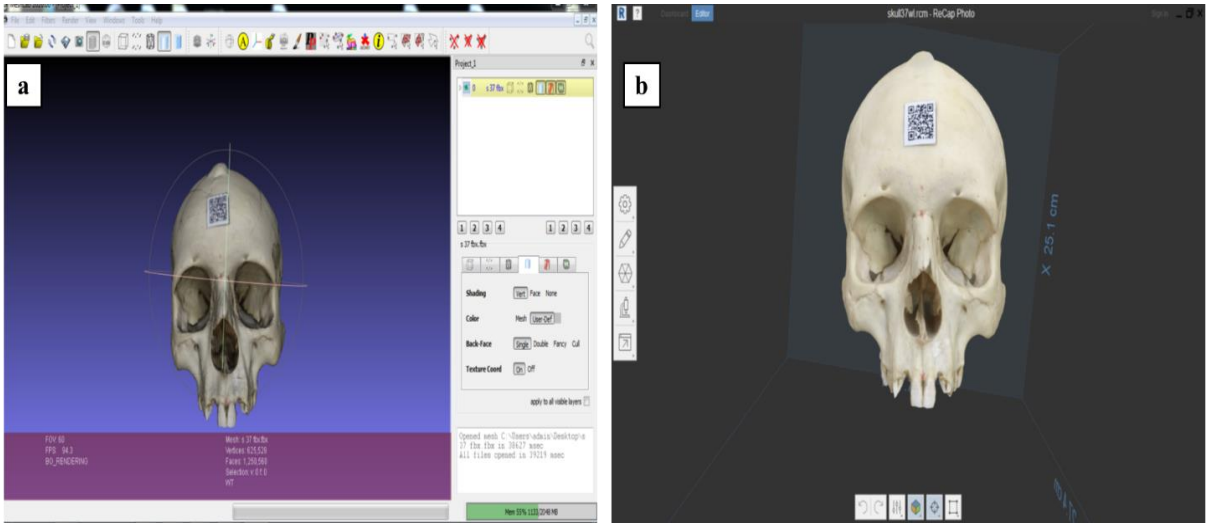

Figure 2: An exported mesh of digitized cranium from NextEngine to Meshlab software on the left side and Autodesk Remake photo 2020 on the right side.

Table 1: Measurements and their landmarks Included in the study

S. No.	Measurement	Acronym	Point A Landmark	Symbol	Point B landmark	Symbol
1.	**Cranial Length**	GOL	Glabella	g	Opisthocranion	op
2.	**Cranial Breadth**	XCB	Euryon	eu	Euryon	eu
3.	**Cranial Height**	BBH	Basion	ba	Bregma	b
4.	**Minimum frontal breadth**	WFB	frontotemporale	ft	Frontotemporale	ft
5.	**Interorbital Breadth**	DKB	Dacryon	d	Dacryon	d
6.	**Upper FacialBreadth**	UFB	frontomalaretemporale	fmt	Frontomalaretemporale	fmt
7.	**Inner Bi-Orbital Breadth**	IBB	Frontomalareorbitale	fmo	Frontomalareorbitale	fmo
8.	**Bi-Zygomatic Breadth**	ZYB	Zygion	zy	Zygion	zy
9.	**Bimaxillary Breadth**	ZMB	zygomaxillare anterior	zm	zygomaxillare anterior	zm
10.	**Upper facial height**	NPH	Nasion	n	Prosthion	pr

RESULTS AND DISCUSSION

Table 2 summarizes the 10 craniometric measurements obtained both by direct and 3D software.

Table 2: Differences between Direct Anthropometry and NextEngine 3D models.

Measurements	Direct (Sliding/ Spreading Caliper) n = 10		Software (Autodesk Recap pro) n = 10		Difference	Percent Difference
	Mean (cm)	SD (cm)	Mean (cm)	SD (cm)	Mean (cm)	%
Cranial Length	16.760	.9276	16.769	.9558	.009	.053
Cranial Breadth	12.544	.6544	12.368	.6344	.176	1.413
Cranial Height	12.796	.7984	12.456	.6415	.340	2.692
Minimum Frontal breadth	9.184	.3672	8.831	.3522	.353	3.918
Interorbital Breadth	2.216	.2179	1.714	.3455	.502	25.547
Upper facial breadth	10.080	.7060	9.760	.4768	.320	3.225
Innerbiorbital breadth	9.390	.4621	9.230	.5135	.160	1.718
Bizygomatic Breadth	12.044	.6506	11.764	1.078	.28	2.352
Bimaxillary Breadth	9.102	.5698	8.745	.4184	.357	4.000
Upper facial height	6.246	.5219	5.932	.4120	.314	5.156

Bland-Altman plot is given in figure 3 (Bland and Altman, 1986). The difference between the two methods was found below 0.5 cm in 9 measurements out of 10. The measurement interorbital breadth (dacryon-dacryon) gave a result of above 0.5 cm with a percentage difference of 25.54. It was found the NextEngine scanner gave a slightly lower reading in comparison to the direct method with a maximum percentage difference of 25.54 to a minimum of .053 based on ten inter-landmark distances included in this study. After calculating the mean difference of all the 10 variables, a comparison between both methods showed that the mean difference was .2793 with a 95% confidence interval. Bland-Altman analysis illustrated that measurements taken after digitization of 3D cranium with NextEngine scanner gives statistically similar measurements in comparison to direct measurements with little percentage difference in most of the Inter-landmark distances and can be applied in the field of forensic science for 3D digitization and measurements of cranium.

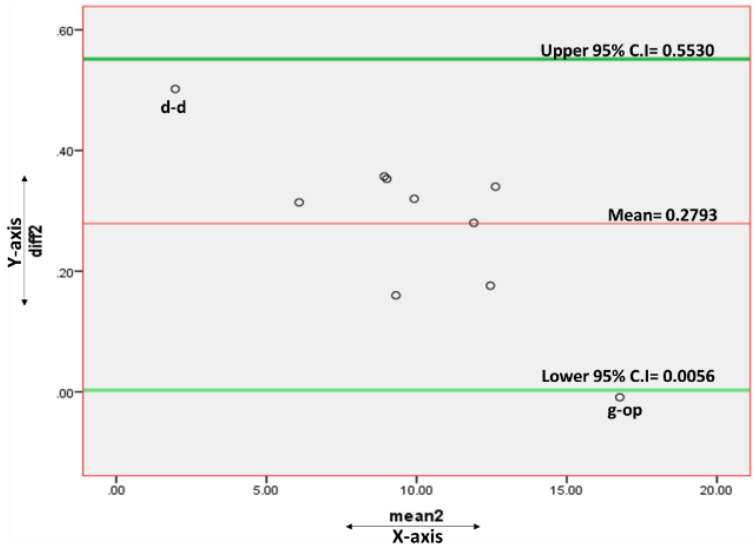

Figure 3: Bland-Altman plot of 10 craniometric measurements

The X-axis shows the mean of the results of the two methods, whereas the y-axis represents the absolute difference between the two methods (difference = Direct measuring-3D laser scanning). The limit of agreement with a 95% confidence interval (C.I) is given in horizontal lines.

CONCLUSION

The 3D file can act as permanent documentation which can be used by researchers, forensic scientists, and teachers in their respective fields. The use of this technique can be valuable when the bones are fragmented or fragile. The 3D model can be digitally stored or shared online to take expert opinion saving the hassle to transport the specimen. In conclusion, it can be said that additional research is still required for 3D digitization of different bones using laser scanning and testing its reliability in comparison to other well-known techniques such as CT scanning when the aim is to capture only the external surfaces of a given specimen. It is recommended that researchers should have knowledge and practice of the scanner before using it on any specimen of interest.

ACKNOWLEDGMENTS

The authors are grateful to Mr. Priyanshu Mehran and his team from Pixel Perfect, Panchkula, India for all the technical support in 3D scanning. The authors would also like to thank Dr. Aanchal Dwevedi, Senior Scientific Officer, Central Forensic Science Laboratory, Chandigarh for valuable scientific guidance.

REFERENCES

Bland, J.M. and D.G. Altman, (1986): Statistical methods for assessing agreement between two methods of clinical measurement. Lancet 1986, 307-310

Chacón, M. G., F., Détroit, A., Coudenneau, and M. H. Moncel, 2016. Morphometric assessment of convergent tool technology and function during the Early Middle Palaeolithic: the case of Payre, France. PloS one, 11(5): e0155316.

Friess, M. 2012. Scratching the surface? The use of surface scanning in physical and paleoanthropology. J. Anthropol. Sci., 90: 1-25.

Garvin, H. M., and M. K. Stock, 2016. The utility of advanced imaging in forensic anthropology. Acad. Forensic Pathol., 6(3): 499-516.

Sholts, S.B., S.K., Wärmländer, L.M., Flores, K.W., Miller, and P.L. Walker, 2010. Variation in the measurement of cranial volume and surface area using 3D laser scanning technology. J Forensic Sci., 55(4): 871-6. DOI: 10.1111/j.1556-4029.2010.01380.x.

Slizewski, A., M., Friess, and P. Semal, 2010. Surface scanning of anthropological specimens: nominal-actual comparison with low-cost laser scanner and high-end fringe light projection surface scanning systems. Quart., 57: 179-187.

Slizewski, A. and P. Semal, 2009. Experiences with low and high-cost 3D surface scanner. Quart., 56: 131-138.

INVESTIGATING MANGANESE DOPED CADMIUM SULPHIDE NANOPARTICLE PROPERTIES

Anil Kumar[1*], Ramesh K Sharma[1], Navdeep Goyal[2], Sanjeev Gautam[3]

[1] CIL/UCIM, Department, Panjab University, Chandigarh – 160014, India

[2] Department of Physics, Panjab University, Chandigarh – 160014, India

[3] UICET, Panjab University, Chandigarh – 160014, India

ABSTRACT

Chemical precipitation method was used to synthesize un-doped and Mn-doped Cadmium Sulphide (CdS) nanoparticle. Various characterizing tools like XRD, UV-Vis, TEM and FESEM with EDS were used for the analysis of the prepared sample. XRD confirmed the structure of the nanoparticles to be Zinc blende with diffraction from (111), (220) & (311) planes. Crystallite size was also calculated from XRD pattern. TEM image gave further endorsement toward average particle size. Optical analysis using UV-Vis showed a blue shift of absorption edge as a function of Mn-doping concentration.

Keywords: CdS, Doping, Manganese, Characterization, Optical properties.

INTRODUCTION

The transition metal (TM) dopants in host semiconductors of group (II-VI) introduces disorder and spin-orbit interactions may induce magnetic ordering that leads to dilute magnetic semiconductor (DMS) (Sharma *et al.* 2003, Furdyna 1988, Diet *et al*. 1994, Ohno 1998, 2010). Semiconductors doped with TM element have attracted much attention due to their applications in spintronics (Akai 1993, Akai and Dederichs 1998, Jiang *et al*. 2009). Spintronic materials open up a faster and more efficient mode of information storage and transfer for quantum computation, electronics, magnetronics and communication (Chelikowsky *et al.* 2006, Boeck *et al.* 2002). Giant Magneto resistance (GMR) has found applications in magnetic field sensors in the heads of magnetic recording disks and magnetic random access memory (MRAM) (Boeck *et al.* 2002), Pang *et al*. 2011). In recent years, major research focus is on the synthesis, characterization and application of semiconductors. In the emerging technologies these semiconductors are explored and used in different forms such as quantum dots, nanoclusters, nanotubes, nanofilms, etc. When the size of semiconductors reduces to nano scale, their properties change dramatically (Diet *et al*. 1994, Ohno *et al.* 1998, Akai 1993, Akai and Dederichs 1998, Jiang *et al*. 2009].

Group II-VI semiconductor with band gap ranging from 1-3 eV is suitable for various scientific and technological applications. CdS is an important semiconductor in this group having attractive optoelectronic & other properties (Kirovskaya *et al.* 2011). Because of size tunable properties of such semiconductors in nano form, the preparation & characterization is an exciting area of material research. Doped semiconductor nanocrystals can be studied to achieve two different material properties viz luminescence & magnetism. It has been reported that a fractional TM substitution will not deteriorate the optical and electronic transport properties of the host but simultaneously introduce large magnetic field effects. The partially filled *d* states or *f* states act as magnetic impurities typically characterized by large magnetic moments. The unpaired electrons and unpaired electron spins of these dopants lead to magnetic behavior in DMS. TM impurities incorporated into II-VI semiconductor act as acceptor which tunes various properties like optical, electrical, luminescence, etc.

Several theoreticians have described the blue shift behavior of a semiconductor as a function of particle size (Brus *et al*. 1986a,b, Kanyanuma 1988, Lippens and Lannoo 1990). The most popular theoretical effort used to understand the size dependent band gap behavior of low dimensional systems is Effective mass approximation (EMA). Tight binding approximation (TBA) is other method used to describe the band gap of nanoparticles. The effective bond orbital model (EBOM), Wannier function method (WFM), empirical pseudo potential method (EPM), density functional theory (DFT) and hyperbolic band model (HBM) are also other methods mentioned (Brus 1986a,b, Kayanuma 1988, Lippens and Lannoo 1990). For nanostructure CdS, the band gap can be tuned between 2.42 eV – 4 eV by varying the size of crystallites. The smaller crystallites are blue shifted w.r.t. the larger ones showing quantum confinement in them. The study of the optical band gap behavior and optical constants of CdS semiconductor near the fundamental absorption edge and sub band gap region is important for optoelectronic applications. The

*Corresponding author: aks_anil@yahoo.com

Received: September 10, 2021, Accepted: November 15, 2021

accurate knowledge of absorption coefficient, band gap, refractive index and extinction coefficient is indispensable for the design and functioning of optoelectronic devices.

The present paper reports the synthesis of Mn-doped CdS nanoparticles using chemical reaction precipitation method. Thereafter Mn doped CdS nanoparticles were investigated and results were interpreted.

EXPERIMENTAL

The chemical method is simple and cost effective technique that has been adopted for synthesis of CdS nanoparticles. To prepare CdS nanoparticle, main chemicals used were Cadmium acetate, Sodium sulphide and Manganese acetate as dopant.

A 0.5M concentration solution of Cadmium acetate and Sodium acetate were prepared in de-ionized water. Sodium acetate was then mixed drop wise in Cadmium acetate solution while solution being constantly stirred at room temperature. Waited for few minutes to settle down their precipitates. Ultrasonically cleaned, centrifuged and repeatedly washed for about eight times. The material was put in furnace for about 80°C for drying. After grinding lightly the dried powder, the final material was obtained as pure CdS nanoparticles. Further for synthesizing doped material, Manganese acetate solution for same molar concentration (e.g. 0.5M) was prepared. For 2% doping, 2ml was taken out from 100ml Manganese acetate and mixed in 95ml of Cadmium acetate (0.5M). Next step is to mix Sodium sulphide (0.5M) dropwise in it as dictated above. Final material prepared as Mn(2%)- doped CdS nanoparticles. Similar procedure was adopted for making Mn doped CdS for 4%, 6%, 8% and 10%.

The structure of pure and Mn-doped CdS nanoparticles were analysed with XRD (PANAlytical, XPertPro with CuK_α radiation, $\lambda = 1.5406$ A°) in the range of 20° - 60° (2θ) at scanning rate of 0.05 °/min. The morphology was examined by FESEM Hitachi (SU 8010). TEM of nanoparticles were taken by Hitachi (H-7500). UV-Vis absorption studies were carried out using spectrophotometer (Lamda 750 Perkin Elmer).

RESULTS AND DISCUSSION

Structural Analysis with XRD

XRD pattern (Fig. 1) with powdered-XRD shows a perfect match with cubic Zinc blende phase of CdS (JCPDS 10-454). Diffraction peaks were found at values of 2θ at 26.49◦, 43.61◦ and 52.23◦ (approx), and these referred to diffraction from (111), (220) and (311) planes respectively(Fig 1). XRD data revealed that broadened diffraction peak of Mn-doped CdS plane has shifted slightly toward higher angle in reference to pure CdS nanoparticle. This small shift may be attributed to presence of doping material in CdS material. Broadening of diffraction peak gives intimation about crystallite size. As the width of peak increases, the size of crystallite decreases.

Values of FWHM were measured from XRD peak list for calculating crystallite size using Scherrer formula:

$$D = 0.9\,\lambda / \beta \cos\theta \qquad (1)$$

where D is the average crystalline size, λ is the x-ray wavelength, β is the full width half maximum (FWHM) of the diffraction peak & θ is the diffraction angle. Size of the crystallite doped Cadmium Sulphide was found decreased with the addition of Mn transition metal ions. (Table1).

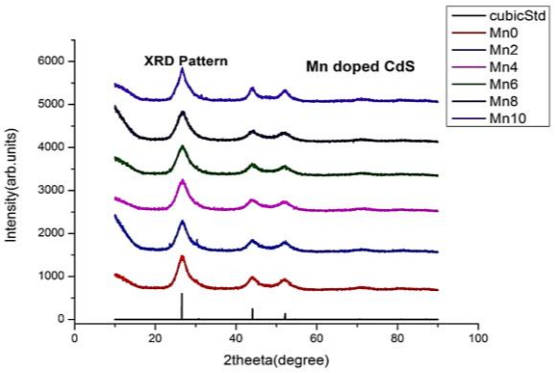

Figure 1: XRD pattern for undoped and Mn-doped CdS

Optical Studies

UV-Vis spectroscopy is commonly used for the calculations of optical constants. No material is fully transparent at all optical wavelengths and hence there will always be some absorption and reflectance.

According to Lambert-Beer Law:

$$I_s = I_o\, e^{-\alpha t} \qquad (2)$$

where I_s is intensity of light passing through a sample, I_o is incident intensity of light, α is absorption coefficient and t is sample thickness.

The ratio I_s / Io is called transmittance. Absorption (A), a fraction of radiation absorbed inside of material is

$$A = \log_{10}(I_s / I_o) = \log_{10}(T) \qquad (3)$$

Absorption coefficient (α) measures the spatial decrease in the intensity of a propagating beam due to progressive conversion into different form of energy. There is minimal absorption for semiconductor materials for photons having energy smaller than band gap and high absorption for photons with energies greater than the band gap. Resulting, there is a sharp increase in absorption at energies close to the band gap that gives an absorption edge in UV-Vis absorption spectrum.

The fundamental absorption edge is given as

$$E_g = h\upsilon = \frac{1238\ Ev}{\lambda(nm)} \qquad (4)$$

where λ is the cut-off wavelength.

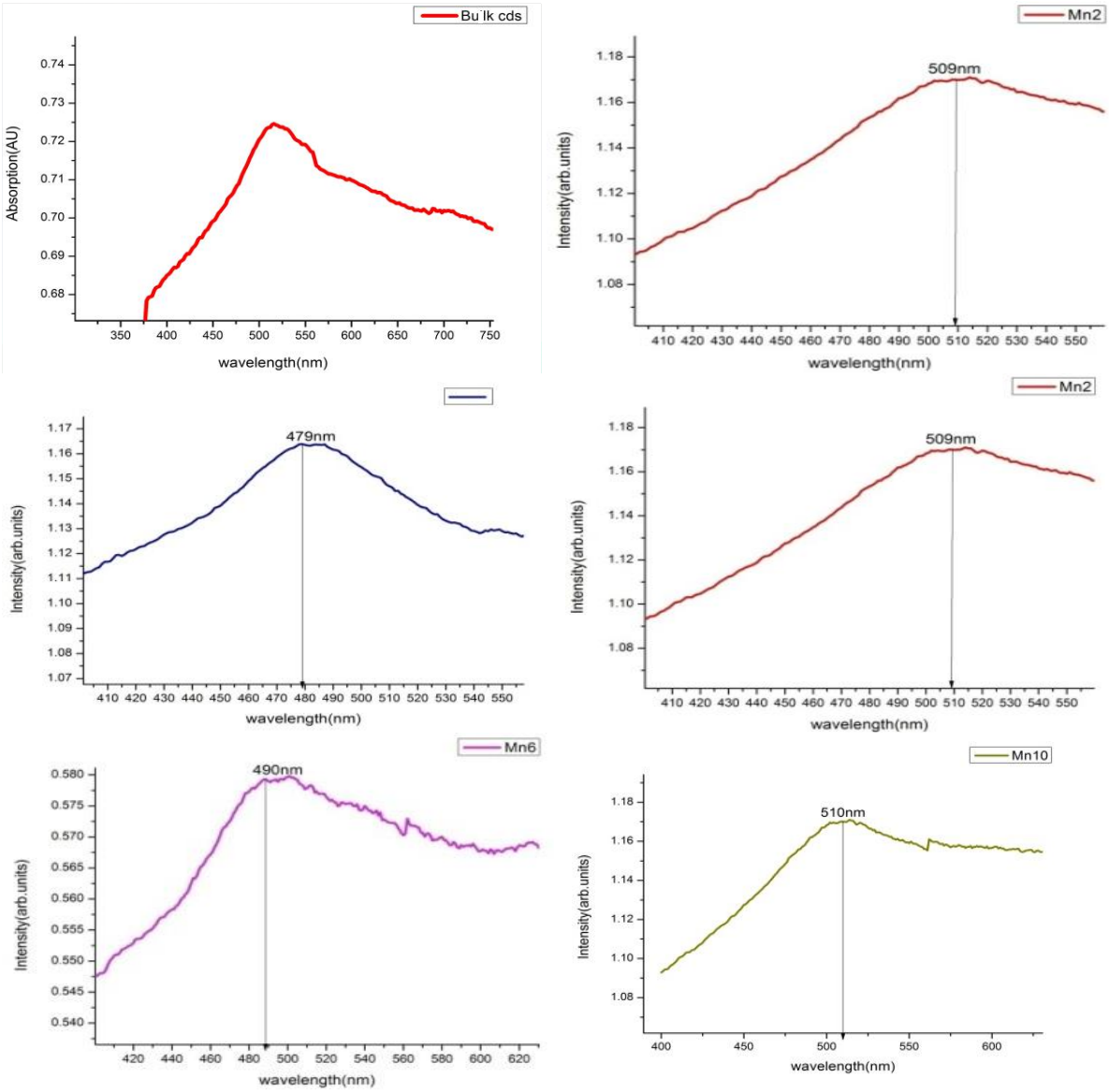

Figure 2: Optical absorption spectra for bulk CdS and doped(Mn) CdS

UV-Vis Analysis

The optical absorption spectra of bulk CdS and Mn doped CdS nanoparticle (Fig2) was recorded as a function of wavelength in the range of 300nm-750 nm and found there is blue shift wrt to bulk CdS. This happens because of quantum confinement effect.

It may be noted that for 10% doped concentration, the band gap shift got reversed and data were repeated to confirm for same value of concentration. Further, one reading for 12% was also taken to see the trend of band gap variation after this doped concentration value, but its value came out almost same as correspond to 10% doped concentration.

The reason for narrowing the band gap could be attributed due to structure disorder & sp-d hybridization effects. Under the action of surrounding crystal field, with particular doping concentration(10%), the 3d-shell of Mn^{+2} forms new localized states in the band gap.

Table1: Crystallite Size and Optical Band gap for Mn-doped CdS

Sr. No.	Doped Conc.	Crystallite Size (nm)	Wavelength (nm)	Optical BG (eV)
1	2%	2.91 nm	509 nm	2.43 eV
2	4%	2.62 nm	490 nm	2.53 eV
3	6%	2.20 nm	490 nm	2.58 eV
4	8%	2.20 nm	479 nm	2.58 eV
5	10%	2.00 nm	510 nm	2.42 eV

TEM Analysis

TEM micrographs (Fig3) shows images correspond to pure 0.5M CdS NPs & with Mn-doped CdS NPs. The images give the information that nanoparticles were well visible & defined and no effected aggregation was formed. So even the absence of capping agent did not disturb the formation of nanoparticles.

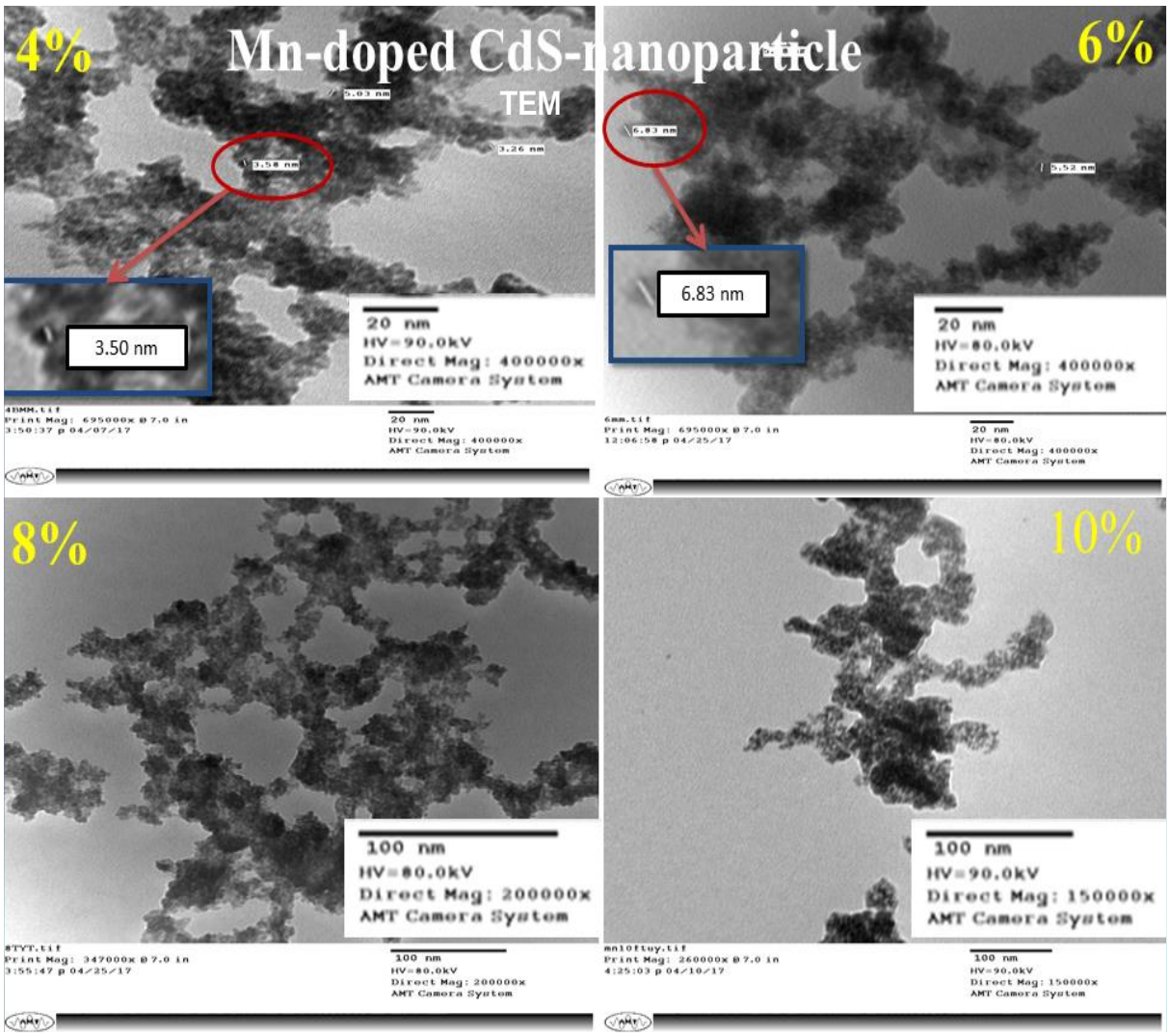

Figure 3: TEM micrographs

Surface morphology

FESEM images of undoped & Mn-doped CdS NPs as shown represented the formation of nanoclusters. The different clusters were formed within various grains. The average grain size diameter for Mn-doped CdS nanoparticles were found to be in the range of 15-32nm.

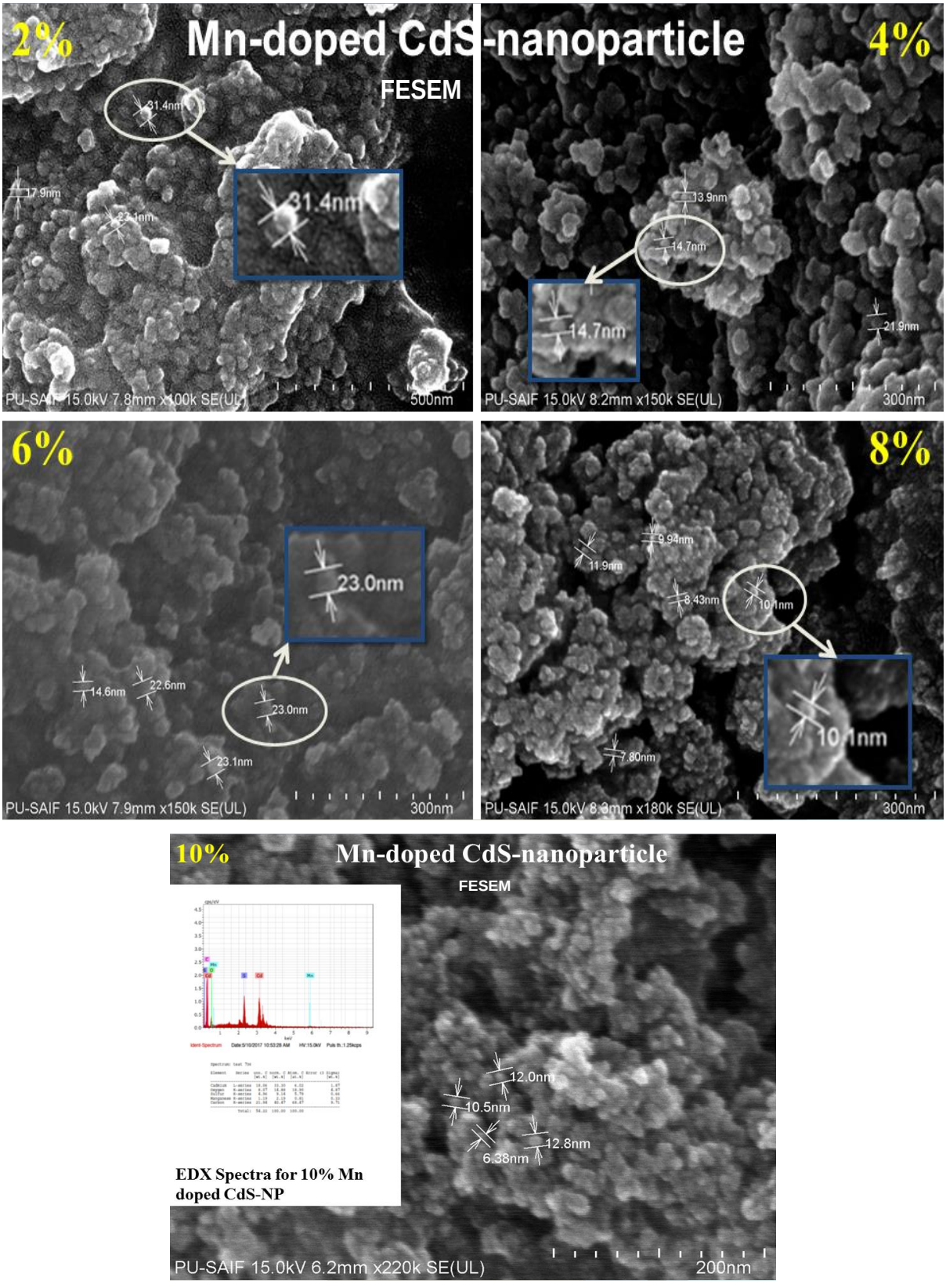

Figure 4: FESEM images

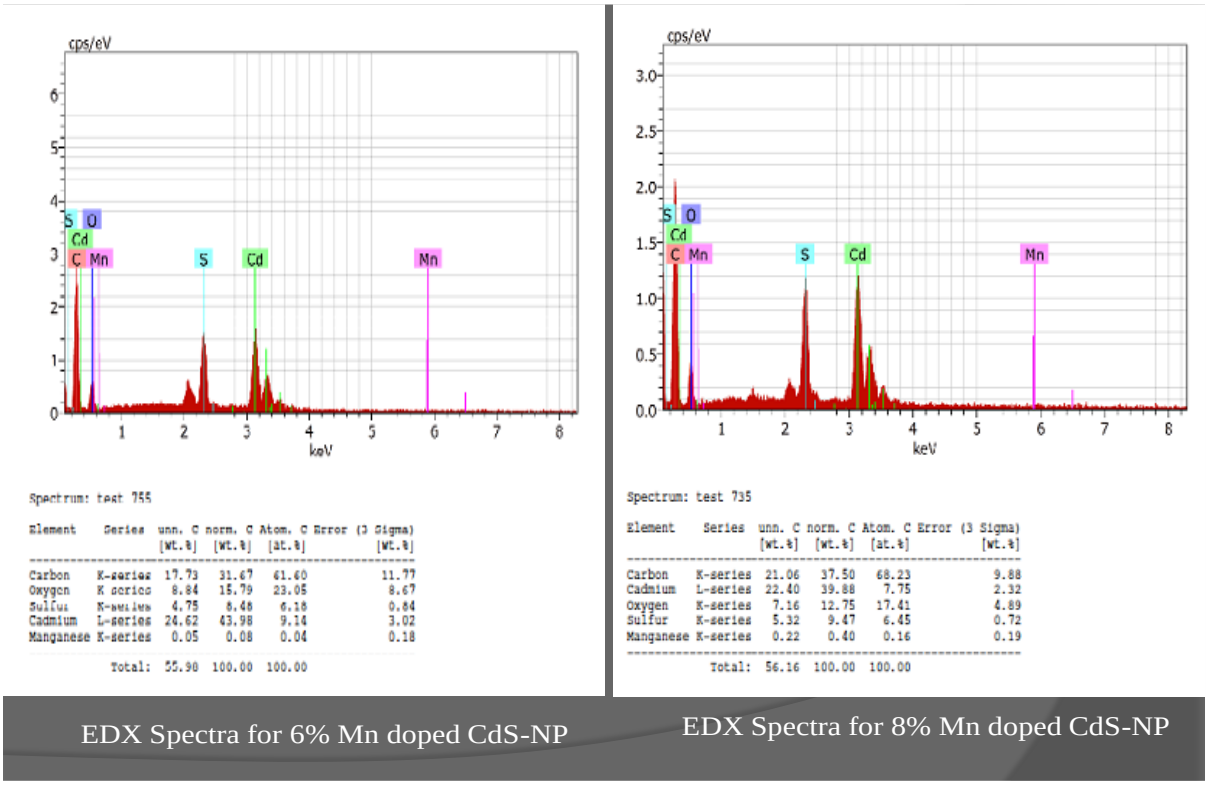

Figure 5: EDX spectra

CONCLUSIONS

Mn-doped & undoped cadmium sulphide (CdS) nanoparticles were synthesized at room temperature. Experiment was progressed without using PVP capping agent and found no agglomeration of nanoparticles. Doping of CdS with Manganease transition metal showed a blue shift in comparison to pure CdS & with respect to bulk counterpart and hence exhibit increase in band gap with decrease in crystallite size of NPs. This material may be considered for fabrication of photoconductive detector with higher efficiency.

ACKNOWLEDGEMENTS

Authors are thankful to Director CIL/SAIF of Panjab University, Chandigarh for permitting to access the facilities of the department.

REFERENCES

Akai, H. and P. H. Dederichs. 1998. Ferromagnetism and Its Stability in the Diluted Magnetic Semiconductor (In, Mn) As. Phys. Rev. Lett., 81 3002-3005.

Akai, H. 1993. Local moment disorder in ferromagnetic alloys. Phys. Rev. B, 47: 8739-8747.

Boeck J D, Roy D V, das J, Motsnyi V, Liu Z, Lagae L, Boeve H, Dessein K and Borghs G 2002. Technology and materials issues in semiconductor-based magnetoelectronics. Semicond. Sci. Technol., 17: 342-354.

Brus, L. E. J., 1986a. A simple model for the ionization potential, electron affinity, and aqueous redox potentials of small semiconductor crystallites. Chem. Phys., 1983. 79: 5566-5571.

Brus, L. E. 1986b. Electronic wave functions in semiconductor clusters: experiment and theory. J. Phys. Chem., 90: 2555-2560.

Chelikowsky, J. R., E. Kaxiras and R. M. Wentzcovitch. 2006. Theory of spintronic materials. Phys. Stat. Sol. (b), 243: 2133-2150.

Diet, I. T. 1994. Diluted Magnetic Semiconductors Chapter 14 in Handbook of Semiconductors vol. 3 B eds Mahajan S (Amsterdam: North Holland) p.1251.

Furdyna, J. K. 1988. Diluted magnetic semiconductors. J. Appl. Phys., 64: R29-R64.

Jiang, Y., W. Yan, Z. Sun, Q. Liu, Z. Pan, T. Yao, Y. Li, Z. Qi, G. Zhang, P. Xu, Z. Wu and S. Wei. 2009. Experimental and theoretical investigations on ferromagnetic nature of Mn-doped dilute magnetic semiconductors. J. Phys.: Conf. Ser., 190: 012100 (11 pages)

Kirovskaya, I. A., O. T. Timoshenko and E. O. Karpova 2011. The catalytic and photocatalytic properties of InP-CdS and ZnTe-CdS system components. Russ. J. Phys. Chem., A 85: 557-560.

Kayanuma, Y., 1988. Quantum-size effects of interacting electrons and holes in semiconductor microcrystals with spherical shape. Phys. Rev. B, 38: 9797-9805.

Lippens, P. E., and M. Lannoo. 1990. Comparison between calculated and experimental values of the lowest excited electronic state of small CdSe crystallites. Phys. Rev. B, 41: 6079-6081.

Ohno, H. 1998. Making Nonmagnetic Semiconductors Ferromagnetic. Science, 281: 951-956.

Ohno, H. 2010. A window on the future of spintronics Nat. Mater., 9: 952-954.

Pang X, J. Zhang, K. Gao and A. A. Volinsky. 2011. Room temperature ferromagnetism in sputtered Zn1− xCrxO thin films. Mater. Lett., 65: 2728.

Sharma P., A. Gupta A, K.V. Rao, F. J. Owens, R. Sharma, R. Ahuja, J. M. O. Guillen, B. Johansson, G. A. Gehring. 2003. Ferromagnetism above room temperature in bulk and transparent thin films of Mn-doped ZnO. Nat. Mater., 2: 673-677.

SYNTHESIS OF TRIFLUOROMETHYLATED OXAZOLINES VIA A VISIBLE-LIGHT-PROMOTED TANDEM DIFUNCTIONALIZATION OF N-ALLYLAMIDES WITH TRIFLUOROMETHYLSULFINATE

Palani Natarajan,*[a] Deachen Chuskit,[a] Priya,[a]

[a] Department of Chemistry & Centre for Advanced Studies in Chemistry,
Panjab University, Chandigarh - 160014, India

ABSTRACT

Using N-allylamides and trifluoromethylsulfinate as precursors, the 9,10-phenanthrenedione (PQ) visible-light photocatalysis for the synthesis of a variety of trifluoromethylated oxazolines in good yield has been established. A plausible mechanism for the reaction is reported. It involves the formation of cascade C-C and C-O bonds in the oxidative difunctionalization of N-allylamides. This new and operationally easy approach is transition-metal-free, cost-effective, and operates in an open environment, with diverse functional group tolerance.

Keywords: Oxazolines, Trifluoromethyl, Metal-free, Photocatalysis, Synthetic Methods,

INTRODUCTION

Oxazoline and its derivatives are a kind of heterocycle that may be found in a wide range of natural products (Hahn *et al*., 2018; Tilvi, 2016; Yeh, 2004) and physiologically active compounds (Luxenhofer *et al*., 2010; Nicolaou *et al*., 2005; Schulz *et al*., 2014). The trifluoromethyl (-CF_3) functionality has also been widely used in a variety of drugs (Chaudhary *et al*., 2020; Chiba *et al*., 2012; Küçükgüzel *et al*., 2013; Penta *et al*., 2013; Zhu *et al*., 2014) and organic functional materials (Garci *et al*., 2006; Katla *et al*., 2018; Lermontov *et al*., 2016; Chang *et al*., 2015; Niu *et al*., 2020; Servnis *et al*., 2015) because the key structural motif improves physical, chemical, and biological properties such as solubility, lipophilicity, metabolic stability, binding selectivity, and so on (Chu and Qing, 2014; Ma and Cahard, 2007; Merino and Nevado, 2014; Muller *et al*., 2007; Purser *et al*., 2008; Shimizu and Hiyama, 2005; Studer, 2012; Schlosser, 2006; Tomshenko *et al*., 2011; T. Liang *et al*., 2013). As a result, chemists, pharmacists, and biologists have been paying close attention to the development of a feasible method for the synthesis of trifluoromethylated oxazolines. In 2017, Kawamuraa and colleagues published a synthetic technique (Scheme 1a) for making CF_3-containing oxazolines by employing N-allylamides and Togni reagent in the presence of alkali metal iodides (Kawamuraa et al., 2017). Deng and colleagues published a visible-light photocatalysis (Scheme 1b) for the production of CF_3-containing oxazolines from N-allylamides, Umemoto's reagent, $[Ru(bpy)_3]^{2+}$ and base in 2015 (Deng et al., 2015). In 2014, Yu and co-workers disclosed a trifluoromethylation of N-allylamides (Scheme 1c) leading to CF_3-containing oxazolines by using iodobenzene diacetate and sodium trifluoromethanesulfinate at 80 °C (Yu *et al*., 2014). These procedures (Scheme 1) are limited to expensive reagents such as transition metals, organoiodines, or Umemoto reagent, while being effective and flexible. As a result, the development of a cost-effective and environmentally benign technique for obtaining trifluoromethylated oxazolines is in high demand.

Quinones, as compared to other organo-photoredox catalysts, are a low-cost and low-molecular-weight organic molecule (Chang *et al*., 2017; Lerch *et al*., 2014; Wendlandt and Stahl, 2015). Many of them have absorption bands in the visible range and demonstrate three easily accessible oxidation states through single electron transfer. Moreover, some quinines include 2,3-dichloro-5,6-dicyano-1,4-benzoquinone (DDQ) (Liu and Floreancig, 2010; Natarajan and Konig, 2021; Shen *et al*., 2011), 9,10-phenanthrenedione (PQ) (Berenguer *et al*., 2018; Natarajan *et al*., 2022; Natarajan *et al*., 2021), and anthraquinone (AQ) (Bardagi *et al*., 2018; Duval *et al*., 2016; Elkazaz and Jones, 2010; Hao and Lang, 2019; Lerch *et al*., 2014) can participate in photoinduced electron transfer processes and can be easily recovered from the reduced compound (dihydroquinone) by using nitrates, metal oxides, or molecular oxygen. To the best of our knowledge, nevertheless, quinone has not yet been employed as a catalyst in the visible-light photocatalysis production of trifluoromethylated oxazolines.

In continuation of our research on visible-light-induced photoredox catalysis (Chaudhary and Natarajan, 2017; Chuskit *et al*. 2018; Natarajan *et al*., 2020; Natarajan *et al*., 2019; Natarajan *et al*., 2018; Natarajan *et al*., 2017; Natarajan *et al*., 2016;

*Corresponding author: pnataraj@pu.ac.in
Received: November 12, 2021, Accepted: December 27, 2021

Natarajan *et al*., 2016), we present a novel, cost-effective, and transition-metal-free protocol for the preparation of trifluoromethylated oxazolines from N-allylamides and trifluoromethylsulfinate using PQ (8 mol%) as a photocatalyst, CH_3CN as a solvent, and a white LED as an irradiation source in an open to air atmosphere at ambient conditions (Scheme 2). A possible mechanism for the reaction is also reported (see infra).

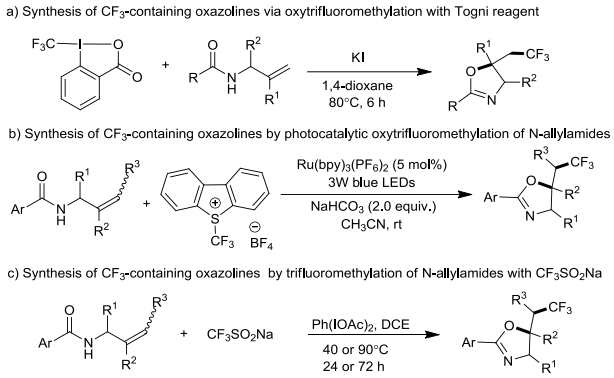

Scheme 1. In the literature, three distinct procedures (a-c) for the synthesis of trifluoromethylated oxazolines have been published.

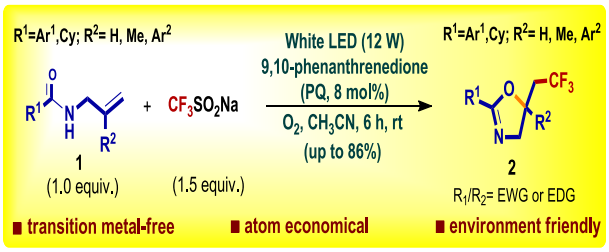

Scheme 2. This paper work on the synthesis of trifluoromethylated oxazolines (**2**) from N-allylamides (**1**) and trifluoromethylsulfinate using PQ, white LED, and CH_3CN in an open to air environment under ambient temperatures.

RESULTS AND DISCUSSION

At ambient conditions, we used N-(2-phenylallyl)benzamide (**1g**, 0.5 mmol, 1.0 equiv.) as a model substrate, trifluoromethyl sulfinate (0.5 mmol, 1.0 equiv.) as -CF_3 source, acetonitrile (4 mL) as a solvent, oxygen from open air as a terminal oxidant, and a white LED (12W, with a distance of 2 cm) as irradiation source. Under these circumstances, a series of quinone photocatalysts (5 mol per cent) were tested, and the findings are described in Table 1 (Entries 1-6). After 20 h, 2,3-dichloro-5,6-dicyano-1,4-benzoquinone (DDQ, entry 1), 9,10-phenanthrenedione (PQ, entry 3) and anthraquinone (AQ, entry 5) gave 28-47 per cent yields of the required 2,5-diphenyl-5-(2,2,2-trifluoroethyl)-4,5-dihydrooxazole (**2g**). NMR analyses were used to characterize the product (**2g**), as described in the experimental section. We opted to continue optimizing reaction conditions utilizing PQ as a photocatalyst due to its good performance (Table 1, entry 3), ready availability, and high stability. The effect of the quantity of PQ on the product yield was then investigated. With an increase in catalyst concentration from 5.0 mol per cent to 6.0-10.0 mol per cent, the reaction time was significantly reduced, yielding 57-65 per cent of **2g** (Table 1, entries 7, 8, 9 and 10). In any event, there was no product without a photocatalyst (Table 1, entry 11). Following that, the effect of solvents on the production of **2g** was investigated (Table 1, entries 12, 13 14, 15 and 16). Among all other solvents examined (Table 1, entries 12-16), including toluene, methanol, $C_2H_4Cl_2$, ethyl acetate, and THF, CH_3CN was shown to be the best match (Table 1, entry 9). Similarly, as compared to processes done with either green LEDs or blue LEDs, irradiation sources such as white LEDs (12W) yielded **2g** in good yield (Table 1, entry 9). The stoichiometry of trifluoromethylsulfinate to substrate (**1g**) was then explored to optimize product yield. Increasing the quantity of trifluoromethylsulfinate to 1.5 equiv. resulted in an outstanding yield (93 per cent) of **2g**; but, further raising the amount of trifluoromethylsulfinate did not improve the reaction efficiency drastically (Table 1, entries 21 and 22). This reaction did not function in the absence of each reaction parameter, according to the control experiments (Table 1). Therefore, the optimal conditions for the synthesis of trifluoromethylated oxazolines from N-allylamides (1.0 equiv.) were trifluoromethylsulfinate (1.5 equiv.), 8.0 mol per cent 9,10-phenanthrenedione, white LED (12W), and CH_3CN in an open air environment at ambient temperature for 6 h stirring (Table 1, entry 20).

Table 1. Results of a screening experiment to find the best conditions for photocatalytic synthesis of trifluoromethylated oxazolines (**2**) from N-allylamides (**1**)[a]

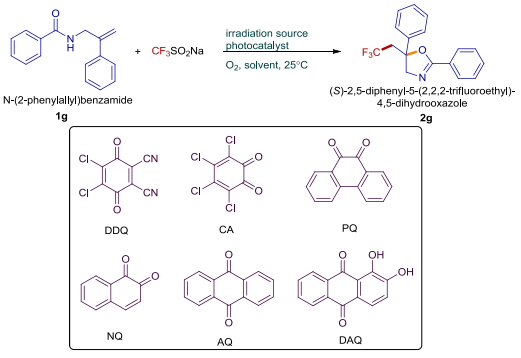

Entry	photocatalyst (mol per cent)[b]	CF_3SO_2Na (equiv.)	solvent[c]	time (h)	yield of 2g (per cent)[d]
1	DDQ (5)	1.0	CH_3CN	20	28
2	CA (5)	1.0	CH_3CN	20	NR
3	PQ (5)	1.0	CH_3CN	20	47
4	NQ (5)	1.0	CH_3CN	20	NR
5	AQ (5)	1.0	CH_3CN	20	34
6	DAQ (5)	1.0	CH_3CN	20	NR
7	PQ (6)	1.0	CH_3CN	20	49
8	PQ (7)	1.0	CH_3CN	15	57
9	PQ (8)	1.0	CH_3CN	11	62
10	PQ (10)	1.0	CH_3CN	11	65
11	PQ (0)	1.0	CH_3CN	24	NR
12	PQ (8)	1.0	toluene	11	16
13	PQ (8)	1.0	CH_3OH	11	NR
14	PQ (8)	1.0	$C_2H_4Cl_2$	11	38
15	PQ (8)	1.0	ethyl acetate	11	NR
16	PQ (8)	1.0	THF	11	22
17	PQ (8)	1.0	CH_3CN	11	37[e]
18	PQ (8)	1.0	CH_3CN	11	40[f]
19	PQ (8)	1.2	CH_3CN	9	71
20	PQ (8)	1.5	CH_3CN	6	93
21	PQ (8)	1.8	CH_3CN	5	95
22	PQ (8)	2.0	CH_3CN	4	94
23	PQ (8)	1.5	CH_3CN	6	NR[g]

[a]Reaction conditions: Unless stated otherwise all reactions were performed in a vial equipped with N-(2-phenylallyl)benzamide (**1g**, 0.5 mmol), photocatalyst and solvent under white LED (12W) irradiation and open to air atmosphere at ambient conditions. [b]Commercially available high purity catalysts were purchased and utilized as such. [c]Solvents were purified before use. [d]Isolated yield of **2g**. [e]Green LED used instead of white LED. [f]Blue LED used instead of white LED. [g]Reaction performed under darkness. NR: no reaction.

Next, the substrate scope and functional group tolerance were investigated using the optimized reaction conditions (Table 1, entry 20), and the findings are provided in Table 2. In general, the reaction tolerated N-allylamides (**1a-n**) with both electron-donating and electron-withdrawing groups and yielded good yield of trifluoromethylated oxazolines (**2a-n**). The substituted electron rich and electron deficient aromatic ring of N-allyl arylamide (**2a-2e**) gave higher yields up to 86 per cent (Table 2). The reaction was well tolerated with N-allyl alkylamide (**2f**) in 49 per cent yield. Next, the scope of substituted alkenes (**2g-2n**) in the reaction system was then investigated. Various substituents at the β position of alkene moiety such as phenyl- (**2g-2k**), methyl- (**2l**), tolyl-(**2m**), and 4-chlorophenyl-(**2n**), yielded outstanding yields.

Table 2. Substrate scope for the synthesis of trifluoromethylated oxazolines from N-allylamides and trifluoromethylsulfinate[a]

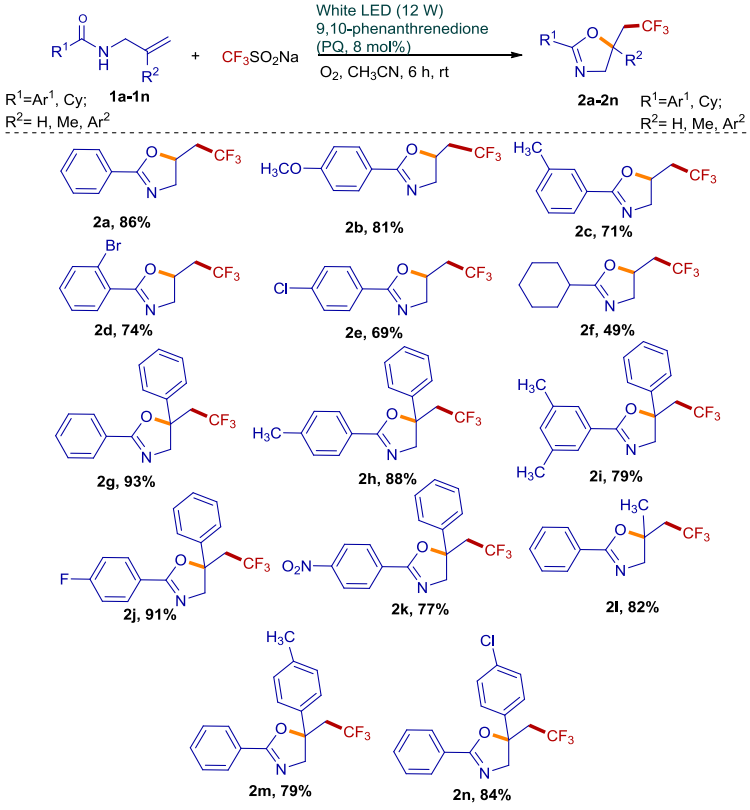

[a]Unless stated otherwise all reactions were performed in a vial equipped with allylamides (**1a-1n**, 1.0 mmol), trifluoromethylsulfinate (1.5 mmol), **PQ** (8 mol%) and CH_3CN (8-10 mL) under white LED (12W) irradiation and open to air atmosphere at ambient conditions for 6 h.

Control tests were carried out as outlined in Scheme 3 to better understand the mechanism of this transition. The addition of 2.5 equiv. of 2,2,6,6-tetramethylpiperidine-1-oxyl (TEMPO, a common radical scavenger) completely inhibited the reactions (Scheme 3), which suggested that the trifluoromethylation reaction proceeds via a radical process. Electron paramagnetic resonance (EPR) spectroscopy was used to further investigate the probable radical species involved in the reactions. ESR clearly recorded a signal with six peaks corresponding to the radical adduct, i.e., CF_3-MNP$^{\bullet}$ (trifluoromethyl·*tert*-butyl nitroxide radical with g = 2.0069, $a_N = a_F$ = 12.26 G) (Hang *et al*., 2014) when PQ and CF_3SO_2Na in DCE were irradiated with white LED in the presence of 2-methyl-2-nitrosopropane (MNP, a typical CF_3-radical scavenger). Despite this, the identical reaction combination of MNP, PQ, and CF_3SO_2Na was found to be EPR quiet in the dark. These results confirmed the formation of CF_3-radical under the experimental conditions.

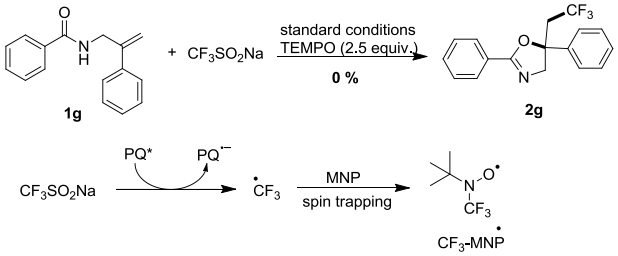

Scheme 3. The control experiments with TEMPO and MNP under optimized reaction conditions.

A reasonable reaction route for the difunctionalization of N-allylamides over 9,10-phenanthrenedione (PQ) is provided in light of the foregoing experimental findings and our experience with visible-light photocatalysis (Scheme 4). When PQ was subjected to visible-light, it got excited, resulting in PQ* [E_{red}(PQ*/PQ$^{\bullet-}$) = +1.6 V versus SCE]. PQ$^{\bullet-}$ and trifuloromethyl radical ($CF_3^{\bullet}$) (**I**) were produced by a single electron transfer from trifluoromethylsulfinate [E_{ox}(CF_3SO_2-/CF_3SO_2•) = +1.05 V versus SCE] to PQ*. Following that, the electron-poor CF_3• (**I**) attacks the electron-rich C-C bond of N-allylamides (**1**) to produce radical intermediate **II**. This radical intermediate **II** is further oxidized by PQ$^{\bullet-}$ to give cation intermediate **III** and **PQH$^-$.** The required trifluoromethylated oxazolines **2** were then obtained by the intramolecular cyclization of **III**. PQ is reduced to PQH$^-$ throughout the process, which is then reoxidized by molecular oxygen to PQ.

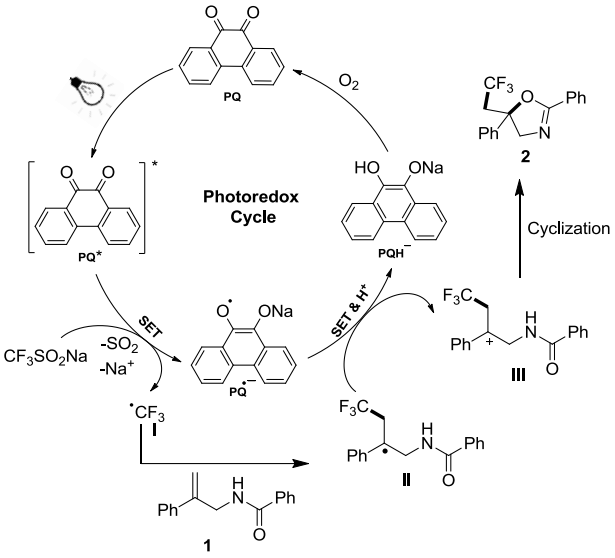

Scheme 4. A plausible mechanism for the production of trifluoromethylated oxazolines from N-allylamides and trifluoromethylsulfinate.

As previously stated, the synthesis of trifluoromethylated oxazolines (**2**) has recently received a lot of interest due to their biological importance (Li *et al*., 2019; Waschinski and Tiller, 2005) and the use of chiral oxazoline-based ligands in asymmetric catalysis (Hargaden and Guiry, 2009; Rasappan *et al*., 2008). Only three synthesis techniques (Scheme 1) have been disclosed thus far, all of which require hazardous and expensive chemicals. The approach described here, on the other hand, relies on the employment of an organic dye, namely PQ, as a catalyst under visible-light irradiation and trifluoromethylsulfinate as -CF_3 source. As a result, we are optimistic that the current methodology will have a bright future, particularly in the pharmaceutical industry, where the need for low-cost and high-purity end products is critical.

CONCLUSIONS

Using 9,10-phenanthrenedione as a catalyst under visible-light irradiation, a novel, cost-effective, and metal-free approach for the synthesis of trifluoromethylated oxazolines from N-allylamides and trifluoromethylsulfinate has been established. The facile formations of new C-C and C-O bonds take place in a one-pot procedure. Moreover, desired products in pure form are obtained in good yield by

small-filtration over silica-gel column chromatography. Further application of this strategy to other substrates is ongoing in our laboratory.

EXPERIMENTAL SECTION

General Information

Unless otherwise noted, all reagents and substrates were bought from reputable commercial sources and utilized without additional purification. All solvents were distilled in accordance with standard methods. All reactions were carried out in an open-air atmosphere. A silica gel with a mesh size of 100-200 was used for column chromatography. Analytical thin layer chromatography on silica gel was used to monitor reactions, and visibility was achieved by irradiation with short wave UV light at 254 nm and near UV 366 nm lights. All of the products are well-known, and their ^{1}H- and ^{13}C NMR spectra were compared to those of authentic samples. The leftover protonated solvent was used to calibrate chemical shifts, which are given as *δ*-value in parts per million (ppm). The peak patterns are indicated as follows: s, singlet; d, doublet; t, triplet; m, multiplet; and so on. The coupling constants, J, are reported in Hertz (Hz).

General procedure for the synthesis of trifluoromethylated oxazolines

Under open-air conditions, N-allylamides (1.0 mmol, 1.0 equiv.), sodium trifluoromethanesulfinate (1.5 mmol, 1.5 equiv.), 9,10-phenanthrenedione (8 mol %), and 5-7 ml of freshly distilled CH_3CN were charged to a vial (20 ml) equipped with a magnetic stir bar. The liquid was agitated for a few minutes in an open-air environment to ensure thorough mixing, and then the vial was irradiated through the plane bottom side of the vial with a 12W white LED at a distance of 2 cm at ambient conditions. After the completion (as determined by TLC, 6 h), volatiles were evaporated under decreased pressure and then admixed with aqueous NaCl solution (10 ml). The organic matter was extracted with ethyl acetate (3-10 ml), dried over Na_2SO_4, and evaporated under reduced pressure to obtain pale-yellow gummy components, which were purified using a combination of ethyl acetate and n-hexane filtration using a short-pad of silica-gel column chromatography. Spectroscopic examination, as well as a comparison with actual sample spectra, was used to establish the product's identification and purity.

Experimental characterization data for few selected products

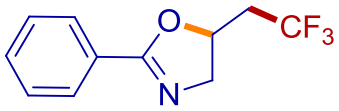

2a

2-Phenyl-5-(2,2,2-trifluoroethyl)oxazoline (**2a**): Colorless amorphous; ^{1}H NMR (400 MHz, $CDCl_3$): δ 2.34-2.52 (m, 1H), 2.58-2.73 (m, 1H), 3.81 (dd, J = 14.8, 7.2 Hz, 1H), 4.28 (dd, J = 14.8, 9.6 Hz, 1H), 4.93-5.01 (m, 1H), 7.41 (t, J = 7.6 Hz, 2H), 7.51 (t, J = 7.6 Hz, 1H), 7.92 (d, J = 7.6 Hz, 2H); ^{13}C NMR (100 MHz, $CDCl_3$): δ 39.6 (q, J = 28.8 Hz), 60.4, 73.2 (q, J = 2.8 Hz), 125.4 (q, J = 274 Hz), 127.2, 128.4, 128.5, 131.7, 163.7; ^{19}F NMR (376 MHz, $CDCl_3$): δ −63.6 (t, J = 10.1 Hz).

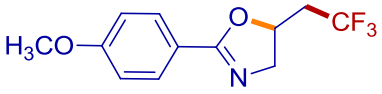

2b

2-(4-Methoxyphenyl)-5-(2,2,2-trifluoroethyl)oxazoline (**2b**): Colorless amorphous; ^{1}H NMR (400 MHz, $CDCl_3$): δ 2.36-2.49 (m, 1H), 2.58-2.74 (m, 1H), 3.77 (dd, J = 14.7, 7.2 Hz, 1H), 3.87 (s, 3H), 4.27 (dd, J = 14.7, 9.4 Hz, 1H), 4.96-5.04 (m, 1H), 6.92-6.96 (m, 2H), 7.89-7.95 (m, 2H); ^{13}C NMR (100 MHz, $CDCl_3$): δ 39.7 (q, J = 27.8 Hz), 55.5, 59.6, 73.7 (q, J = 1.8 Hz), 114.1 (2C), 119.0, 125.3 (q, J = 277 Hz), 130.6 (2C), 162.8, 164.1; ^{19}F NMR (376 MHz, $CDCl_3$): δ −63.6 (t, J = 10.2 Hz).

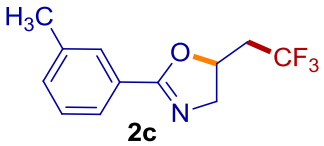

2c

2-(3-Methylphenyl)-5-(2,2,2-trifluoroethyl)oxazoline (**2c**): Colorless oil; ^{1}H NMR (400 MHz, $CDCl_3$): δ 2.36-2.49 (m, 1H), 2.38 (s, 3H), 2.57-2.72 (m, 1H), 3.78 (dd, J = 14.8, 7.2 Hz, 1H), 4.26 (dd, J = 14.8, 9.4 Hz, 1H), 4.92-5.02 (m, 1H), 7.29-2.35 (m, 2H), 7.72-7.78 (m, 2H); ^{13}C NMR (100 MHz, $CDCl_3$): δ 21.5, 39.8 (q, J = 27.8 Hz), 60.2, 73.3, 125.5 (q, J = 275 Hz), 125.4, 127.1, 128.6, 129.1, 132.8, 138.4, 164.2; ^{19}F NMR (376 MHz, $CDCl_3$): δ −63.8 (t, J = 11.4 Hz).

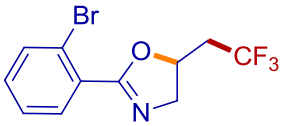

2d

2-(2-Bromophenyl)-5-(2,2,2-trifluoroethyl)oxazoline (**2d**): Colorless oil; ^{1}H NMR (400 MHz, $CDCl_3$): δ 2.38-2.52 (m, 1H), 2.64-2.81 (m, 1H), 3.87 (dd, J = 14.8, 7.4 Hz, 1H), 4.34 (dd, J = 14.8, 9.6 Hz, 1H), 4.97-5.06 (m, 1H), 7.28-7.40 (m, 2H), 7.67 (dd, J = 7.8, 1.4 Hz, 1H), 7.74 (dd, J = 7.8, 1.6 Hz, 1H); ^{13}C NMR (100 MHz, $CDCl_3$): δ 39.7 (q, J = 27.8 Hz), 60.7, 73.5, 122.2, 125.3 (q, J = 276 Hz), 127.5, 129.1, 131.4, 132.2, 134.2, 162.8; ^{19}F NMR (376 MHz, $CDCl_3$): δ −63.6 (t, J = 10.2 Hz).

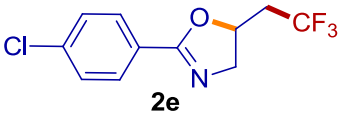

2e

2-(4-Chlorophenyl)-5-(2,2,2-trifluoroethyl)oxazoline (**2e**): Pale yellow solid; ^{1}H NMR (400 MHz, $CDCl_3$): δ 2.34-2.48 (m, 1H), 2.58-2.72 (m, 1H), 3.78 (dd, J = 15.2, 7.4 Hz, 1H), 4.26 (dd, J = 15.2, 9.6 Hz, 1H), 4.95-5.03 (m, 1H), 7.86-7.91 (m, 2H), 7.77-7.84 (m, 2H); ^{13}C NMR (100 MHz, $CDCl_3$): δ 39.7 (q, J = 27.8 Hz), 60.3, 73.7 (q, J = 1.8 Hz), 125.5 (q, J = 275 Hz), 125.7, 128.8, 129.6, 138.2, 163.1; ^{19}F NMR (376 MHz, $CDCl_3$): δ −63.5 (t, J = 10.4 Hz).

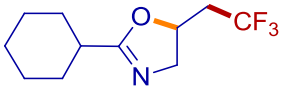

2f

2-Cyclohexyl-5-(2,2,2-trifluoroethyl)oxazoline (**2f**): Colorless oil; ^{1}H NMR (400 MHz, $CDCl_3$): δ 1.16-1.47 (m, 5H), 1.61-1.95 (m, 5H), 2.21-2.36 (m, 2H), 2.42-2.54 (m, 1H), 3.51 (dd, J = 14.4, 6.8 Hz, 1H), 3.96 (dd, J = 14.2, 9.4 Hz, 1H), 4.67-4.78 (m, 1H); ^{13}C NMR (100 MHz, $CDCl_3$): δ 25.6, 25.9, 29.8, 29.8, 37.4, 39.7 (q, J = 27.8 Hz), 59.7, 72.4, 125.6 (q, J = 276 Hz), 171.2; ^{19}F NMR (376 MHz, $CDCl_3$): δ −63.8 (t, J = 11.5 Hz).

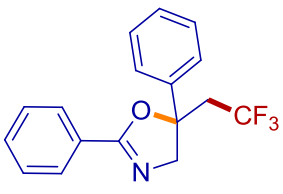

2g

2,5-Diphenyl-5-(2,2,2-trifluoroethyl)oxazoline (2g): Colorless amorphous solid; ^{1}H NMR (400 MHz, $CDCl_3$): δ 2.84-3.01 (m, 2H), 4.25 (d, J = 14.6 Hz, 1H), 4.42 (d, J = 14.7 Hz, 1H), 7.31-7.38 (m, 1H), 7.36-7.42 (m, 4H), 7.45-7.51 (m, 2H), 7.51-7.57 (m, 1H), 8.06-8.10 (m, 2H); ^{13}C NMR (100 MHz, $CDCl_3$): δ = 44.3 (q, J = 27.9 Hz), 67.8, 85.2, 124.4, 125.1 (q, J = 276 Hz), 127.2, 128.3, 128.6, 128.7, 128.8, 132.2, 142.4, 163.3; ^{19}F NMR (376 MHz, $CDCl_3$): δ −60.2 (t, J = 10.3 Hz).

ACKNOWLEDGMENTS

The authors gratefully acknowledge financial support from the Council of Scientific & Industrial Research (CSIR), New Delhi, India, through an extra mutual research grant with project number 02(0380)/19/EMR-II. D. C. and Priya are grateful for their senior research fellowships from the CSIR, New Delhi.

REFERENCES

Bardagi J. I., I. Ghosh, M. Schmalzbauer, T. Ghosh and B. König. 2018. Anthraquinones as Photoredox Catalysts for the Reductive Activation of Aryl Halides. Eur. J. Org. Chem., 2018 (1): 34–40.

Berenguer J. R., G. Blay, J. R. Pedro and C. Vila. 2018. 9, 10-Phenanthrenedione as Visible-Light PhotoredoxCatalyst: A Green Methodology for theFunctionalization of 3, 4-Dihydro-1, 4-Benzoxazin-2-Ones through a Friedel-Crafts Reaction. Catalysts, 8 (12): 653.

Chang B., H. Shao, P. Yan, W. Qiu, Z. Weng and R. Yuan. 2017. Quinone-Mediated Trifluoromethylation of Arenes and Heteroarenes with Visible Light. ACS Sustainable Chem. Eng., 5: 334−341.

Chang J., W. Liu, M. Zhang, L. Cao, Q. Ge, H. Niu, G. Sui and D. Wu. 2015. Structures and properties of polyimide fibers containing fluorine groups. RSC Adv., 5: 71425-71432.

Chaudhary B., N. Kulkarni, N. Saiyed, M. Chaurasia, S. Desai, S. Potkulea and S. Sharma. 2020. β-Trifluoromethyl α,β-unsaturated Ketones: Efficient Building Blocks for Diverse Trifluoromethylated Molecules. Adv. Synth. Catal., 362 (22): 4794-4819.

Chaudhary R. and P. Natarajan. 2017. Visible Light Photoredox Activation of Sulfonyl Chlorides: Applications in Organic Synthesis. ChemistrySelect, 2: 6458–6479.

Chiba A., M. Mizuno, C. Tomi, R. Tajima, I. Alloza, A. Penta, T. Yamamura, K. Vandenbroeck and S. Miyake. 2012. A 4-trifluoromethyl analogue of celecoxib inhibits arthritis by suppressing innate immune cell activation. Arthritis Res. Ther., 14: 1-9.

Chu L. and F.-L. Qing. 2014. Oxidative Trifluoromethylation and Trifluoromethylthiolation Reactions Using (Trifluoromethyl)trimethylsilane as a Nucleophilic CF_3 Source. Acc. Chem. Res., 47: 1513.

Chuskit D., R. Chaudhary, P. Venugopalan, B. König and P. Natarajan. 2018. Oxidative homodimerization of substituted olefins by DDQ visible light photocatalysis. Org. Chem. Front., 5: 3553–3556.

Deng Q. –H., J. –R. Chen, Q. Wei, Q. –Q. Zhao, L. –Q. Lua and W. –J. Xiao. 2015. Visible-light-induced photocatalytic oxytrifluoromethylation of N-allylamides for the synthesis of CF3-containing oxazolines and benzoxazines. Chem. Commun., 51: 3537-3540.

Duval J., V. Pecher, M. Poujol and E. Lesellier. 2016. Research advances for the extraction, analysis and uses of anthraquinones: A review. Ind. Crops and Prod., 94: 812–833.

Elkazaz S. and P. B. Jones. 2010. Photochemical Hydroxylation of 1-Methyl-9,10-anthraquinones: Synthesis of 90-Hydroxyaloesaponarin II. J. Org. Chem., 75: 412-416.

Garcı´ O., R. Sastre, D. Agua, A. Costela, I. G.-Moreno and A. Roig. 2006. Optical materials based on fluorinated-polymeric silica aerogels. Chem. Phys. Lett., 427: 375-378.

Hahn L., M. M. Lü btow, T. Lorson, F. Schmitt, A. A. -Menzel, R. Schobert and R. Luxenhofer. 2018. Investigating the Influence of Aromatic Moieties on the Formulation of Hydrophobic Natural Products and Drugs in Poly(2-oxazoline)- Based Amphiphiles. Biomacromolecules, 19: 3119−3128.

Hang Z., Z. Li and Z. –Q. Liu. 2014. Iodotrifluoromethylation of Alkenes and Alkynes with Sodium Trifluoromethanesulfinate and Iodine Pentoxide. Org. Lett., 16: 3648-3651.

Hao H., X. Lia and X. Lang. 2019. Anthraquinones as photoredox active ligands of TiO2 for selective aerobic oxidation of organic sulfides. Appl. Catal. B., 259: 118038.

Hargaden G. C. and P. J. Guiry. 2009. Recent Applications of Oxazoline-Containing Ligands in Asymmetric Catalysis. Chem. Rev., 109, 6: 2505–2550.

Katla J., A. J. M. Nair, A. Ojha and S. Kanvah. 2018. Organogels composed of trifluoromethyl anthryl cyanostyrenes: enhanced emission and self-assembly. Photochem. Photobiol. Sci.**,** 17**:** 395-403.

Kawamuraa S., D. Sekineb and M. Sodeokaa. 2017. Synthesis of CF3-containing oxazolines via trifluoromethylation of allylamides with Togni reagent in the presence of alkali metal iodides. J. Fluor. Chem., 203: 115–121.

Küçükgüzel Ş. G., İ. Coşkun, S. Aydın, G. Aktay, Ş. Gürsoy, Ö. Çevik, Ö. B. Özakpınar, D. Özsavcı, A. Şener, N. K.-Basu, A. Basu and T. T. Talele. 2013. Synthesis and Characterization of Celecoxib Derivatives as Possible Anti-Inflammatory, Analgesic, Antioxidant, Anticancer and Anti-HCV Agents. Molecules, 18(3): 3595-3614.

Lerch S., L. –N. Unkel and M. Brasholz. 2014. Tandem Organocatalysis and Photocatalysis: An Anthraquinone-Catalyzed Indole-C3 Alkylation/ Photooxidation/1,2-Shift Sequence. Angew. Chem. Int. Ed., 53: 6558–6562.

Lerch S., L. –N. Unkel, P. Wienefeld, M. Brasholz. 2014. Ground- and Excited-State Quinones: Perspectives in Organocatalysis and Visible-Light Photocatalysis Quinone Organocatalysis and Photocatalysis. Synlett, 25: 2673–2680.

Lermontov S. A., N. A. Sipyagina, A. N. Malkova, A. V. Yarkov, S. G. Vasil'ev, N. P. Simonenko, A. E. Baranchikovbd and V. K. Ivanov. 2016. SiO_2 aerogels modified by perfluoro acid amides: a precisely controlled hydrophobicity. RSC Adv., 6: 80766–80772.

Liu L. and P. E. Floreancig. 2010. 2,3-Dichloro-5,6-dicyano-1,4-benzoquinone-Catalyzed Reactions Employing MnO2 as a Stoichiometric Oxidant. Org. Lett., 12(20): 4686-4689.

Li W., G. Wang, J. Lai and S. Li. 2019. Multifunctional isoquinoline-oxazoline ligands of chemical and biological importance. Chem. Commun., 55: 5902-5905.

Luxenhofer R., A. Schulz, C. Roques, S. Li, T. K. Bronich, E. V. Batrakova, R. Jordan, A. V. Kabanov. 2010. Doubly amphiphilic poly(2-oxazoline)s as high-capacity delivery systems for hydrophobic drugs. Biomaterials, 31 (18): 4972−4979.

Ma J.-A., D. Cahard. 2007. Strategies for nucleophilic, electrophilic, and radical trifluoromethylations. J. Fluorine Chem., 128: 975-996.

Merino E. and C. Nevado. 2014. Addition of CF_3 across unsaturated moieties: a powerful functionalization tool. Chem. Soc. Rev., 43: 6598-6608.

Müller K., C. Faeh and F. Diederich. 2007. Fluorine in pharmaceuticals: looking beyond intuition. Science, 317(5846): 1881-1886.

Natarajan P. and B. König. 2021. Excited-State 2,3-Dichloro-5,6-dicyano-1,4-benzoquinone (DDQ*) Initiated Organic Synthetic Transformations under Visible-Light Irradiation. Eur. J. Org. Chem., 15: 2145-2161.

Natarajan P., A. Bala, S.K. Mehta and K.K. Bhasin. 2016. Visible-light photocatalyzed synthesis of 2-aryl N-methylpyrroles, furans and thiophenes utilizing arylsulfonyl chlorides as a coupling partner. Tetrahedron, 72: 2521-2526.

Natarajan P., D. Chuskit and Priya. 2019. Metal-free, visible-light-promoted oxidative radical cyclization of N-biarylglycine esters: one-pot construction of phenanthridine- 6-carboxylates in water. Green Chem., 21: 4406–4411.

Natarajan P., D. Chuskit, Priya and Manjeet. 2021. 9, 10-Phenanthrenedione-Catalyzed, Visible-Light-Promoted Radical Intramolecular Cyclization of N-Biarylglycine Esters: One-Pot synthesis of Phenanthridine-6-Carboxylates. ChemistrySelect, 6 (42): 11838-11844.

Natarajan P., D. Chuskit, Priya and Manjeet. 2022. Transition-metal-free synthesis of trifluoromethylated benzoxazines via a visible-light promoted tandem difunctionalization of o-vinylanilides with trifluoromethylsulfinate. New J. Chem., 46: 322-327.

Natarajan P., Manjeet, Muskan, N. K. Brar and J. J. Kaur. 2018. Visible Light Photoredox Catalysis: Conversion of Mixture of Thiophenols and Nitriles into 2-Substituted Benzothiazoles via Consecutive C-S and C-N Bonds Formation Reactions.Org. Chem. Front., 5(9): 1527-1531.

Natarajan P., Manjeet, N. Kumar, S. Devi, K. Mer. 2017. Visible-light assisted one-pot preparation of aryl glyoxals from acetoarylones via in-situ arylacyl bromides formation: Selenium-free approach to acetoarylones oxidation. Tetrahedron Lett., 58: 658–662.

Natarajan P., N. Kumar and M. Sharma. 2016. Visible light-mediated intramolecular C–H arylation of diazonium salts of N-(2-aminoaryl) benzoimines: a facile synthesis of 6-arylphenanthridines. Org. Chem. Front., 3: 1265–1270.

Natarajan P., N. Kumar and Priya. 2020. Eosin Y-Catalyzed Visible-Light-Mediated Synthesis of 2- Mercaptobenzothiazoles from 2-Azidoarenediazonium Tetrafluoroborates and Carbon Disulfide. ChemistrySelect, 5: 4862–4865.

Nicolaou K. C., D. Schlawe, D. W. Kim, D. A. Longbottom, R. G. Noronha, D. E. Lizos, R. R. Manam and D. J. Faulkner. 2005. Total Synthesis of Halipeptins: Isolation of Halipeptin D and Synthesis of Oxazoline Halipeptin Analogues. Chem. Eur. J., 11 (21): 6197–6211.

Niu H., M. Zhang, A. Li, Z. Wang, X. Wang, D. Wu and T. Su 2020. Microstructure evolution and properties of polyimide fibers containing trifluoromethyl units. High Perform. Polym., 32 (1): 39-46.

PentaA. D., A. Chiba, I. Alloza, A. Wyssenbach,T. Yamamura, P. Villoslada, S. Miyake and K. Vandenbroeck. 2013. A Trifluoromethyl Analogue of Celecoxib Exerts Beneficial Effects in Neuroinflammation. PLoS One, 8 (12): 83119.

Purser S., P. R. Moore, S. Swallow and V. Gouverneur. 2008. Fluorine in medicinal chemistry. Chem. Soc. Rev., 37: 320-330.

Rasappan R., D. Laventine, O. Reiser. 2008. Metal-bis(oxazoline) complexes: From coordination chemistry to asymmetric catalysis. Coord. Chem. Rev., 252 (5-7): 702-714.

Schlosser M. 2006. CF(3)-bearing aromatic and heterocyclic building blocks. Angew. Chem. Int. Ed., 45: 5432.

Schulz A., S. Jaksch, R. Schubel, E. Wegener, Z. Di, Y. Han, A. Meister, J. Kressler, A. V. Kabanov, R. Luxenhofer, C. M. Papadakis and R. Jordan. 2014. Drug-induced morphology switch in drug delivery systems based on poly(2-oxazoline)s. ACS Nano, 8 (3): 2686−2696.

Servinis, L., L. C. Henderson, L. M. Andrighetto, M. G. Huson, T. R. Gengenbach and B. L. Fox. 2015. A novel approach to functionalise pristine unsized carbon fibre using in situ generated diazonium species to enhance interfacial shear strength. J. Mater.Chem. A., 3: 3360-3371.

Shen Z., J. Dai, J. Xiong, X. He, W. Mo, B. Hu, N. Sun and X. Hua. 2011. 2,3-Dichloro-5,6-dicyano-1,4-benzoquinone (DDQ)/tert-Butyl Nitrite/ Oxygen: A Versatile Catalytic Oxidation System. Adv. Synth. Catal. , 353 (16): 3031-3038.

Shimizu M. and T. Hiyama. 2005. Modern Synthetic Methods for Fluorine-Substituted Target Molecules. Angew. Chem. Int. Ed., 44: 214–231.

Studer A. 2012. A “Renaissance” in Radical Trifluoromethylation. Angew. Chem. Int. Ed., 51: 8950.

T. Liang T., C. N. Neumann and T. Ritter. 2013. Introduction of fluorine and fluorine-containing functional groups. Angew. Chem. Int. Ed., 52 (32): 8214-64.

Tilvi S. and K. S. Singh. 2016. Synthesis of Oxazole, Oxazoline and Isoxazoline Derived Marine Natural Products: A Review. Curr. Org. Chem., 20 (8): 898-929.

Tomashenko O.A. and V. V. Grushin. 2011. Aromatic Trifluoromethylation with Metal Complexes. Chem. Rev., 111 (8): 4475–4521.

Wendlandt A. E. and S. S. Stahl. 2015. Quinone-Catalyzed Selective Oxidation of Organic Molecules. Angew. Chem. Int. Ed., 54 (49): 14638-14658.

Waschinski C. J. and J. C. Tiller. 2005. Poly(oxazoline)s with Telechelic Antimicrobial Functions. Biomacromolecules, 6 (1): 235–243.

Yeh V. S. C. 2004. Recent advances in the total syntheses of oxazole-containing natural products. Tetrahedron, 60: 11995–12042.

Yu J., H. Yang and H. Fua. 2014. Transition Metal-Free Trifluoromethylation of N-Allylamides with Sodium Trifluoromethanesulfinate: Synthesis of Trifluoromethyl- Containing Oxazolines. Adv. Synth. Catal., 356: 3669–3675.

Zhu W., J. Wang, S. Wang, Z. Gu, J. L. Acen˜, K. Izawa, H. Liu and V. A. Soloshonok. 2014. Recent advances in the trifluoromethylation methodology and new CF3-containing drugs. J. Fluor. Chem., 167: 37-54.

SYNTHESIS AND POTENTIAL ANTIMICROBIAL APPLICATIONS OF SILVER NANOPARTICLE-PEPTIDE CONJUGATES

Alisha Lalhall[1,2], Rohit Sharma[3], Neha Devi[2,4], Rohit K Sharma[4]* and Nishima Wangoo[2]*

[1]Centre for Nanoscience and Nanotechnology, Panjab University, Chandigarh-160014, India
[2]Department of Applied Sciences, University Institute of Engineering & Technology (U.I.E.T.), Panjab University, Chandigarh-160014, India
[3]Centre for Stem Cell and Tissue Engineering, Panjab University, Chandigarh 160014, India
[4]Department of Chemistry & Centre for Advanced Studies in Chemistry, Panjab University, Sector-14, Chandigarh-160014, India

ABSTRACT

Silver nanoparticles have attracted increasing attention in recent years for the wide range of applications such as in biomedicine, sensing, as antimicrobial agents, due to their biocompatibility, ease of synthesis, reliability, and cost effectiveness. Various synthetic methodologies have been used ranging from green synthesis to electrochemical synthesis of nanoparticles. Herein, we have synthesized biocompatible and functionalized silver nanoparticles (Ag NPs) at room temperature by sodium borohydride-mediated reduction of silver nitrate with various cationic peptides. The resulting metallic nanoparticles displayed a narrow size distribution comparable to or better than those achieved with other synthetic methods. UV-visible spectroscopy was used to monitor the formation of silver nanoparticles. Functionalized silver nanoparticles were further characterized using UV-visible spectroscopy.

Keywords: Silver nanoparticles, cationic peptides, antimicrobial agents

INTRODUCTION

Over the past few decades, the emergence of multi-drug resistance in the pathogens has become increasingly prevalent transforming into a global healthcare threat. Bacterial infections are a major cause of chronic infections and mortality, and the widespread use of broad-spectrum antibiotics has produced antibiotic resistance for many human bacterial pathogens.[1] Therefore, there is a pressing need to overcome the limitations of the conventional antibiotics. Recently, advancements in nanotechnology have led to the development of nanoparticles with unique physiochemical properties and functionalization which are strong candidates to overcome drawbacks posed by conventional antimicrobial agents[2]. For this purpose, different nanoparticles and nano-sized carrier-based formulations are being widely used as potential antimicrobials for microbial infections, including antibiotic-resistant microbes. Metallic nanoparticles, such as gold and silver, owing to their extraordinary optoelectronic and antimicrobial properties can be used as antimicrobial agents.[3] Especially silver nanoparticles (AgNPs) have been known to be extremely useful for treating microbial infections due to their small size, high water solubility, biocompatibility, and stability in physiological conditions.[4]

Biomolecule assisted synthesis and stabilization of nanoparticles has shown colossal potential application in widespread areas of research. Several methods are available for the synthesis of nanoparticles using conventional organic and inorganic reducing agents, however the usage of biological molecules is more favourable attributing to their non-toxic, non-hazardous and environment friendly capabilities.[5] In particular, peptide[6,7] and amino acid-based[8] biomolecules have been known to be a significant component of the innate immune system of a wide variety of animals, plants and microbes. Most of these compounds have demonstrated adequate antimicrobial activities. Both natural and synthetic antimicrobial peptides[9] are known to exhibit a broad spectrum of bactericidal and fungicidal actions. Based on this, many reports are available describing short peptide-based molecules that display excellent antimicrobial activities. The combined activities of naturally occurring antimicrobial peptides[10] (polymyxin B and gramicidin S) and AgNPs against microbes have resulted in the enhancement of the antimicrobial activity. An enhancement in the antimicrobial activity of various antibiotics such as penicillin G, amoxicillin, erythromycin, clindamycin, and vancomycin was observed in the presence of AgNPs.[11] Similarly, ampicillin,[12] tetracycline, and streptomycin in combination with AgNPs possess potent antimicrobial activity against both Gram-negative and Gram-positive bacteria. Taking into account the synergistic effects of biomolecule-nanoparticle conjugates and the growing significance of nanomedicine, herein, peptide conjugated AgNPs have been synthesized and

*Corresponding author: nishima.research@gmail.com
Received: May 15, 2021, Accepted: June 30, 2021

characterized by using UV–visible (UV–vis) spectroscopy and transmission electron microscopy (TEM). Further, these conjugates were evaluated for their antimicrobial efficacy against different bacterial (scheme 1).

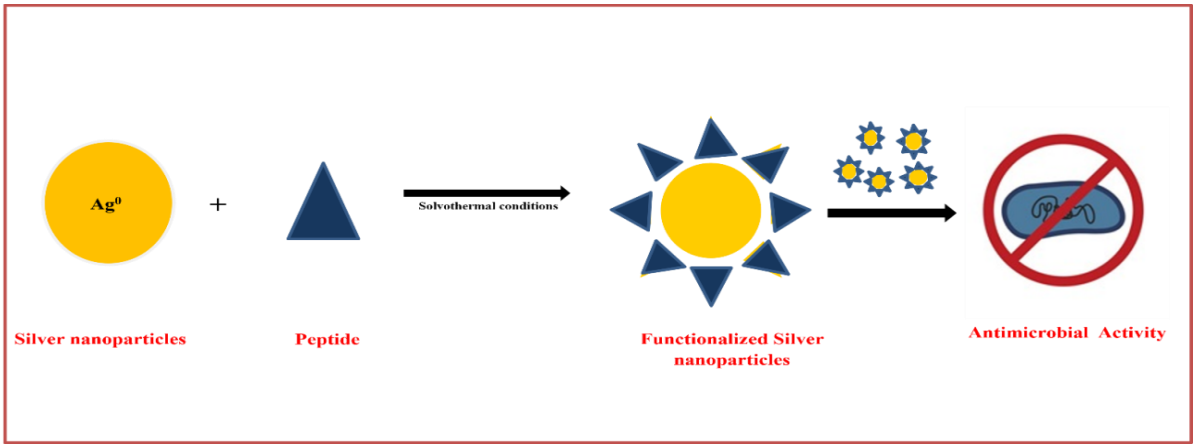

Scheme 1: Representative scheme illustrating the electrostatic conjugation of AgNPs with synthesized peptides

MATERIALS AND METHODS:

Materials:

Silver nitrate ($AgNO_3$), sodium borohydride ($NaBH_4$), tri-sodium citrate (TSC), Boc-L-His-OH, L-Arg-OMe, Boc-L-Phe-OH, L-Arg-OMe, diisopropylcarbodimide (DIC), N-hydroxy-5-norborene-2,3-dicarboximide (HONB) and hydrochloric acid (HCl) were obtained from Sigma. The DI water having resistivity of 18.2 MΩcm was used for the synthesis.

Synthesis of AgNPs:

The AgNPs were synthesized by chemical reduction method using $NaBH_4$ as reducing agent and TSC as stabilizing agent. Briefly, 0.1 ml of 100 mM $AgNO_3$ and 0.1 ml of 34 mM TSC were added to 10 ml of DI-water. Then, 0.1 ml of 2 mM $NaBH_4$ was added dropwise and the mixture was stirred for 1 hr and centrifuged at 10000 rpm for 30 min.[7] The size and morphology of synthesized AgNPs were analysed using UV–Visible spectroscopy and TEM.

Synthesis of peptides:

The peptides were synthesized using t-Butyloxycarbonyl (t-Boc) chemistry protocols using reported method [4]. Initially, commercially available Boc protected amino acid precursors (1) were coupled with amino acid methyl ester (2) of the other amino acid followed by deprotection of Boc group yield desired dipeptides (Scheme 2).

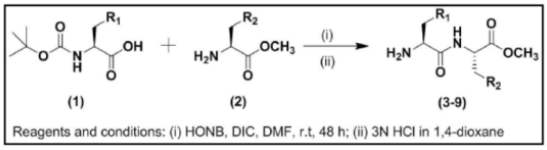

Scheme 2. Generalized scheme depicting synthesis of dipeptides

Synthesis of L-His-L-Arg-OMe:

For, the synthesis of this dipeptide, solution phase peptide synthesis protocol was adopted. The commercially available amino acid, Boc-L-His-OH (1) was coupled with L-Arg-OMe (2) in presence of HONB and DIC; using DMF as a solvent under constant stirring for 48 h at room temperature to afford Boc-L-His-L-Arg-OMe. The formation of Boc-L-His-L-Arg-OMe was confirmed by MALDI-TOF with molecular ion peak appeared at m/z 426.27 $[M+H]^+$. After that, the Boc group was removed using 3N HCl to obtain required dipeptide L-His-L-Arg-OMe (scheme 2). The crude product was purified using column chromatography in basic alumina as a stationary phase and DCM: MeOH as a solvent system. The purified cream solid dipeptide was characterized using ^{1}H-NMR spectroscopy and mass spectrometry. Similarly, in ^{1}H-NMR spectrum, a singlet at δ 7.79 and δ 6.92 was observed for aromatic protons. The two triplets at δ 4.67-4.71 and δ 3.90-3.95 indicate the presence of two α-CH protons whereas a singlet at δ 3.14 indicated the presence of OCH_3 group protons. The presence of Im-CH_2 protons was indicated by a multiplet at δ 3.39-3.42 and CH_2 protons of arginine side chain exhibited multiplets at δ 2.88-2.94, δ 1.71-1.78 and δ 1.30-1.32 respectively. The molecular ion peak at *m/z* 326.27 $[M+H]^+$ in MALDI-TOF spectrum also showed the formation of dipeptide (Figure 1a). The RP-HPLC analysis of dipeptide was performed using flow rate of 1 mL/min for 30 min at a gradient run of 95-0 % (A:B), where buffer A was 0.1% TFA in water and

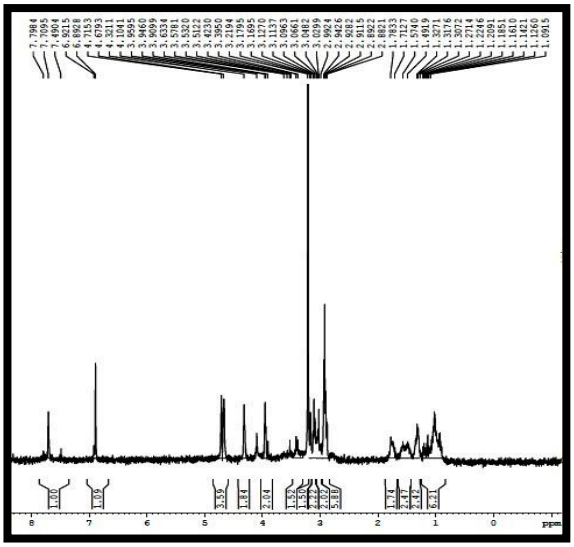

Figure 1: (a) MALDI-TOF (b) RP-HPLC of dipeptide

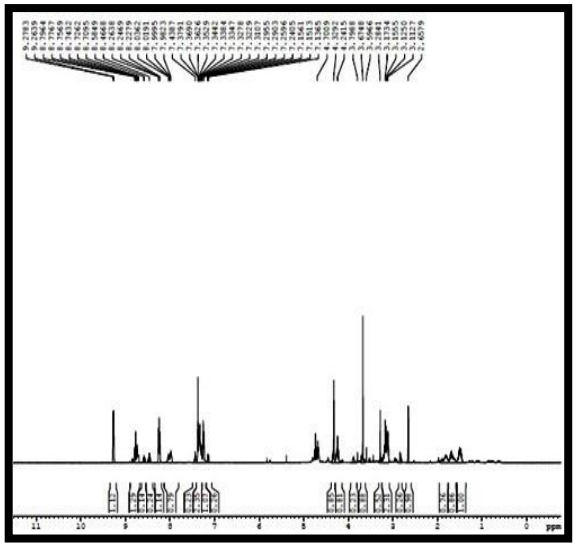

Figure 2. (a) ^{1}H-NMR (b) MALDI-TOF of dipeptide

buffer B was 0.1% TFA in CH_3CN and detection at 220 nm. The retention time of 3.039 minutes was observed in chromatogram (Figure 1b) confirming the purity of the synthesized product to be 95.37 %.

Synthesis of L-Phe-L-Arg-OMe:

The dipeptide was synthesized using solution phase peptide synthesis protocol. For this purpose, commercially available amino acid, Boc-L-Phe-*O*H (**1**) was coupled with L-Arg-*O*Me (**2**) in the presence of HONB and DIC; using DMF as a solvent under constant stirring for 48 hr at room temperature. It resulted in the formation of Boc-L-Phe-L-Arg-*O*Me which was confirmed using LC-MS with molecular ion peak observed at *m/z* 436.41 $[M+H]^+$ (Fig. 2a). Finally, the Boc group was removed using 3N HCl to obtain desired dipeptide L-Phe-L-Arg-*O*Me. The crude product was purified using column chromatography in basic alumina as a stationary phase and DCM: MeOH as a solvent system. The purified white solid dipeptide was characterized using ^{1}H-NMR spectroscopy and mass spectrometry.The ^{1}H-NMR spectrum of the dipeptide exhibited multiplets at δ 7.13-7.43 corresponded to aromatic protons of Phe and multiplets at δ 4.32 and δ 4.24 confirmed the presence of two α-CH protons. A singlet δ 3.67 indicated the presence of OCH_3 group protons and multiplets appeared at δ 3.28 which corresponded to Ph-CH_2 protons. The CH_2 protons of arginine side chain showed multiplets at δ 3.11-3.17 and δ 2.65 respectively. The molecular ion peak at *m/z* 336.33 $[M+H]^+$ in LC-MS also showed the formation of dipeptide (Figure 2b).

Synthesis of H-Lys-Lys-Lys-Arg-Arg-Arg-OH (KRKRKR peptide**)**

KRKRKR peptide was also synthesized using solid phase peptide synthesis method as shown in scheme 3. Firstly, the rink amide resin (**1**) (200 mg, 0.65 m mol/g) was taken and Fmoc group in Rink amide resin was removed using 20% piperidine in DMF for 15 min to yield free resin (**2**). The free resin (**2**) was coupled with the Fmoc-Arg(Pbf)-OH (4 eq) in the presence of TBTU (4 eq) as coupling agent and DIEA as activating reagent in DMF for 3-4 h. The Fmoc group was removed using 20% piperidine in DMF for 15 min to afford resin coupled arginine. This rotation of coupling and deprotection was repeated with Fmoc-Arg(Pbf)-OH (4eq), Fmoc-Arg(Pbf)-OH (4 eq), Fmoc-Lys(Boc)-OH (3eq), Fmoc-Lys(Boc)-OH (3eq) and Fmoc-Lys(Boc)-OH(3eq) to give the resin coupled peptides **(4), (5), (6), (7) and (8)** respectively. Finally, the resin and orthogonal protecting groups were cleaved using TFA in the presence of TIPS as scavenger and small amount of water for 3 h to get the desired peptide KKKRRR (**9**). The synthesized peptide was further characterized using MALDI-TOF. The KKKRRR peptide was purified and analyzed using HPLC. The HPLC analysis of peptide 9 showed purity of 95% (Fig. 3b). Molecular ion peak $[M^+H]^+$ for KKKRRR peptide was observed at 870 (Figure 3a) in MALDI-TOF MS.

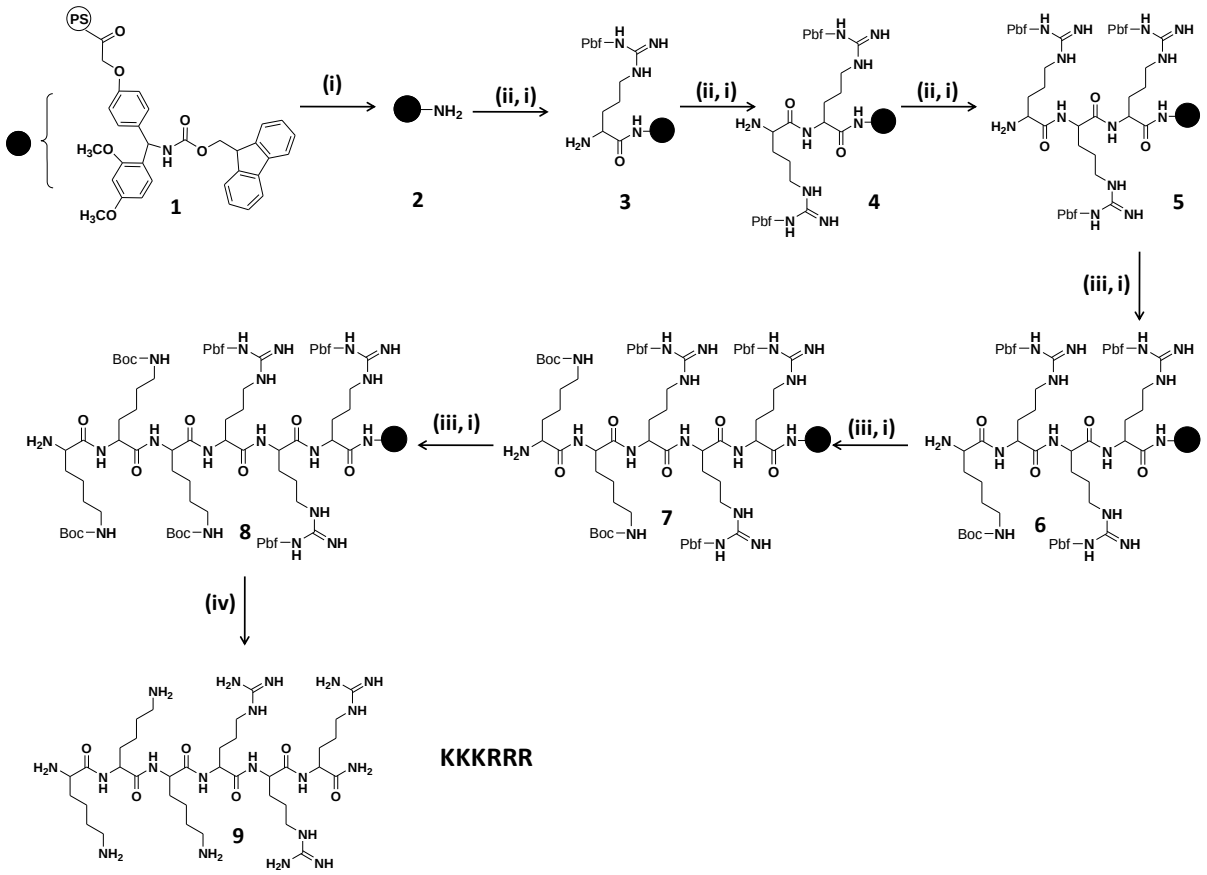

Scheme 3: SPPS based scheme KKKRRR-amide, reagents and conditions: (i) 20% piperidine in DMF,15 min; (ii) Fmoc-Arg(Pbf)-OH, TBTU, DIEA, DMF, 3h; (iii) Fmoc-Lys(Boc)-OH, TBTU, DIEA, DMF, 3h; (iv) TFA, Triisopropylsilane, water, 2.5 h

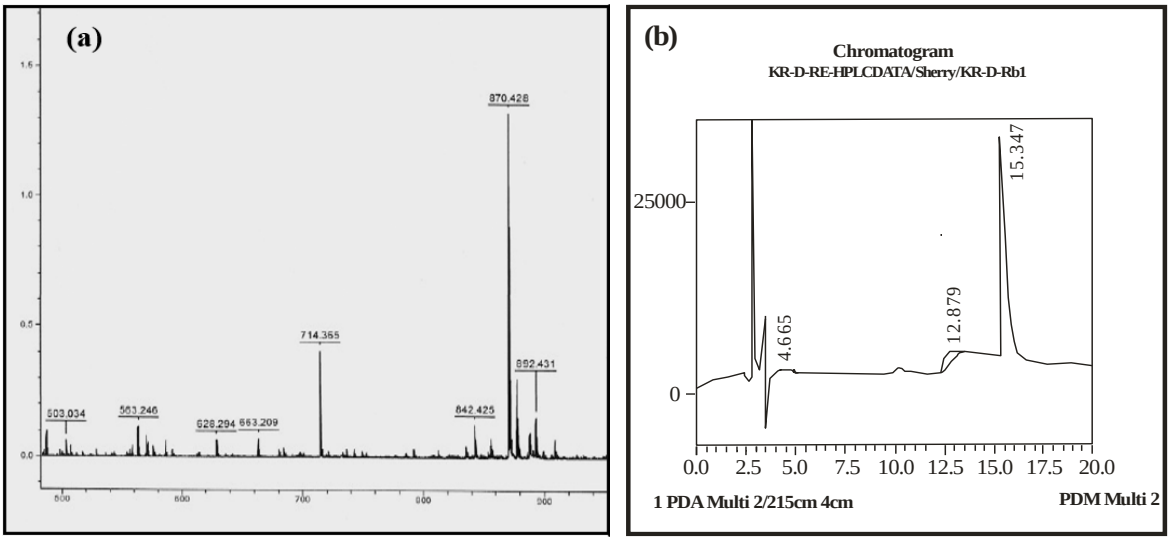

Figure 3 (a) MALDI-TOF spectrum and (b) HPLC chromatogram of synthesized KKKRRR peptide

Conjugation of the AgNPs with peptides:

Peptides-capped AgNPs were prepared by incubating AgNPs with peptides (10:1 v/v) in DI. The resulting nanoconjugates were characterized using UV–Visible spectroscopy.

Characterization of the AgNPs, peptides and peptides conjugate AgNPs

UV–Visible spectroscopy:

The optimum concentrations of peptides conjugated to AgNPs were determine using UV–Visible spectrophotometer (Jasco, V-530).

HR-TEM analysis:
The shape and size of the nanoparticles as well as nanoconjugates were analysed using HR-TEM analysis. Peptides conjugated AgNPs were prepared as described above and were observed under TEM (H-7500, Hitachi) operating at an acceleration voltage of 40 kv to 120 kv. Samples were adsorbed on carbon coated copper grid and after air drying used for analysis.

NMR and Mass spectroscopy:
The synthesized dipeptides were characterized using ^{1}H-NMR [AVANCE III 400 Bruker (400 MHz)] and mass spectrum was recorded on MAXIS-Bruker using APCI-TOF method.

HPLC:
The purity of dipeptides was checked by (HPLC) on Waters 2996 system using Supelcosil TM LC-18 column (25 cm × 4.6 mm, 5dm) run for 30 min with a flow of 1 ml/min, using a gradient of 95-0% (A:B) where buffer A was 0.1% TFA in H_2O and buffer B was 0.1% TFA in CH_3CN and detection at 220 nm.

Antimicrobial studies

Microbial strains
The two bacterial strains, *Escherichia coli* and *Staphylococcus aureus* used in the present study were procured from Microbial Culture Collection Centre (MTCC), Institute of Microbial Technology (IMTECH), Chandigarh, India. The bacterial strains were cultured in Luria broth (Hi-Media) and were freshly revived on respective agar plates from the stock before each experiment.

Antimicrobial activity

Antimicrobial activity was assessed using optical density method. Briefly, bacteria were grown overnight in Luria broth (LB), followed by 100 µl of sample treatment in respective test tubes having total volume 1000 µl. After 24 hrs of incubation along with continuous shaking at 37◦C, O.D at 600 nm was measured using the spectrophotometer. The minimum inhibitory concentration (MIC) of samples against bacterial was determined by a broth micro dilution method based on Clinical and Laboratory Standards Institute (CLSI). These bacteria were grown overnight and diluted in Luria broth (LB) to a cell density of 10^5 colony forming unit (CFU)/mL into 96-well flat-bottomed microtiter plate. Thereafter, AgNPs, dipeptides and dipeptide capped Ag-NPs (in the range of 1–100 µM) were added into the 96-well microtiter plates in respective wells. The plate was incubated at 37◦C for 24 hr. The optical density at 600 nm was measured using microplate reader. Kanamycin, a well-known standard antibacterial drug was used as a positive control.

Results and Discussions

Peptide design, synthesis and characterization
The peptides for conjugation with nanoparticles were selected on the bases of their conjugation abilities with AgNPs. For this objective, the peptides possessing positively ionizable feature(s) were expected to perform better, given their tendency to adhere to a negatively charged metallic surface. Moreover, cationic peptides are known to have comparatively better antimicrobial activity compared to the non-cationic peptides. Taking these factors into considerations, two cationic dipeptides: L-His-L-Arg-OMe and L-Phe-L-Arg-OMe were selected as these are easy to synthesize and cost effective. These peptides were synthesized using standard Boc chemistry protocols. Initially, commercially available Boc protected amino acid (**1**) was coupled with amino acid methyl ester (**2**) of the other amino acid in the presence of HONB as additive and DIC as coupling reagent in DMF as solvent to yield desired protected dipeptide followed by purification using column chromatography. At the end, the Boc group was removed under acidic condition. The crude product was purified using column chromatography and characterized using 1H NMR, mass spectrometry and HPLC.

Synthesis and characterization of citrate capped silver nanoparticles
AgNPs were synthesized by reducing silver nitrate with sodium borohydride in the presence of tri-sodium citrate as a capping agent followed by analysis using UV–vis spectroscopy (Figure 4 a). Citrate was used as the capping agent owing to its biocompatibility and ability to stabilize AgNPs. Moreover, the citrate ion has the capability to act as a cross-linker between positively charged/terminated peptides and negatively charged nanoparticles. It was observed that AgNPs displayed plasmon peak at 400 nm. During TEM analysis, the particles were observed to be spherical and monodispersed with particle diameter of 5 ± 2 nm (Figure 4b b).

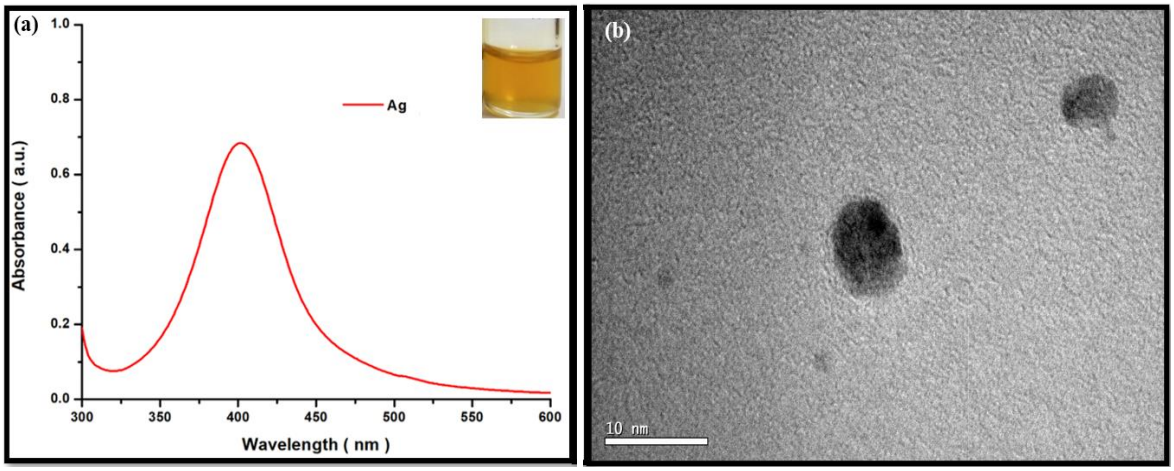

Figure 4 : (a) Absorption spectrum and (b) HR-TEM image of AgNPs

Conjugation of peptides with AgNPs

It is important to optimize the concentration of peptide for conjugation to nanoparticles, in order to prepare stable nanoparticle-peptide conjugates. For this, varying concentrations (0.1–100 M) of synthesized peptides were added individually to a colloidal suspension (1 ml) of AgNPs. The constituents were thoroughly mixed at room temperature for 24 h followed by stability analysis of AgNPs using UV–vis spectroscopy (Figure 6). It was observed that interaction between AgNPs and synthesized dipeptides progressed with visible colour changes.

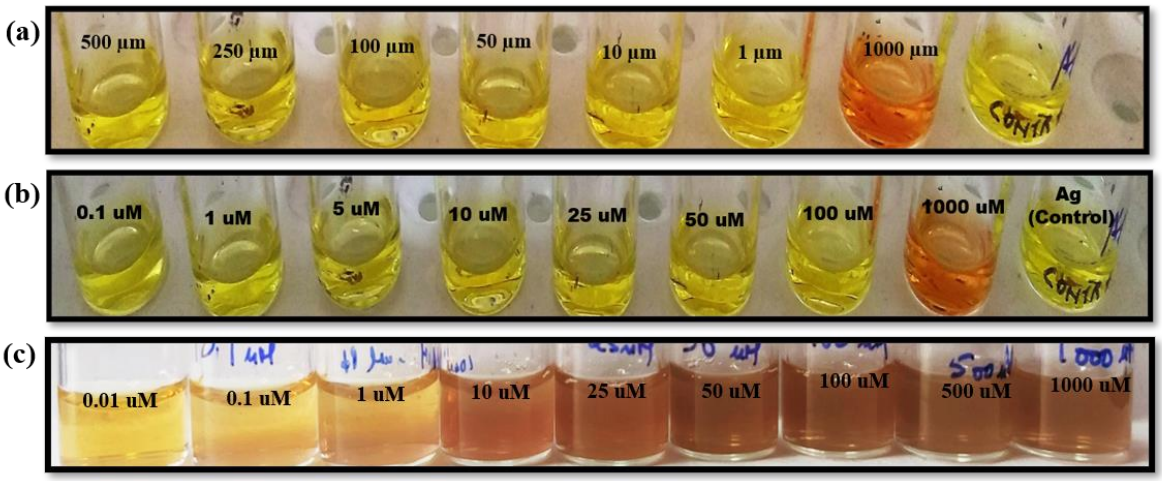

Figure 5: Various concentrations (0.01-100 µM) of (a) HR peptide (b) FR reptide (c) KRKRKR peptide in colloidal suspensions of AgNPs

AgNPs were yellow in colour, prior to the addition of peptides owing to their SPR. However, when peptides were added to AgNPs at varying concentrations (0.01–100 uM), the colour changes from yellow to brown with increasing concentrations of peptides. AgNPs with various concentrations of FR peptides was also analyzed using UV-spectroscopy as seen in fig 6. It was observed that the AgNPs are quite stable under lower concentrations probably due to the affinity of arginine towards the nanoparticle surface through side chain guanidinium group.

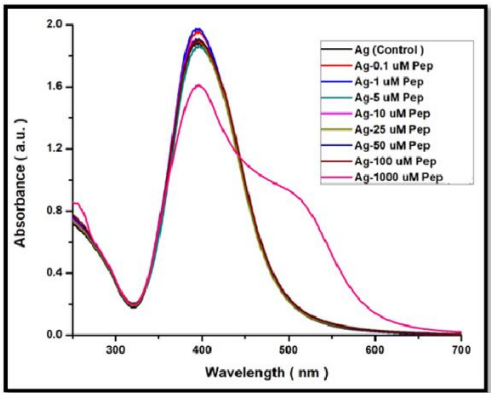

Figure 6 : UV-Vis absorption spectrum of Ag-FR conjugates at various concentrations

Antimicrobial assay

Antimicrobial activity of cationic peptides and AgNPs are well known and therefore, synthesized AgNPs peptide conjugates were further evaluated for antibacterial activity against *E. coli* and *S. aureus*. It was observed that conjugation enhances the antimicrobial property synergistically. In O.D method, it was observed that Ag-FR conjugates exhibited maximum killing, followed by Ag-HR conjugates as seen in figure 7. Even in case of MIC determination, FR conjugated AgNPs showed least concentration followed by HR conjugated AgNPs. Based on these observations, it can be stated that cationic peptide conjugated AgNPs revealed potent antimicrobial activity against tested bacterial strains, thereby opening a new dimension for using nanoparticle-based compounds as effective and novel antibacterial agents.

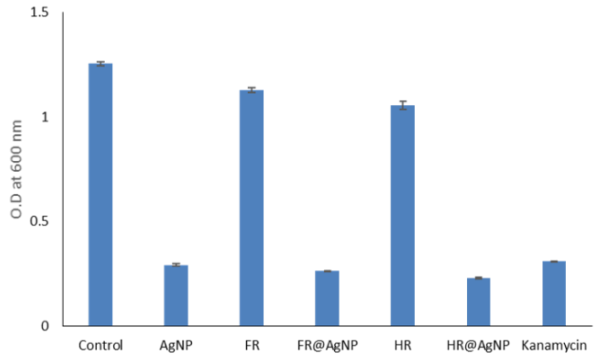

Samples	MIC for *E.coli* (µM)	MIC for *S.aureus* (µM)
AgNP	7.5	3.5
FR	40	75
HR	35	60
FR@AgNP	5	2
HR@AgNP	2.5	1.5
Kanamycin	10	15

Figure 7 : Antimicrobial assay of Ag-HR and Ag-FR conjugates

CONCLUSION

Herein, we report a simple and cost-effective approach for the conjugation of cationic peptides with AgNPs. Cationic peptides are known to possess antimicrobial characteristics and based on this and varying cationicity which is crucial for interaction with negatively charged cell membrane, these peptides were chosen. These peptides were conjugated with AgNPs and the concentration of peptides used for conjugation was optimized using UV–vis spectroscopy. Further, synthesized peptides and peptide capped AgNPs were evaluated for antimicrobial activity against two bacterial strains. It was observed that peptide capped AgNPs demonstrated slightly higher activity against tested strains as compared to alone AgNPs and native peptides. The fact that peptide-nano conjugates were prepared based on electrostatic interactions adds to the applicability of the current approach for future synthesis of antimicrobial peptides and nanoconjugates. This in turn can lead to the design and synthesis of peptide/biomolecule labelled nanostructures as efficient and novel antimicrobial agents overcoming microbial resistance and for further applications in drug delivery and bio-imaging.

ACKNOWLEDGEMENTS

Alisha Lalhall thank Technical Education Quality Improvement Programme (TEQIP-III), MHRD, and Rohit Sharma and Neha thank SERB for Senior Research Fellowship, India. The authors are also thankful to SAIF, Panjab University, Chandigarh for the characterizations. Financial support from DST-PURSE grant is also acknowledged.

REFERENCES

Gupta, A.; S. Mumtaz; C. H. Li; I. Hussain; V. M. Rotello, Combatting antibiotic-resistant bacteria using nanomaterials. *Chemical Society reviews* **2019,** *48* (2), 415-427.

Hemeg, H. A., Nanomaterials for alternative antibacterial therapy. *International journal of nanomedicine* **2017,** *12*, 8211-8225.

Shaikh, S.; N. Nazam; S. M. D. Rizvi; K. Ahmad; M. H. Baig; E. J. Lee; I. Choi, Mechanistic Insights into the Antimicrobial Actions of Metallic Nanoparticles and Their Implications for Multidrug Resistance. **2019,** *20* (10), 2468.

Rai, M. K.; S. D. Deshmukh; Ingle, A. P.; Gade, A. K., Silver nanoparticles: the powerful nanoweapon against multidrug-resistant bacteria. **2012,** *112* (5), 841-852.

Kumar, M.; R. Bala; V. S. Gondil; D. V. S. Jain,; S. Chhibber; R. K. Sharma; N. Wangoo, Efficient, Green and One Pot Synthesis of Sodium Acetate Functionalized Silver Nanoparticles and Their Potential Application as Food Preservative. *BioNanoScience* **2017,** *7* (3), 521-529.

Bajaj, M.; S. K. Pandey; T. Nain; S. K. Brar; P. Singh; S. Singh; N. Wangoo; and R. K. Sharma, Stabilized cationic dipeptide capped gold/silver nanohybrids: Towards enhanced antibacterial and antifungal efficacy. *Colloids and surfaces. B, Biointerfaces* **2017,** *158*, 397-407.

Bajaj, M.; S. K. Pandey; N. Wangoo and R. K. Sharma, Peptide Functionalized Metallic Nanoconstructs: Synthesis, Structural Characterization, and Antimicrobial Evaluation. *ACS Biomaterials Science & Engineering* **2018,** *4* (2), 739-747.

Kumar, M.; K. Bansal; V. S. Gondil; S. Sharma; D. V. S. Jain; S. Chhibber; R. K. Sharma and N. Wangoo, Synthesis, characterization, mechanistic studies and antimicrobial efficacy of biomolecule capped and pH modulated silver nanoparticles. *Journal of Molecular Liquids* **2018,** *249*, 1145-1150.

Mohanty, S.; P. Jena; R. Mehta; R. Pati; B. Banerjee; S. Patil and A. Sonawane, Cationic Antimicrobial Peptides and Biogenic Silver Nanoparticles Kill Mycobacteria without Eliciting DNA Damage and Cytotoxicity in Mouse Macrophages. **2013,** *57* (8), 3688-3698.

Berditsch, M.; T. Jäger; N. Strempel; T. Schwartz; J. Overhage; A. S. Ulrich, Synergistic effect of membrane-active peptides polymyxin B and gramicidin S on multidrug-resistant strains and biofilms of Pseudomonas aeruginosa. *Antimicrobial agents and chemotherapy* **2015,** *59* (9), 5288-96.

Kaur, A.; S. Preet; V. Kumar; R. Kumar and R. Kumar, Synergetic effect of vancomycin loaded silver nanoparticles for enhanced antibacterial activity. *Colloids and surfaces. B, Biointerfaces* **2019,** *176*, 62-69.

Khatoon, N.; H. Alam; A. Khan; K. Raza; and M. Sardar, Ampicillin Silver Nanoformulations against Multidrug resistant bacteria. *Sci Rep* **2019,** *9* (1), 6848-6848.

EFFECT OF GRAPHITIC CARBON NITRIDE (G-C_3N_4) NANOSHEET EXFOLIATION ON STRUCTURAL, MORPHOLOGICAL BEHAVIOR FOR EFFICIENT PHOTOCATALYTIC ACTIVITY

Rajender Singh[a*] and Ramesh Sharma[a]

[a]Department of Central Instrumentation Laboratory (CIL), Panjab University, Chandigarh, India-160014

ABSTRACT

In current time development of graphitic carbon nitride (g-C_3N_4) based photocatalyst through their dynamic exfoliations ways is burning area in sustainable photocatalysis. As compared to bulk g-C_3N_4, its exfoliated form shows characteristics diffraction fingerprints by X-ray diffraction (XRD) confirms its crystal structure formation. Effect of exfoliation of bulk g-C_3N_4 nanosheet has been clearly observed with nanosheet monolayer formation under HRTEM study. Exfoliated g-C_3N_4 nanosheets through delayed electron/hole recombination bring methylene dye (MB) dye (10ppm) degradation to 98.00% in 90 min. as compared to bulk g-C_3N_4 91.80% degradation under the exposure of visible light. Finally, visibly active g-C_3N_4 shown excellent photocatalytic behavior which needs further exploration to establish it as a emerging and efficient sustainable photocatalyst for future.

Keywords: Nanosheet, X-ray diffraction, Electron microscope, Dye degradation, photocatalysis

INTRODUCTION

Global rise in population of world bring alarming situation for every working sector to work for maintaining environment sustainable growth. Load on environment's maximum resources all the time for fulfillment of basic need bring challenges like global warming and climate change (Sampaio and Gonzalez 2017, Pelletier *et al.* 2019). Sustainable growth of environment cannot be progressed until environmentalist, policymakers, economist, state & federal governments collectively working to find applied solutions of social challenges (Usher 2019, Huq 2020). Day by day rising population bring rapid industrialization which brings maximum discharge of leftover into open air or water without any proper treatments. Water pollution comes out from above ill practices as a major challenge for policy makers and governments to maintain the quality and availability of water usable and drinkable. Different sectors like pharmaceutical, textiles, cosmetics, food industries are the main source for spreading water pollution in environment (Khin *et al*. 2012).

Water contamination proceed through presence of different colored dyes from textiles, pharmaceutical industries, discharge of contaminated water from effluent treatment plants (ETP) of industries without proper standard operating procedure(SOP) to open environment. To minimize and control and remove the unwanted particulate from polluted water, photocatalysis process has been found to be milestone to tackle the problem (Pelaez *et al.* 2012). In photocatalysis behavior, semiconductor feature of material has been further shows excellent properties due to their comparable band gap with respect to sunlight energy or UV-visible light region. Still there are lot of efficient semiconductor are working on photocatalysis behavior i.e. TiO_2 (Yu *et al.* 2013, Yu *et al.* 2014), ZnO (Jang *et al.* 2006), Fe_2O_3 (Cao and Zhu 2008, Zhou *et al.* 2014), $BiVO_4$ (Liu et al. 2012), CdS (Hu et al. 2013), Ta_3N_5 (Chen *et al.* 2015) etc. to remove or degrade hazaderous components present in polluted water. The basic requirements for the operation of photocatalysis behavior is maximum incident light absorption absorption ability, with maximum generated charge separation having minimum charge recombination ability bring ideal photocatalysis (Liu *et al.* 2010, Zhang *et al.* 2010a, Ismael 2020). In addition, the inclination of researchers towards photocatalysis application also due to its hydrogen generation (Wang *et al.* 2016, Maeda *et al.* 2006), hydrocarbon based fuel generation (Mao *et al.* 2013, White *et al.* 2015), ability during water splitting mechanism under exposure of appropriate light energy.

Even after the major breakthrough on photocatalysis in 1972 by Fujishima and Honda (1972) on water splitting via photocatalysis, lot of work has been performed and reported on photocatalysis behavior but still desired performance and efficiency in water splitting has not been still achieved in sustainable manner (Low *et al.* 2017, Yang *et al.* 2020). Use of carbon based materials viz. graphene, graphitic carbon nitride, fullerenes, carbon nanotubes etc. have been found very effective in different applications viz. Li ion batteries (Reddy *et al.* 2010), supercapacitors (Zhang *et al.* 2010b), biosensor

*Corresponding author: rajenderphysics@gmail.com
Received: September 15, 2021, Accepted: November 27, 2021

(Pumera 2011), fuel cell (Qu *et al.* 2010), catalysis (Zheng *et al.* 2013). Out of them graphitic carbon nitride (g-C_3N_4)(gCN), has been found most appropriate w.r.t. band gap(~2.7eV) (Lin *et al.* 2019), thermal stability (Tang *et al.* 2016), easy processing (Gao *et al.* 2017). In addition to structural properties of gCN, it can be utilized in in photocatalytic degradation of different organic dyes, antibiotics (Wen *et al.* 2017) from water. Due to structural deformities like crystalline behavior, defects states (Zhang *et al.* 2019), bring limited photo catalytic behavior. Modification in gCN properties w.r.t. their defects states, crystalline behavior, conduction ability etc. will bring efficient sustainable photocatalytic degradation behavior (Ong *et al.* 2016).

gCN can be synthesized through different precursor viz. cyanamide (Tong *et al.* 2017), dicyanamide (Liang *et al.* 2015), melamine (Shi *et al.* 2015), urea (Liu *et al.* 2015) and thiourea (Xiao *et al.* 2016) etc. In current manuscript we have studied the effect of exfoliation behavior on bulk gCN from melamine precursor for structural and morphological for photocatalytic degradation of methylene dye (MB) under visible light exposure.

EXPERIMENTAL SECTION

MATERIALS AND METHODS

All chemical used in this study were of analytical grade and used without further purification. Melamine extra pure has been purchased from loba chemie. Triple distilled water has been used in whole purification process of samples.

Synthesis

In typical synthesis process, 10.0g of melamine powder was placed in 50ml of aluminum crucible which was covered with lid and placed inside the muffle furnace. Further, sample was heated at 500°C for 4hrs, followed by cooling and grind to fine powder. The bulk sample was coded as MB. Furthermore, exfoliation of MB sample has been performed with putting 5 g MB into 50 ml of ethanol and stirred for 6hrs at 100rpm/minute. Sample obtained after exfoliation of gCN coded as MLF. Reported sample has been studied under XRD, HRTEM and dye degradation behavior.

Characterization techniques

The crystal structure of gCN samples were studied with the help of X-pert pro diffractometer (Panalytical) at λ=1.54Å. High Resolution TEM (HRTEM) Joel 2100 Plus have been used to explore ultra-structural information of synthesized gCN samples. 100Watt tungsten lamp has been used for MB dye degradation study.

RESULTS AND DISCUSSION

XRD

To investigate and authenticate the crystal structure of as synthesized gCN samples, XRD techniques have been used. Two diffraction peaks appear at 13.1°(100 plane) & 27.6°(002 plane) related with in plane repeated units and inter layer stacking unit of conjugated aromatic system respectively. Under figure 1(b) w.r.t. (002) peak exfoliated samples shows drastic of respective peak as compared to MB. This will clearly indicate formation of MB sample nanosheet based formation in MLF (Ganchang *et al.* 2019).

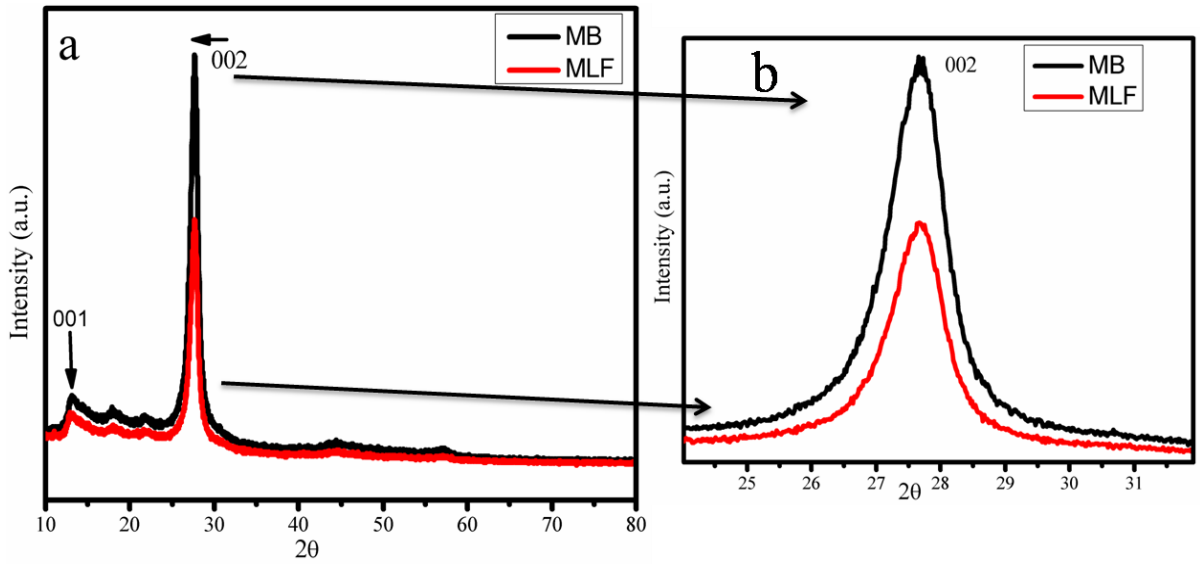

Figure 1: (a) XRD pattern of MB and MLF, (b) Zoomed view of (002) hkl peak respectively.

HRTEM

The hypothesis of gCN exfoliation as indicated in XRD diffraction has been confirmed by HRTEM technique. Figure 2(a & b) shows state of gCN sheet with its diffraction behavior. Figure 2(a) shows stacked sheets with crystalline nature through observation of dull diffraction rings in SAED study. After the uniform magnetic stirring of MB sample for 6hrs bring stacked nanosheet to maximum exfoliated nanosheet which is shown in figure 2(c). Under figure 2(d), sharp SAED pattern has been observed confirmed monolayer formation. The observation under XRD study for exfoliation of gCN has been authenticated and visualized by HRTEM figure 2 (a-d) observations, which can be utilized in coming applications (Ganchang *et al.* 2019).

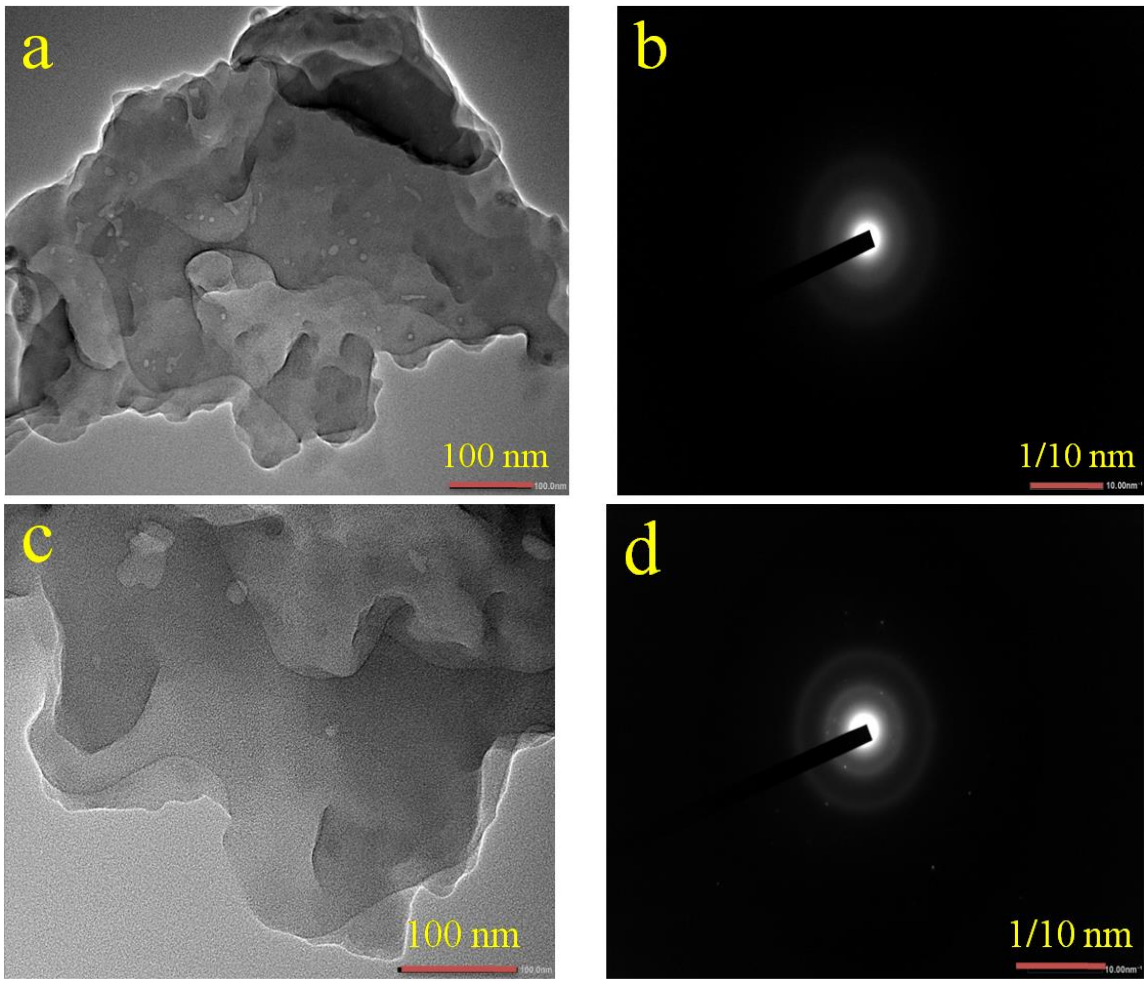

Figure 2: (a) HRTEM image of MB, (b) its SAED pattern,(c) HRTEM image of MLF, (d) its SAED pattern respectively.

MB dye degradation

After proper investigation of gCN material for structural and morphological properties, its application has been extended to methylene blue (MB) dye degradation behavior. 10ppm MB dye degradation behavior has been studied under 100 watt W lamp for 90 minutes exposure with 30 mg of nanoparticles (NPs). Before studying the photocatalytic behavior of semiconducting features based gCN, adsorption behavior has been studied for 60 minutes in dark environment, which was ~33.30%. The drastic adsorption % has been observed may be due to maximum availability of adsorbing and porous sites of studied bulk sample.

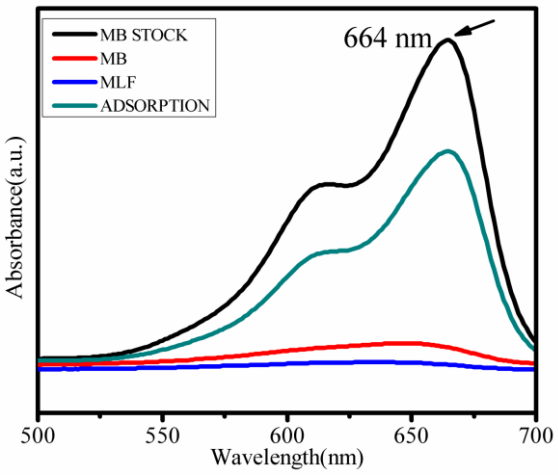

After 90 minute of adsorption observation, two sample set up one with MB sample i.e. 30mg NPs in 50 ml of 10ppm dye and second with sample amount of MLF NPs in 50ml of dye. Both beaker were placed in inside the 100Watt W lamp for 90 min with uniform stirring. After 90 minute of reaction, sample was collected, filtered and analyzed under UV-Vis spectrophotometer. MB sample have degraded dye to 91.80% in 90 minutes whereas MLF sample shows 98.00% degradation in same time. Nearly, 7% enhanced degradation behavior of gCN against MB dye has been observed may be due to maximum electron/hole recombination delay with maximum incident light absorption ability features. Through these conditions, maximum dye degrading species viz. OH°, O_2° etc. get generated during whole photocatalysis process (Zhao *et al.* 2015, Xia *et al*. 2017). Finally, plenty of latent aspect through visible light active photocatalysis stiil needs to explored for coming future. This approach will enhance the applicability of photocatalysis in sustainable growth of environment.

CONCLUSION

In current manuscript, we have reported thermal polycondensation method based synthesis of gCN for visible dominated MB dye degradation behavior. Reported NPs has been authenticated with XRD for its crystal structure formation. Further, initial proposed hypothesis of exfoliated nanosheet formation from MB sheets has been demonstrated and confirmed by HRTEM analysis. One of major organic pollutants i.e. MB dye has been degraded through exfoliated gCN under visible light exposure to 98% in 90 min. It will bring environment to minimum hazard, and metal free nature have propose researcher for a better substitute in photocatalysis applications in comparison to existing options in related area.

ACKNOWLEDGEMENT

The author would like to thank SAIF, Panjab University, Chandigarh for providing different characterization (XRD, FESEM) facilities

Conflict of interest: There is no conflict of interest in this study.

REFERENCES

Cao, S. W., and Y. J. Zhu. 2008. Hierarchically Nanostructured α-Fe_2O_3 Hollow Spheres: Preparation, Growth Mechanism, Photocatalytic Property and Application in Water Treatment. J. Phys. Chem. C 112: 6253-6257.

Chen, S., S. Shen, G. Liu, Y. Qi, F. Zhang and C. Li, Angew. 2015. Interface Engineering of a CoO_x/Ta_3N_5 Photocatalyst for Unprecedented Water Oxidation Performance under Visible-Light-Irradiation‡. Chem. Int. Ed. 54: 3047- 3051.

Fujishima A. and K. Honda. 1972. Electrochemical Photolysis of Water at a Semiconductor Electrode, Nature 238: 37-38.

Gao, J., Wang Y, Zhou S, Lin W, Kong Y. 2017. A Facile One-Step Synthesis of Fe-Doped g-C_3N_4 Nanosheets and Their Improved Visible-Light Photocatalytic Performance. Chem Cat Chem 2017, 9:1708-1715.

Hu, Y., X. Gao, L. Yu, Y. Wang, J. Ning, S. Xu and X. W. D. Lou. 2013. Highly Photoluminescent Carbon Dots for Multicolor Patterning, Sensors, and Bioimaging‡. Angewandte Chemie 125: 5746-5749.

Huq, M., 2020. Science, Technology and Development: North-South Co-operation, Routledge, New York.

Ismael, M., 2020. The photocatalytic performance of the ZnO/g-C_3N_4 composite photocatalyst toward degradation of organic pollutants and its inactivity toward hydrogen evolution: The influence of light irradiation and charge transfer, Chem. Phys. Lett. 739: 136992 (10 pages).

Jang, E. S., J. H. Won, S. J. Hwang and J. H. Choy. 2006. Fine Tuning of the Face Orientation of ZnO Crystals to Optimize Their Photocatalytic Activity. Adv. Mater. 18: 3309-3312.

Khin, M. M., A. S. Nair, V. J. Babu, R. Murugan, and S. Ramakrishna. 2012. A review on nanomaterials for environmental remediation. Energy Environ. Sci. 5: 8075-8109.

Lei, G., Y. Cao, W. Zhao, Z. Dai, L. Shen,, Y. Xiao and L. Jian. 2019. Exfoliation of Graphitic Carbon Nitride for Enhanced Oxidative Desulfurization: A Facile and General Strategy, ACS Sustainable Chem. Eng. 7: 4941−4950.

Liang, Q., Z. Li, Z.-H. Huang, F. Kang, Q.-H. Yang. 2015. Holey Graphitic Carbon Nitride

Nanosheets with Carbon Vacancies for Highly Improved Photocatalytic Hydrogen Production. Adv. Funct. Mater. 25: 6885.

Lin W, Lu K, Zhou S, Wang J, Mu F, Wang Y, Wu Y, Kong Y. Appl Surf Sci 2019,474:194-202.

Liu, G., L.Z. Wang, H.G. Yang, H.M. Cheng, G.Q. Lu. 2010. Titania-based photocatalysts—crystal growth, doping and heterostructuring. J. Mater. Chem. 20: 831-843.

Liu, S., K. Yin, W. Ren, B. Cheng and J. Yu. 2012. Tandem photocatalytic oxidation of Rhodamine B over surface fluorinated bismuth vanadate crystals. J. Mater. Chem. 22: 17759-17767.

Liu, J. , W. Li, L. Duan, X. Li, L. Ji, Z. Geng, K. Huang, L. Lu,L. Zhou, Z. Liu, W. Chen, L. Liu, S. Feng, Y. Zhang. 2015. A Graphene-like Oxygenated Carbon Nitride Material for Improved Cycle-Life Lithium/Sulfur Batteries. Nano Lett. 15: 5137-5142.

Low, J., C. Jiang, B. Cheng, S. Wageh, A. A. Al-Ghamdi, J. Yu. 2017. A Review of Direct Z-Scheme Photocatalysts, Small Methods 1:1700080.

Maeda, K., K. Teramura, D. Lu, T. Takata, N. Saito, Y. Inoue and K. Domen. 2006. Photocatalyst releasing hydrogen from water, Nature, 440: 295-295.

Mao, J., K. Li and T. Peng. 2013. Recent advances in the photocatalytic CO_2 reduction over semiconductors. Catal. Sci. Tech. 3: 2481-2498.

Ong, W. J., L. L. Tan, Y. H. Ng, S. T. Yong, S. P. Chai. 2016. Graphitic Carbon Nitride (g-C_3N_4)-Based Photocatalysts for Artificial Photosynthesis and Environmental Remediation: Are We a Step Closer To Achieving Sustainability?. Chem Rev 116:7159-7329.

Pelaez, M., N. T. Nolan, S. C. Pillai, M. K. Seery, P. Falaras, A. G. Kontos, P. S. M. Dunlop, J. W. J. Hamilton, J. A. Byrne, K. Oshea, M. H. Entezari, D. D. Dionysiou. 2012. A review on the visible light active titanium dioxide photocatalysts for environmental applications. Appl. Catal. B Environ. 125 331-349.

Pelletier, C., Y. Rogaume, L. Dieckhoff, G. Bardeau, M. N. Pons, A. Dufour. 2019. Effect of combustion technology and biogenic CO_2 impact factor on global warming potential of wood-to-heat chains. Appl. Energy 235: 1381–1388.

Pumera, M. 2011. Graphene-based nanomaterials for energy storage. Energy Environ. Sci. 4: 668-674.

Qu, L., Y. Liu, J. -B. Baek, L. Dai, 2010. Nitrogen-Doped Graphene as Efficient Metal-Free Electrocatalyst for Oxygen Reduction in Fuel Cells, ACS Nano 4: 1321-1326.

Reddy, A. L. M., A. Srivastava, S. R. Gowda, H. Gullapalli, M. Dubey, P. M. Ajayan. 2010. Synthesis of nitrogen-doped graphene films for lithium battery application, ACS Nano 4: 6337-6342.

Sampaio, P. G. V., M. O. A. Gonzalez. 2017. Photovoltaic solar energy: Conceptual framework. Renew. Sust. Energy Rev. 74: 590-601.

Shi, L., T. Wang, H. Zhang, K. Chang, J. Ye. 2015. Electrostatic Self-Assembly of Nanosized Carbon Nitride Nanosheet onto a Zirconium Metal–Organic Framework for Enhanced Photocatalytic CO_2 Reduction. Adv. Funct. Mater. 25: 5360.

Tang, H., S. Chang, L. Jiang, G. Tang, W. Liang. 2016. Novel spindle-shaped nanoporous TiO_2 coupled graphitic g-C_3N_4 nanosheets with enhanced visible-light photocatalytic activity. Ceram. Int. 2016,42:18443–52.

Tong, Z., D. Yang, Z. Li, Y. Nan, F. Ding, Y. Shen, Z. Jiang. 2017. Thylakoid-Inspired Multishell g-C_3 N_4 Nanocapsules with Enhanced Visible-Light Harvesting and Electron Transfer Properties for High-Efficiency Photocatalysis. ACS Nano 11: 1103-1112.

Usher, B. 2019. Renewable Energy: A Primer for the Twenty-First Century, Columbia University Press: New York.

Wang, Q., T. Hisatomi, Q. Jia, H. Tokudome, M. Zhong, C. Wang, Z. Pan, T. Takata, M. Nakabayashi, N. Shibata, Yanbo Li, Ian D. Sharp, A. Kudo, T. Yamada, K. Domen. Scalable water splitting on particulate photocatalyst sheets with a solar-to-hydrogen energy conversion efficiency exceeding 1. 2016. Nat. Mater. 15(6): 611-615.

Wen, J., J. Xie, X. Chen, X. Li. 2017. A review on g-C_3N_4-based photocatalysts. Appl Surf Sci 391:72- 123.

White, J. L., M. F. Baruch, J. E. Pander III, Y. Hu, I. C. Fortmeyer, J. E. Park, T. Zhang, K. Liao, J. Gu and Y. Yan. 2015. Light-Driven Heterogeneous Reduction of Carbon Dioxide: Photocatalysts and Photoelectrodes, Chem. Rev. 115: 12888-12935.

Xia P., B. Zhu, Y. Jiaguou, C. Shaowen and M. Jaroniec. 2017. Ultra-thin nanosheet assemblies of graphitic carbon nitride for enhanced photocatalytic CO_2 reduction. J. Mater. Chem. A 5: 3230-3238.

Xiao, J., Y. Xie, F. Nawaz, Y. Wang, P. Du, H. Cao, 2016. Dramatic coupling of visible light with ozone on honeycomb-like porous g-C_3N_4 towards superior oxidation of water pollutants. Appl. Catal. B Environ. 183: 417-425.

Yang, C., R. Li, K. Zhang, W. Lin, K. Landfester, X. Wang. 2020. Heterogeneous photoredox flow chemistry for the scalable organosynthesis of fine chemicals. Nat. Commun. 11: 1-8.

Yu, J., Q. Li, S. Liu and M. Jaroniec. 2013. Ionic-Liquid-Assisted Synthesis of Uniform Fluorinated B/C-Codoped TiO_2 Nanocrystals and Their Enhanced Visible-Light Photocatalytic Activity. Chem. Eur. J. 19: 2433-2441.

Yu, J., J. Low, W. Xiao, P. Zhou and M. Jaroniec. 2014. Enhanced Photocatalytic CO_2-Reduction Activity of Anatase TiO_2 by Coexposed {001} and {101} Facets. J. Am. Chem. Soc. 136: 8839-8842.

Zhang, D. Q., G. S. Li, J. C. Yu. 2010a. Inorganic materials for photocatalytic water disinfection. J. Mater. Chem. 20: 4529-4536.

Zhang, L. L., Zhou, R., Zhao, X. S. J. 2010b. Graphene-based materials as supercapacitor electrodes, J. Mater. Chem. 20: 5983-5992.

Zhang, S., P. Gu, R. Ma, C. Luo, T. Wen, G. Zhao, W. Cheng, X. Wang. 2019. Recent developments in fabrication and structure regulation of visible-light-driven g-C_3N_4-based photocatalysts towards water purification: A critical review. XCatal Today 335: 65–77.

Zhao, Z., Y. Sun, F. Dong, Y. Zhang and H. Zhao. 2015. Template synthesis of carbon self-doped g-C_3N_4 with enhanced visible to near-infrared absorption and photocatalytic performance. RSC Adv. 5: 39549-39556.

Zheng, Y., Jiao, Y., Ge, L., Jaroniec, M., Qiao, S. Z. 2013. Two-Step Boron and Nitrogen Doping in Graphene for Enhanced Synergistic Catalysis. Angew. Chem. 125: 3192–3198.

Zhou, X., Q. Xu, W. Lei, T. Zhang, X. Qi, G. Liu, K. Deng and J. Yu. 2014. Effects of the preparation method on the structure and the visible-light photocatalytic activity of Ag_2CrO_4.Small 10: 674-679.

INSIGHTS INTO MUSHROOM POLYSACCHARIDE AND THEIR POTENTIAL APPLICATIONS

Navdha Sharma, Ekta Chaudhary, Harpreet Kaur, Aruna Singh Parmar, Maninderjeet Kaur, Devender Kumar Sharma and Deepak K. Rahi

Affiliation: Department of Microbiology, Panjab University, Chandigarh – 160014, India

ABSTRACT

Mushrooms have been eaten and valued for many years for their nutritious value and medicinal properties. More than 2000 species of mushrooms have been identified so far which are widely known for their health promoting benefits. These health promoting benefits are attributed to a variety of bioactive compounds produced by them which include polysaccharides, unsaturated fatty acids, proteins, mineral substances, terpenoids, sterols, and other secondary metabolites etc. which have been more recently isolated from different type of mushrooms. Of all these compounds polysaccharide is considered to be one of the major groups which has found huge applicability in various fields. The extracellular, intracellular, or the cell wall polysaccharides produced by the mushrooms are known to exhibit immuno-stimulating, antitumor, antimicrobial, anti-inflammatory, antioxidant, prebiotic, hypoglycemic, and hypo-cholesterolemic effects. However, their application in fields apart from the pharmaceutical applications is still at an early stage. So, here an inclusive and illustrative review is given on mushroom polysaccharides. The goal of this review is to provide thoroughly restructured information on the development, extraction and purification of mushroom polysaccharides, their structural characteristics, their biological structure and their industrial applications.

Key-words: Exopolysaccharide, Anti-oxidant, Immuno-stimulating, Antimicrobial, Nutraceuticals

INTRODUCTION

The most important building blocks are naturally occurring and well distributed carbohydrates. These organic compounds of evolutionary and biological significance take various forms on the earth. Carbohydrates are categorized into three classes according to the number of sugar units into monosaccharide, oligosaccharides and polysaccharides. Natural macromolecules consisting of multiple monosaccharide units (more than ten) are classified as polysaccharides and are metabolized for various purposes at various stages of each living organism's life cycle. The polysaccharide monosaccharide units are linked by an acetal linkage to each other. Polysaccharides have different monomeric sequences and furthermore varying glycosidic linkages including various branching forms. In water, they might maybe amorphous and immiscible. Every one of these point together give polysaccharides an extraordinary variety of structure, property, and capacities (Sutherland, 1996). Polysaccharides utilized at the modern level are practically the entirety of plant and kelp starting point. These long-chain and high sub-atomic weight polymers, for example, starch, alginate, Arabic gum, carrageenan, agar, and gaur gum, are generally utilized in the food, drug, and restorative ventures (Roller and Dea, 1992; Wang and McNeil, 1996; Manzi *et al*., 2000). Interestingly, microorganisms are known for their capacity to metabolize various structural complexities of polysaccharides (Seviour *et al*., 1992; Sutherland, 1994). These polysaccharides remain either bound to the exterior of the cell or are found in the outer membrane (Banik *et al*., 2000). 200 years back Henri Braconnot found chitin, first sugar polymer from consumable mushrooms yet polymer research doesn't stand out enough to be noticed like genomes and proteins (Muzzarelli *et al*., 2012; Mahapatra and Banerjee, 2012). Exploration in glycoscience particularly fungal exopolysaccharide (EPS) had broadly been expanding throughout the previous years because of their various uses in both medicines, pharmacy, (Lee *et al*., 1996; Lee *et al*., 2003; Muzzarelli *et al*., 2012) business for example, thickening and stabilizing for instance immunostimulating agents (Lee *et al*., 2003) and antitumor specialists part of different beauty care products (Czop and Kay, 1991) ,immunotherapeutic specialist for malignancy treatment, (Lee *et al*., 2003) and anti-anemics (Podkolzin *et al*., 1996). The EPS from fungi has been extensively explored over the last two generations. There have been reports of various EPS development through submerged species including *Ganoderma lucidum, Agaricus Blazei, Cordyceps* sp., *Lentinus edodes*, and *Grifola frondosa* all of which have different and fascinating biological activities (Yang and He, 2008).

STRUCTURE AND BIOLOGICAL ACTIVITY

Natural polymers which are present in all living organisms are polysaccharides. More than 75% of carbohydrates, including primarily glucans and mannans can consist of these molecules, located

*Corresponding author: deepakraahi10@gmail.com
Received: August 18, 2021, Accepted: October 30, 2021

mainly in the cell wall of fungi. Some polysaccharides form an extracellular sheath around the mycelium and facilitate the adhesion of lignin- degrading enzymes, an indirect source of hydrogen peroxide, in addition to protecting the cells from dehydration, serving as a support factor for the hyphae (Da Silva *et al*., 2006). The entire complex of a polysaccharide is described by its sugar composition, the glycoside bond arrangement, the monosaccharide series, the length of the chain, as well as the nature, amount, and number of the polysaccharides and the position of classes of non-carbohydrates attached. In addition, monosaccharide polymerization may take place at various sugar unit locations, creating a wide range of linear or branched chains with high structural variation and various functions (Da Silva *et al*., 2006; Hu *et al*., 2013). Depending on the composition of its components, molecular mass and inter and intra- chain reactions, the secondary structures of the molecule can also differ (Paulsen, 2002). The structural diversity of polysaccharides is also supported by modification process, such as sulfation, which occurs naturally in marine organisms and in the extracellular matrix of vertebrates (Kirkwood, 1974). The formation of polysaccharides is linked to species and strain and is associated with several different factors, such as collection location and time, life cycle phase, cultivation process, isolation and drying. Throughout this, the classification of polysaccharides is important to ensure their effectiveness and protection and because of its complexity, is a concern for industrial processing. (Hu *et al*., 2013; Giavasis, 2014).

FUNGAL EXOPOLYSACCHARIDES SOURCES

Fungi are hypothetically viewed as superior reservoirs of various polysaccharides based on their structural and cellular complexities. In the past, mushrooms and endophytic fungi were used as reliable sources of useful industrial exopolysaccharides (Sood *et al*., 2013; Orlandelli *et al*., 2016). *Phellinus linteus* (medicinal mushroom), *Fusarium* sp., *Ganoderma lucidium, Pleurotus* sp., (Oyster mushroom) and *Inonotus obliquus* (Chaga mushroom) are the examples of the wide variety of fungi that have been studied for exopolysaccharides (Guo *et al*., 2013; Smiderle *et al*., 2012; Xiang *et al*., 2012; Hwang *et al*., 2003). The EPS, especially the β-(1,3) and (1,6) glucans can be excreted by several fungal species, for its chemical structure, two major fungal neutral extracellular Homopolysaccharides, called scleroglucan and schizophyllan, are widely studied, closely resembling the curdlan and lentinan backbone.

Pleurotus: In comparison with other restorative mushrooms occurring in an upsurge the past two decades, *Pleurotus* is becoming more relevant as a well-being promoter and environmental restorer. *Ganoderma* is number one in the world of restorative mushrooms and was regarded as the ruler of restorative mushrooms taken after *Lentinula* and others counting *Pleurotus*, after which oyster mushrooms are made. In addition, fruiting bodies and complex *Pleurotus* mycelia have a range of therapeutic properties, such as anti-inflammatory, immunostimulatory, immunomodulatory (Wang *et al*., 2000), anti-cancer action (Wasser *et al*., 2000; Tzaniabos, 2000) and several other exercises. *Pleurotus* species have a place to send oyster-formed mushrooms (basidiocarps) to the phylum *Basidiomycota* and have been referred to as oyster mushrooms in the same way (OM). In addition, OM appreciates worldwide transport from temperate to tropical districts growing saprophytic species and has a variety of therapeutic species at a temperature range of 12-32 °C. On various kinds of lignocellulosic, un-composted agro-squanders, *Pleurotus* species grows and generates OM rich in high-esteem proteins, vitamins and minerals; OM produces unusually lower quantities of carbohydrates, sugars and cholesterol (Waseer *et al*., 2009). OM has been investigated to fight *Escherichia coli, Staphylococcus epidermidis*, *S. aureus* and various drug resistant isolates (Akyuz *et al*., 2010) such as *Streptococcus, Enterococcus* and *Candida* species (Kotra *et al*., 1998; Morschhäuser *et al*., 2000; Sandven, 2000; Thomson and E.S, 2000).

DIFFERENT POLYSACCHARIDES PRODUCED BY MUSHROOMS

Lentinan: Lentinan is a β-(1→3), β-(1→6)-D-glucan (Figure 1) with viable antitumor and immunopotentiating activity supplied from the fruiting bodies of Shiitake mushroom *Lentinus edodes* (Vannucci *et al*., 2013). Since 1985, Lentinan has been Japan's key reported mushroom polysaccharide for therapeutic use as an immune adjuvant to chemotherapy for the treatment of stomach cancer in Japan (Higashi *et al*., 2012). An antitumor sedate, Lentinan, hinders tumor growth by invigorating the immune structure, but is rather non-toxic to tumor cells. (Chihara *et al*., 1970; Chihara, 1978). In the arrangement of 400,000-1, daltons, the atomic weight of lentinan is particularly massive. (1→3)-β-glucan may be its basic structure featuring

five (1→3)-β-glucose buildups in a direct association and two (1→6)-β-glucopyranoside branching in side chains, resulting in a triple helical structure of the right hand (Chihara, 1992). Lentinan extraction can be categorized into two main forms more often than not: one could be a dissolvable form of extraction, using hot water, soluble base arrangement, and polyethylene glycol; and the other could use ultrasonic or ultra-high weight to eliminate the polysaccharides (Chihara *et al*., 1969, 1970). Lentinan seem to have an unmistakable anti-tumor activity against allogeneic tumors, such as sarcoma 180, but also against various synergistic and autochthonous tumors. It recognizes chemical and viral oncogenesis and also suppresses and repeats cancer metastasis in creature models. (Zakany *et al*., 1980; Suga *et al*., 1984). In addition, Lentinan is able to restore the smothered behavior of helper T-cells inside the tumor-bearing state to their normal state, leading to complete restoration of healthy humoral reactions (Maeda *et al*., 1988). With the antitumor movement of lentinan inside the tumor-bearing mice, the lentinan-induced delayed type hypersensitivity reaction is accurate (Suzuki *et al*., 1994). It is suggested that the delayed-type contact reaction triggered by lentinan at the tumor sites and the consequent invasion into the tumor burden of resistant effector cells, such as natural executioner cells and cytotoxic T-lymphocytes, are essential mechanisms of lentinan antitumor operation. Lentinan's antitumor operation demands an intact T-cell component and a thymus-dependent safe instrument intercedes with this antitumor motion.

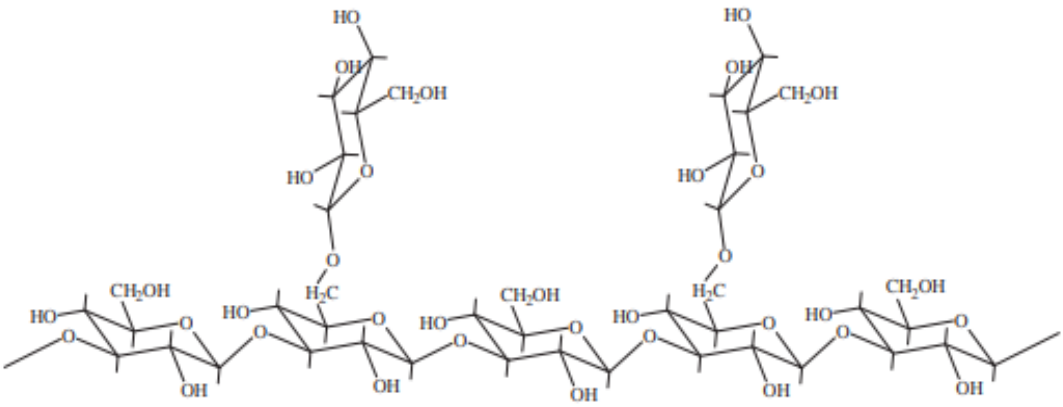

Figure 1: Repeating unit of lentinan
Source: (Zhang et al., 2008b)

Scleroglucan is a neutral homopolymer that is soluble in water and composed of branching consisting of (1,3)-linked units of β-D-glucopyranosyl with β-D-glucosyl linked to each third unit of β-D-glucosyl (1,6) synthesized by the fungus *Sclerotium*. Halleck first stimulated the explanation and interest of these polysaccharides in 1967 (Halleck, 1967). Rather, scleroglucan disperses quickly at ambient temperature in water due to the presence of groups of 1,6-β-D-glucopyranosyls that increase solubilization of the polysaccharide and the capacity to form gels decreases (Sandford 1979; Moresi *et al*. 2001). It has been used mostly for various industrial applications (Halleck, 1972; Doster *et al*., 1984). Scleroglucan chains presume that there is a triple helical rod-like structure Composition (Yanaki et al. 1981; Yanaki and Norisuye 1983; Palleschi et al. 2005). The intra- and intermolecular hydrogen bonds stabilize the triple helix structure and show strong stability over a broad temperature range. Scleroglucan has a variety of fascinating properties by way of its structure and high molecular weight. Scleroglucan has several industrial uses, but it has been initially used for moistening in the oil industry, discharge of drilling muds and improved recovery of oil, which shows greater performance and stability compared to other polymers (Davison and Mentzer 1982; Doster et al., 1984; Pirri 1996; Johnson 1996). It is used in paintings as a thickener, stabilizer in fire drencher foams and in agricultural as pesticides (Sieber et al. 2005). Scleroglucan will be perfectly acceptable in the food industry for the stabilisation of ice creams and dressings. In gastroenterology or as an antitumor, antiviral and antimicrobial agent, laxative as tablet coatings it also displays some interesting pharmacological properties (Singh *et al*., 1974; Pret *et al*., 1991; Mastromarino *et al*., 1997; Duc 1982).

Schizophyllan is a neutral polysaccharide made up of a (1, 3)-β-D- linked glucose residue backbone with (1, 6)-β-D glucosyl side groups formed by

processed mycelia branches excreted by the fungus *Schizophyllan commune*. Schizophyllan (also called sizofiran) is comparable to lentinan. It contains a lower atomic weight compared to lentin (within a range of 100–200 kDa) and offers triple helical compliance. The whole polymer is shown to be a novel potential candidate for the carrier of anti sense oligonucleotides when chemically modified with different functional groups, such as polyethylene glycol, (Karinaga *et al*., 2005) spermine, octa arginine. Both schizophyllan and lentinan are immunotherapeutic glucans that have been used clinically for cancer care since 1986, typically in conjunction with traditional cancer therapies. Schizophyllum is popular and has numerous potential applications, such as oil recovery, remediation thickener, oxygen-impermeable food-preservation films, and high-value pharmaceutical applications. It can restore mitosis in bone marrow cells that are suppressed by antitumour drugs (Zhu, 1987). Schizophyllan is a T-cell-oriented immunopotentiator and therefore needs a functional T-cell therapeutic portion for its natural action and this can increase helper T cell production; macrophage production in immune system of human body and can increase non-immunological tolerance in host body. Schizophyllan, which was administered alongside antineoplastic medications, tended to increase the lifespan of patients with lung, gastric or cervical cancer (Furue, 1987; Wasser, 2002).

Pulluan is one of the most widespread and well-studied fungal polysaccharides and is synthesized by the polymorphic fungus *Aureobasidium* in the family of alpha D- glucans in a number of liquid fermentation systems, pullulans are made up of linear alpha (1,6) interactions between the molecules of maltotriose and maltotetraose. Pullulan is a white, tasteless, water soluble glucose homopolymer. Even in the presence of ions, the pullulan has very high solubility in water. This polymer is used mainly for food processing in Japan and can be mixed into nylon- like and polystyrene – like fibres and also have an application in cosmetics, pharmaceuticals etc. (Vandamme *et al*., 1996). Pullulan has been suggested as a replacement for starch in solid and liquid food, in particular pasta and heated goods, where it improves food quality, dampness and gas maintenance and dispersibility. It has been associated as a dietary fibre and as a prebiotic to advance the growth of *Bifidobacterium* spp. leading to its halfway degradation of toxic short-chain oligomers by human salivary amylase (Okada *et al*., 1990; Singh *et al*., 2008; Cheng *et al*., 2011). Pullulan can also frame oil-resistant, water-soluble, scentless, lean and clear films with low oxygen permeability that can serve as edible food coatings that drive life forward (Leathers, 2003; Gounga *et al*., 2008; Cheng *et al*., 2011)

Figure 2 shows the basic structure of Scleroglucan, Schizophyllan and Pullulan polysaccharide.

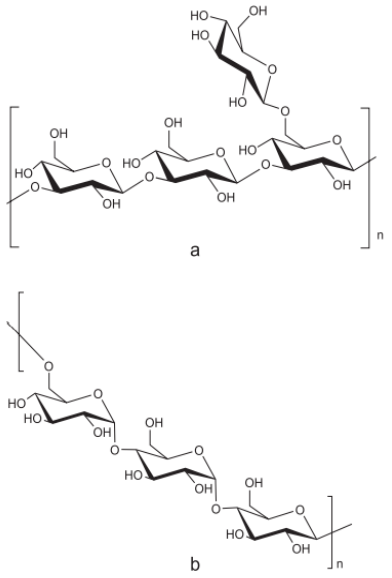

Figure 2: **Chemical Structure of mains fungal Exopolysaccharides (a): Scleroglucan and Schizophyllan; (b): Pullulan**

Production extraction and concentration of Mushroom exopolysaccharides

The word exo is best able to establish when a compound of fungi has taken place in the outermost portion of the compound in which all the cells are closely bound to the structure or released into the world in other stable forms of infinite structures, such as protective shields, signals and ligands, etc. Discharged biopolymers are present as a suitable loosely cell atmosphere interface that is almost easier to isolate

and disinfect (Nwodo *et al*., 2012). The selection of methods documented in research journals was determined on the basis of their non-drastic approach, which retains physiological properties and functionality. As a result, a blend of physical, chemical and analytical methods have been adapted for the separation of fungi exopolysaccharide, in particular food grade types (Donot *et al*., 2012; Su *et al.*, 2013). The exopolysaccharide architecture is characterized in nature by the repetition of monomeric sugar moieties whose individual and combined chemical characteristics provide a variety of attempting to respond and functions. The secretion of a number of other metabolic by-products during isolation may have been related to this. Affinity, ion exchange, size exclusion, and chromatographic thin-layer techniques have been reported to be sufficient for exopolysaccharide isolation. Under anaerobic conditions, fermentation utilizes the metabolic activities of organisms for the bioconversion of complex substrates. Around the same moment, new compounds called secondary metabolites, that might contain exopolysaccharides, are released from species.

Two main methods of fermentation are used in the production: Solid State Fermentation (SSF) and Submerged Fermentation (SmF). The compounds released during the fermentation process differ from different species and are largely affected by prevailing environmental conditions. A few of the natural bioactive substances reportedly generated by fermentation processes are enzymes, hyperglycemic agents, and antioxidants, antibiotics, preservatives and pigments (Subramaniyam and Vimala, 2012).

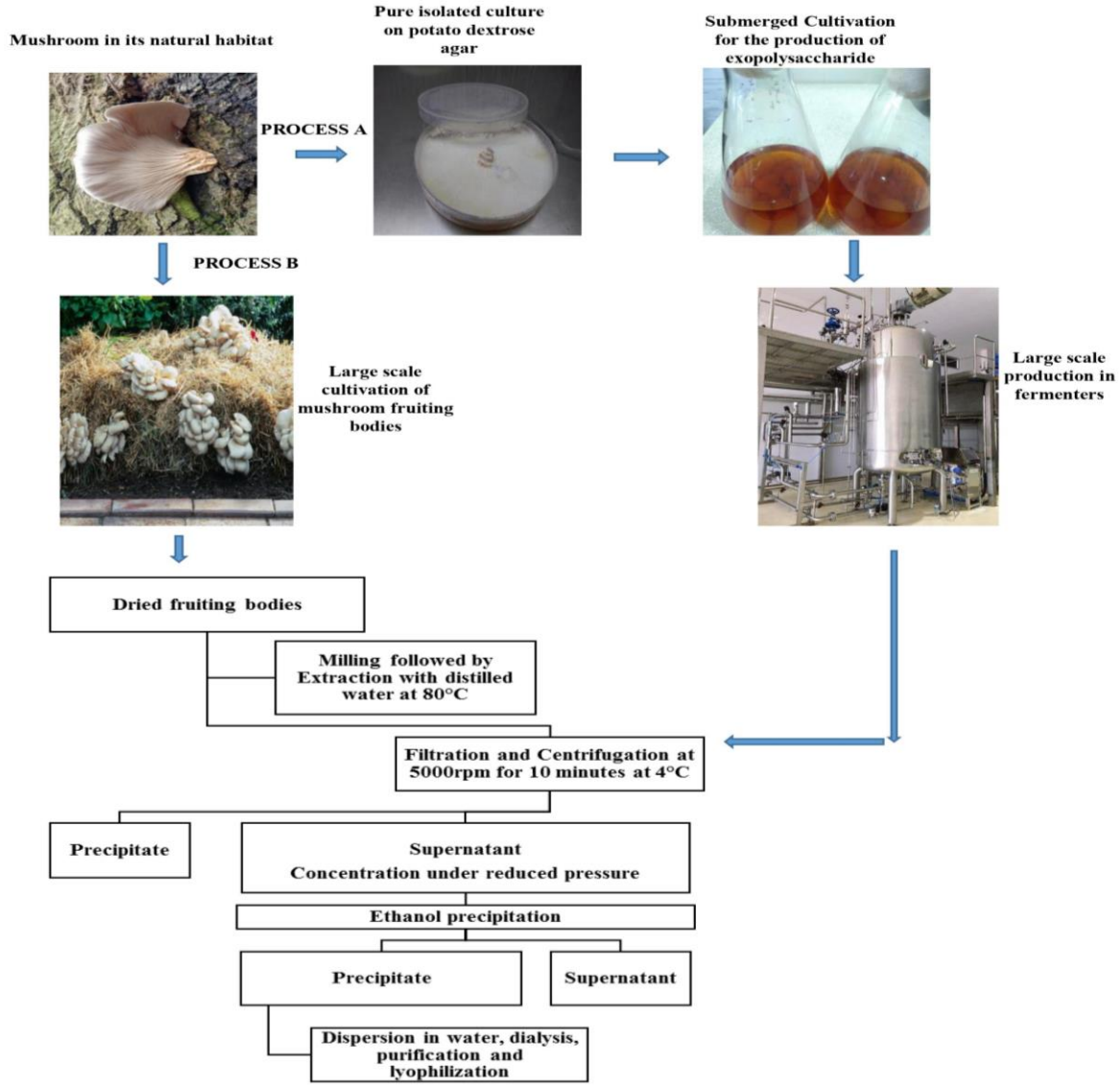

Figure 3: Submerged (Process A) and Solid (Process B) fermentation for the production of mushroom polysaccharide

Above flow chart shows the method for the production of pleuran by *Pleurotus ostreatus* by means of submerged fermentation of mycelium (Process A) or solid state fermentation (Process B). Process A starts with the spread of mushroom cells on agar plates, followed by submerged cell cultivation in shake flasks as an intermediate stage for the preparation of the inoculum for culture of a bioreactor. The bioreactor cultivation is carried out by increasing the process from a limited to a large bioreactor. If the processed polysaccharides are extracellular, removal is typically done either by direct precipitation with cold ethanol or by lyophilization to acquire the crude extract. A solvent-free technique is also developed to directly isolate high molecular weight compounds by ultrafiltration followed by direct lyophilization. The endopolysaccharides are obtained from mushroom fruiting bodies normally (Process B) using the traditional procedure of polysaccharides production. The cells are washed and dried first with fruiting bodies as starting materials in Process B, accompanied by homogenization prior to several hours of boiling water extraction. Crude polysaccharide water extract is concentrated using vacuum extraction, followed by precipitation of alcohol using cold ethanol. Then the precipitate is lyophilized. Further purification may also be achieved in this process by repeating the steps between the stage of water extraction and lyophilization. The majority of today's methods available for the extraction of polysaccharides are substantially time bound, energy consuming and requiring a significant amount of organic polysaccharide precipitation solvents, this leads to the critical problem of the recovery of solvents and environmental pollution. After production, bioactive polysaccharides can be extracted and concentrated by means of porous membranes (Charcosset, 2006). Isolation of the membrane is most often used in industries and pilot sizes for size based separations with the aid of high-throughput screening. It is also eco- sustainable and particularly suitable for isolating molecular weight-specific polysaccharides with specific biological activity (Xiao *et al*., 2007). The use of membrane technology to fractionate polysaccharides from *A. subrufescens* is stated by Silveira *et al*., (2012). Both the microfiltration and ultra-filtration membrane films are equipped for isolating high-sub-atomic weight polysaccharides from the two concentrates. As intended, when the nominal porosity of membranes decrease, higher retention levels were achieved, irrespective of the source of the extracts. All the components of polysaccharide were detected in the modules of the nano-filtration membrane producing higher retention yields. Therefore, for scaling- up processes, this system is an effective alternative. Among the accessible membrane separation systems, tangential flow filtration is an option, also known as cross – flow filtration. The system works on the basis of a feeding stream mode where the system works under strain, the liquid phase moves through a membrane positioned parallel to the fluid current. A proportion of the fluid passes via the membrane each time its components in the liquid state are smaller than the pores of the membrane. The part that flows through the membrane denounced as permeate. The current applied would be driving force to eliminate contaminants that are not pervaded by the membrane. The use of membranes has certain benefits over alternative technologies which include the use of low temperature, low energy consumption, decreased impact on the environment, particularly due to reduction in the use of solvents and preservation of the inherent properties of the compounds (Xu and Wang 2005; Mello *et al*., 2010; Hsieh *et al*., 2014).

Potential applications

Over the past several decades, microbial EPS's, including fungal EPS's, have gained significance as several studies have shown distinct applications that not only indicate the alternate source of marketed plant or seaweed polysaccharides, but also some modern and interesting bioapplicability. Moreover, upstream and downstream handling of these EPSs is simpler and one can create a lot bigger sum in a more limited time when contrasted with plant or algal polysaccharide creation. Among the distinctive EPS's: Pullulan, Scleroglucan, and Botryosphaeran are notable for their applications in various fields. Mushrooms are a commonly eaten food that promotes low-calorie, low-cholesterol, and low-sodium health. In any case, the manner in which a large number of these mushrooms are digestible (and consequently non-toxic) just as they or their polysaccharides make them conceivably ideal elements for the creation of novel utilitarian foods and nutraceuticals. The extracellular, intracellular, or cell wall polysaccharides, which exhibit immunostimulating, antitumor, antimicrobial, anti-inflammatory, antioxidant, prebiotic, hypoglycemic, and hypocholesterolemic effects, are the most popular active ingredients in these higher fungi (Figure 4).

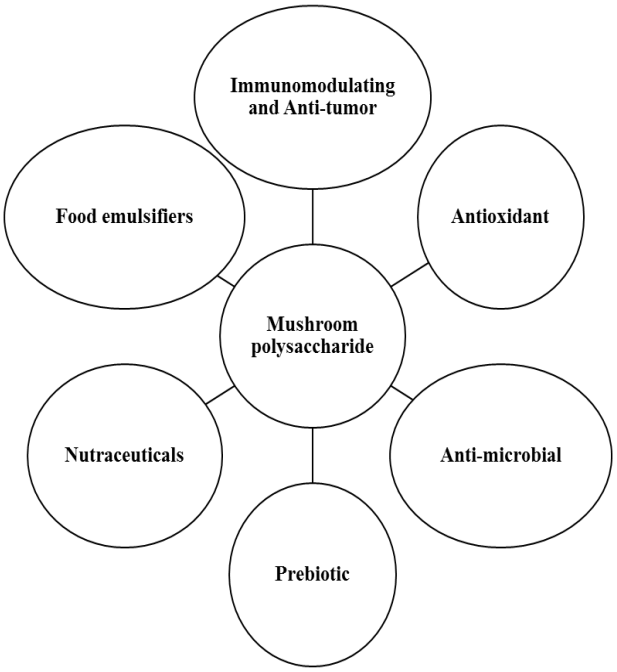

Figure 4: Potential applications of mushroom polysaccharides

1. Immunostimulating and Antitumor Properties: Mushrooms, having a place to the lesson *basidiomycetes* and some of the time *ascomycetes*, are a broadly disseminated nourishment asset on oil and have been devoured since of their wholesome esteem. Mushrooms can act as hypolipidemic, hypoglycemic, antiatherogenic or prebiotic dietary fiber (Giavasis 2013, Kim *et al*., 2006, Mizuno and Nishitani, 2013, Stachowiak and Reguła, 2012, Wasser 2002). Lentinan and schizophyllan are two of the most all around examined mushroom glucans and numerous analysts underline their immunostimulating properties (incitement of emission of tumor rot factor-α (TNF-α) by human monocytes and enactment of macrophages, or platelet haemopoietic movement (Chang and Wasser 2012, Giavasis 2013, Ikekawa 2001, Lo *et al.*, 2011, Stachowiak and Reguła, 2012).

Mushroom polysaccharides apply their antitumor activity generally through activation of the insusceptible reaction of the host life form. These substances are known as biological response modifiers (BRM'S Wasser and Weis, 1999). This fundamentally implies that: they do not cause damage, and they position no extra body stress; they assist the body adapting to different ecological and biological stresses; and they exert on the body a non-specific movement promoting certain or all of the major structures, including as well as regulatory mechanisms, the nervous, hormonal, and immune systems (Brekhman, 1980).

Clinical preliminaries on the remedial impacts of lentinan have indicated that when utilized in mix with traditional chemotherapy, it incredibly expands the survival of patients with advanced gastric cancer (Oba *et al*., 2009). Such β-glucans do not demonstrate toxicity also at high dosages, human beings are more affected when offered in the early stages of cancer treatment. It is understood that fungal polysaccharides activate natural killer cells, T cells, B cells and macrophage-dependent immune system cells. Lentinan is recognized as being able to recover the suppressed helper T-cell development in the tumor-bearing host to their normal state, which leads to full restoration of humoral immune responses (Ooi and Liu 1999). The medicinal biopolymer, Krestin (also known as PSK), derived from *Trametes versicolor* is used in Asia because of its immuno-stimulating, anti-metastatic and direct antitumor effects as a complementary cancer treatment (Kobayashi *et al.*, 1995). It was additionally shown that Krestin has TLR2-agonist operations and Stimulate nerve fiber cells (DC) and T cells in carcinoma murine models wherever cancer growth has been considerably smothered (Lu *et al*., 2011). Ganoderan is another plant life biopolymer that has been used as adjuvant cancer medical care, because it will increase the cytotoxic result of therapy and enhances the immune responses in patients with adenocarcinoma (Mahajna *et al*., 2009, Vannucci *et al*., 2013, Yuen and Gohel 2005). *Agaricus blazei* mushroom is one of recently discovered healthful mushrooms. The proteoglucans and glucans from *A. blazei* was very efficient in promoting the excretion of IFN-γ and also in suppressing allergic reactions (antiallergic immunomodulation) against various forms of sarcomas and carcinomas in mice (Firenzuoli *et al.*, 2008, Mizuno and Nishitani, 2013). *A. blazei* proteoglucans activate assortment of framework cells (macrophages, interferons, T cells, and NK cells) to end the increase, metastasis, and rehash of disease cells (Fujimiya *et al*., 1998, Lakhanpal 2005). Table 1 presents the immune-modulating and antitumor activities of different mushroom polysaccharides.

Table 1: Mushroom polysaccharides and their immune-modulatory and anti-tumor activities

Mushroom	Common name	Active compound	Immunomodulatory/ Antitumor activity
Agaricus blazei	Royal sun agaricus	Glycoprotein (ATOM), β-1,3-D-glucan, with β-1,6-D-glucan branch	Induction of TNF, IFN-γ and IL-8 production
Agaricus subrufescens	Almond portobello		
Cordyceps sinensis	Caterpillar fungus	β-D- glucan, heteroglycan, cordyglucan	Increase in IL-5 induction with decrease in IL-4 and IL-17
Ganoderma lucidum	Reishi, Ling-zhi, Spirit plant	Ganoderan, heteroglycan, Mannoglucan,glycopeptide	Stimulate TNF-α, IL-1, IFN-γ production, activateNF-$_k$B
Grifola frondosa	Hen of the woods, Maitake	Grifolan (1-6 monoglucosylbranched β-1,3-d-glucan), proteoglycan,heteroglycan, galactomannan	Macrophage activation, induction of IL-1, IL-6, and TNF-α secretion
Hericium erinaceus	Lion's Mane mushroom, bearded tooth, Monkey head mushroom	Heteroglycan, heteroglycan-peptide, β-1,3 branched-β-1,2-mannan	Induce NO production, increase expression of TNF-α, IL-1β, IL-12
Lentius edodes	Shiitake, black forest mushroom, golden oak mushroom	Lentinan, glucan, mannoglucan, proteoglycan	Induces non-specific cytotoxicity in macrophage and enhance cytokine production
Phellinus linteus	Mesima, Black Hoof fungus	Acidic polysaccharides	Activation of murine B cells, induce IL-19 anf IFN-γ production
Pleurotus ostreatus	Oyster mushroom	Pleuran, heterogalactan, proteoglycan	Induce IL-4 and IFN-γ production
Polyporus umbellatus	Umbrella polypore	Polysaccharides	Enhances TNF-α,IL-1β, and NO production

2. Antioxidant properties: Polysaccharides extracated from *G. lucidum, T. versicolor, L. edodes, P. linteus, and Agaricus* mushrooms have decreasing control capacities and chelating properties and can repress lipid oxidation or diminish oxidative stress. The phenolic compounds display in *G. lucidum* fruiting bodies and mycelia are the compounds with the most noteworthy antioxidant movement, *G. lucidum* polysaccharides showing free radical-scavenging properties, decreasing lipid peroxidation regulation and hindrance (Heleno *et al.*, 2012, Tseng *et al*., 2008). *G. lucidum* peptidoglucan can provide chemical-acting damage and malfunction to the mitochondria, endoplasmic reticulum, and microvilli of macrophages. In expansion, methanolic extractes of *G. lucidum* and *G. tsugae* glucans and proteoglucans act as cancer prevention agents by rummaging receptive oxygen species (ROS), which are connected both to oncogenesis and to lipid oxidation (Lakhanpal and Rana, 2005). The ability of certain mushroom polysaccharides (e.g., those of *G. lucidum*) to restrict the production of oxygen-free radicals is another instrument of antioxidant movement. The polysaccharides from water-soluble extracts of *A. auricula* and *C. militaris* fruiting bodies, demonstrated free radical properties of scavenging, chelating, and decreasing strength, and an increase in total antioxidant ability (Chen *et al.*, 2008; Luo *et al*., 2009; Wu *et al*., 2011).

3. Antimicrobial properties: Mushroom polysaccharides are adaptive *in vitro* or *in vivo* against bacterial and viral diseases, as they can strengthen the neutrophil and macrophage phagocytosis of species. Lentinan has shown antimicrobial activity against *Listeria monocytogenes*, *Staphylococcus aureus*, *Salmonella enteritis*, *Escherichia coli*, as well as tuberculosis (Giavasis 2013, Mattila *et al.*, 2000, van Nevel *et al.*, 2003). Crude extracts from various fruiting bodies of *Agaricus* have limited the development of *Bacillus subtilis*, *S. aureus* and *B. cereus*, although the antimicrobial effect of these extracts may also be linked to the non-polysaccharide components (Barros *et al*., 2008). Lentinan and an acidic *Ganoderma* proteoglucan, particularly in conjunction with anti-HIV drugs, has been effectively utilized as an elective treatment for HIV, because it increases resistance to the HIV infection and restrain the poisonous quality of engineered anti- HIV drugs (Giavasis and Biliaderis 2006, Lindequist *et al*., 2005, Markova *et al*., 2002, Sasidhara and Thirunalasundari 2012; Selegean *et al*., 2009). A few mushroom glucans are detailed to have anti viral action, which is accepted to occur via the expanded discharge of IFN- γ and upgraded multiplication of peripheral blood mononuclear cells (PBMC) (Lindequist *et al*., 2005, Markova *et al*., 2002, Sasidhara and Thirunalasundari, 2012). Since the antimicrobial activity of mushroom glucans appears to be indirect and linked to immunomodulation (Giavasis and Biliaderi, 2006) and to the verbal organization of the gut mucosa (van Nevel *et al.*, 2003), it seems possible to identify nutraceuticals based on glucan with prophylactic antimicrobial properties.

4. Prebiotics: Mushrooms appear to be a potential source for prebiotics as they contain various polysaccharides such as chitin, hemicellulose, alpha- and β-glucans, mannans, xylans and galactans. The

term prebiotic is described as "a non-digestible nutritional fixation that selectively stimulates the development and/or action of one or a limited number of microscopic organisms in the colon. The crucial increase in the number of probiotics such as *Bifidobacteria* and *Lactobacilli* represents one critical positive influence of prebiotics, while negatively affecting the progress of the subgroup *Histolyticum* (Palframan *et al*., 2003). Among the polysaccharides of mushrooms, β-(1 →3)-D-glucans and their proteoglycans, peptide/protein derivatives (polysaccharide-peptide/protein complexes), are vital prebiotics. Some of them are true heteroglycans containing, or in varying combinations, arabinose, mannose, fructose, galactose, xylose, glucose and glucuronic acids as major components of the side chain (Wasser, 2002; Giavasis and Biliaderis, 2006). As it is impossible for the human digestive enzyme to completely digest the polysaccharide several mushroom polysaccharides are able to serve as a source of prebiotics and hydrolyze β-glucosidic bond (Aida *et al.*, 2009). Mushroom (*Pleurotus ostreatus* and *Lentinus edodes*) can altogether adjust vegetation composition by promoting the digestion system and expansion of advantageous microorganism such as *Lactobacilli* and *Bifidiobacteria* as well as by repressing pathogenic microscopic organisms such as *E.coli, Clostridium* and *Salmonella* (Zhou *et al*., 2011). In order to stimulate the growth of probiotic bacteria, especially those from *P. eryngii*, alkali-soluble linear alpha-1,3-glucans both water-soluble β-1,3/β-1,6-glucans from these mushrooms have been identified. Mushrooms too anticipate viral contamination by improving the development of probiotic microbes within the huge digestive tract (Villares *et al*., 2012). Pleuran from oyster (*Pleurotus ostreatus*) mushrooms and lentinan from shiitake (*Leninus edodes*) mushrooms are currently the most regularly utilized β- glucans as prebiotics. They improve intestinal mucosal tolerance to inflammation (Zeman *et al*., 2001) and prevent the production of rat intestinal ulcers. Chou *et al.* (2013) considered the prebiotic action of unrefined polysaccharides from *Lentinula edodes* stipe, *Pleurotus eryngii* base, and *Flammulina velutipes* base which were found to improve the survival rate of probiotics (*Lactobacillus acidophilus, Lactobacillus casei*, and *Bifidobacterium longum* subsp. *longum*) amid cold capacity. In addition, in recreated gastric and bile juice environments, they had notable protective effects on these probiotics in order to achieve useful effects in the host.

5. Nutraceuticals: The premise of novel drugs (particularly anticancer drugs) has been influenced by a few of mushrooms, but few have been marketed as novel nutraceuticals worldwide. Under various brand names such as Ganodex, Immuna, Lentinex, Immunoglukan, Unadulterated Ruddy Reishi Capsule, LifeShield, Bene-X, and Zymucan, polysaccharides are available as nutraceuticals inside the showcase. In order to solidify a well-being argument for nutraceuticals based on mushroom polysaccharides, isolated from pharmacological thought by unadulterated polysaccharide arrangements, the possible impact of food preparation should be considered. There are a few examples of novel nutraceuticals and useful nutrients that have been developed on the basis of bioactive mushroom polysaccharides as of late. Glucans by *L. edodes* were effectively linked in fiber-rich, low-calorie useful heated foods (with up to 2 percent glucan concentration) as a halfway replacement of wheat flour, where gluing parameters, player consistency and flexibility were advanced, or in noodles where antioxidant and hypocholesterolemic effects and advanced quality characteristics were conferred (Kim *et al*., 2009, 2011). Fan *et al*., (2006) delivered a useful bread where wheat flour was incompletely substituted with *A. auricula* polysaccharides. The antioxidant capability of bread (tried as DPPH free radical-scavenging capacity) was significantly expanded by up to 9 percent by replacement of flour with bioactive polysaccharides without altering the acceptability and recognition of the mixed bread. A utilitarian cheese-like food containing live societies of *S. commune* produced by Okamura-Matsui *et al.,* (2001) included as a starter culture of proteolytic, milk-clotting, which was too capable of ageing lactose and providing up to 0.58 percent β-glucan in this fresh "cheese," which had notable antithrombotic impacts. The use of mushroom polysaccharides or mushroom powder for the concept of utilitarian nibble nourishment has been suggested. An Indian papad has been incorporated with oyster mushroom powder to advance the fiber content although *Agaricus* extracts have been used in snacks, advertising high antioxidant and free radical-scavenging properties (Parab *et al*., 2012; Singla *et al*., 2009). In addition, *A. brasiliensis* polysaccharides have been suggested as a utilitarian fixation in useful foods for antiobesity and antidiabetic medicines (Yamanaka *et al*., 2013). In a conventional Chinese medication formula a soup of *A. auricula* and *Tremella* mushrooms is suggested for the treatment of hypertension (Xu, 2001).

Garden of Life (RM-120), which includes 10 restorative mushrooms on the side of Aloe vera and *Uncaria tomentosa* and is said to stimulate the healthy structure, offers direct blood cholesterol, antitumor, antiviral and antibacterial protection, and facilitates the treatment of cardiovascular infections (Lakhanpal and Rana, 2005). Further research shows that pleuranium-based nutraceutical product (Immunoglukan P4H) decreases the awful essence of repetitive respiratory tract diseases by altering humoral and cellular resistance (Jesenak *et al*., 2013). *Hericium erinaceus***,** moreover known as lion's Mane mushroom or hedgehog mushroom is a consumable organism, which includes a long history of utilization in conventional Chinese medication. This mushroom has a place to the lesson of Agaricomycetes beneath the phylum basidiomycota. A notable increase in healthy reaction and resistance to *Vibrio* disease of white shrimp (*Litopenaeus vannamei*) was achieved using nutrition supplemented with small particles of monkey head mushroom *Hericium erinaceumum*. This was attributed to the improvement in the efficiency of phenoloxidase, superoxide dismutase and glutathione peroxidase. Most of the helpful polysaccharides found in *H. erinaceus,* are β glucans (Lee *et al*., 2009; Kim *et al*., 2011). Table 2 presents the bioactive polysaccharides produced by mushroom and their health benefits.

Table 2: Bioactive polysaccharides produced by mushrooms and their health benefits

Bioactive polysaccharides	Health Benefits
B-glucans polysaccharides e.g (β-1,3-branched-beta-1,6-glucan with laminarin- like trile helix conformation)	Anti-cancerous, Immuno-modulatory, Neuro-protective and Antioxidant
HEP1(a heteropolysaccharide, with a (1>6)-linked α-D-galactopyransol backbone)	Anti-cancerous and Immuno-modulatory
HEP3 (a hetero-polysaccharide, with a branched penta-saccharide repeating unit)	Anti-cancerous and Immunomodulatory
Other polysaccharides: 6-methyl-2,5 dihydroxymethyl-γ-pyranone; 2-hydroxymethyl-5-α-hydroxy-ethyl- γ pyranone;4-chloro-3,5-dimethoxybenzoic-o-arbitol ester; 4-chloro-3,5- dimethoxybenzoic methyl ester and 4-chloro-3,5-dimethoxybenzoic acid	Hepato-protective and antioxidant

6. Food emulsifiers: The emulsifiers stabilize the emulsion by forming a physical barrier in order to prevent the droplets from coalescing (Calvo *et al*., 2004). The currently used chemical emulsifiers are generally toxic and often non-biodegradable posing a serious threat to human health and the environment. Thus, there is an urgent need to look for non-toxic, environmentally friendly alternatives. At present, a growing interest has led to the discovery of new sources and among natural emulsifiers, bio surfactants of microbial origin have dominated in the research during last decades. Since the mushroom polysaccharides are largely explored for their therapeutic potential very few studies are available where in their emulsifying aspect has been studied. Guo *et al*., (2018), reported that the *Ganoderma luicidium*-derived polysaccharide, when integrated with coix oil resulted in enhancing the emulsion stability and in turn, its anti-tumor activity. In another study carried out by Gallotti *et al*., (2020), it was found that the beta-glucan extracts of *Pleurotus ostreatus* were capable of providing suitable emulsifying properties in spray drying as well as liquid emulsions. In a similar study by Veverka *et al*., (2018), beta-glucan isolated from *P. ostreatus* was found capable of forming stable emulsion gels with various natural oils (olive oil, cocoa butter, coconut oil and linolenic acid) without addition of any consolvent or surfactant.

CONCLUSIONS

In various areas of human endeavours, mushroom exopolysaccharides carry great promises even more than actually imagined. Since the 1940s, fungi have been used extensively in industry for diverse bioactive metabolite processing. Efforts have been made to classify varieties and origins of natural exopolysaccharide. Against this background, the identification of the exopolysaccharide with new sugars or sugars in the future, substitutions could lead to new applications. The importance put on the exopolysaccharide market and commercial applications globally stimulates the rapid development of research into new strategies for sourcing, processing, isolating, purifying and restoring functional derivatives. So, it can be said that biologically active polysaccharides are value-added products with significant applications especially in the pharmaceutical sector and there still is a need to dig deeper into this prospect in order to open new avenues to different industrial applications of these polysaccharides.

References

Aida, F. M. N. A., M. Shuhaimi, M. Yazid, and A. G. Maaruf, 2009. Mushroom as a potential source of prebiotics: A review. Trends, Food Science and Technology 20:567–575.

Akyuz, M., A.N. Onganer, P. Erecevit and S. Kirbag, 2010. Antimicrobial activity of some edible mushrooms in the eastern and southeast anatolia region of Turkey. GU Journal of the Science of Food and Agriculture. 23(2): 125-130.

Asfors, K.E. and K. Ley, 1993. Sulfated polysaccharides in inflammation. Journal of Laboratory and Clinical Medicine., 121: 201-202

Banerjee, D., M. Jana, and S. Mahapatra, (2009). Production of exopolysaccharide by endophytic Stemphylium sp. Micologia Aplicada International, 21, 57–62.

Banik RM, B. Kanari, and SN. Upadhyay. 2000 Exopolysaccharide of the gellan family: prospects and potential. World Journal of Microbiology and Biotechnology.;16(5):407–14

Batista, A.C.M., F.E.S. Neto, and W.S. Paiva, 2018. Review of fungal chitosan: past, present and perspectives in Brazil, Polimeros 28 (3) 275–283.

Bouveng, H. O., H. Kiessling, B. Lindberg, and J. McKay, 1962. Polysaccharides elaborated by *Pullularia pullulans*. I. The neutral glucan synthesized from sucrose solutions, Acta Chemica Scandinavica 16, 615,

Brekhman II (1980) Man and biologically active substances. Pergamon Press, New York

Calvo, C., F. L. Toledo, C. Pozo, M. V. Martínez-Toledo, & J. González-López, (2004). Biotechnology of bioemulsifiers produced by micro-organisms. *Journal of Food Agriculture and Environment*, *2*(3), 238-243.

Charcosset, C (2006) Membrane processes in biotechnology: an overview. Biotechnology advances 24:482–492

Chen W, Z. Zhao, SF. Chen, YQ. Li, 2008. Optimization for the production of exopolysaccharide from *Fomes fomentarius* in submerged culture and its antitumor effect in vitro. Bioresource technology;99(8):3187–94.

Chen, G., Y. C. Luo, B. P. Ji et al. 2008. Effect of polysaccharide from *Auricularia auricula* on blood lipid metabolism and lipoprotein lipase activity of ICR mice fed a cholesterol-enriched diet. Journal of Food Science and Technology 73:103–108

Chen, Y., W. Mao, H. Tao, W. Zhu, X. Qi, Y. Chen, et al. (2011). Structural characterization and antioxidant properties of an exopolysaccharide produced by the mangrove endophytic fungus *Aspergillus* sp. Y16. Bioresource Technology, 102, 8179–8184.

Cheng, K.C., A Demirci and J.M. Catchmark (2011), 'Pullulan: biosynthesis, production, and applications', Applied microbiology and biotechnology. 92, 29–44.

Chihara, G. (1992). Immunopharmacology of Lentinan, a polysaccharide isolated from *Lentinus edodes*: its application as a host defence potentiator. International Journal of Oriental Medicine, 17, 57-77.

Chihara, G., J. Hamuro, Y. Maeda, Y. Arai, and F. Fukuoka, (1970). Fractionation and purification of the polysaccharides with marked antitumour activity, especially lentinan, from *Lentinus edodes* (Berk.) Sing, an edible mushroom Cancer Research, 30, 2776e2781.

Chihara, G., J. Hamuro, Y.Y. Maeda, Y. Arai, and F. Fukoeka (1970). Fractionation and purification of the polysaccharides with marked antitumour activity, especially lentinan from *Lentinan edodes* (Berk) Sing (an edible mushroom) Cancer Research, 30(11), 2776-2781.

Chihara, G., Y. Maeda, J. Hamuro, T. Sasaki, and F. Fukuoka, (1969). Inhibition of mouse sarcoma 180 by polysaccharides from *Lentinus edodes* (Berk.) Sing Nature, 222, 687e688

Chinese Herbalism Editorial Board, Zhonghua Bencao, Shanghai Science and Technology Press, Shanghai, 1999, pp. 202–203.

Chou, W.-T., I.-C. Sheih, and T.J. Fang, (2013). The applications of polysaccharides from various mushroom wastes as prebiotics in different systems. Journal of Food Science, 78(7), M1041-M1048

Christodoulidou, A., V. Bouriotis, and G. Thireos, 1996. Two sporulation-specific chitin deactylase-encoding genes are required for the ascospore wall rigidity of *Saccharomyces cerevisiae*, Journal of Biological Chemistry 271 (1996) 31420–31425.

Czop, J. K., and J. Kay, (1991). Isolation and characterization of -glucan receptors on human mononuclear phagocytes. Journal of Experimental Medicine, 173, 1511–1520.

Da Silva MDLC, Martinez PF, Izeli NL, Silva IR, Vasconcelos AFD, De Stefani Cardoso M, Stelutti RM, Giese EC, De Melo Barbosa A (2006) Caracterização química de glucanas

fúngicas e suas aplicações biotecnológicas. Quim Nova 29(1):85–92

Davison P, E Mentzer (1982) Polymer flooding in North Sea reservoirs .Society of Petroleum Engineers journal. 22(3):353–362

Donot. F., A. Fontana, J.C. Baccou, S. Schorr-Galindo, (2012) Microbial exopolysaccharides: main examples of synthesis, excretion, genetics and extraction, Carbohydrate polymers. 87 951–962.

Doster MS, AJ Nute and CA Christopher (1984). Recovering petroleum from underground formations, U.S. Patent 4, 457-372.

Doster. M, S Martha, AJ Nute., and CA Christopher. (1984) Method of recovering petroleum from underground formations. USA Patent 4,457,372

Duc ANC (1982) .Glucosylglucans and their use in gastroenterology, especially in the treatment of colon disorders. Europe Patent 45,338

Fan, L., S. Zhang, L. Yu, and L. Ma. 2006. Evaluation of antioxidant property and quality of breads containing *Auricularia auricula* polysaccharide flour. Food chemistry 101:1158–1163.

Firenzuoli, F., L. Gori, and G. Lombard. 2008. The medicinal mushroom *Agaricus blazei* Murrill: Review of literature and pharmaco-toxicological problems. Evidence-based complementary and alternative medicine 5:3–15.

Fujimiya, Y., Y. Suzuki, K. Oshiman et al. 1998. Selective tumoricidal effect of soluble proteoglucan extracted from the basidiomycete *Agaricus blazei* Murill, mediated via the natural killer cell activation and apoptosis. Cancer immunology, immunotherapy 46:147–159.

Furue. H (1987), 'Biological characteristics and clinical effects of sizofi lan (SPG)', Drugs Today, 23, 335–46.

Gallois, M. et al. (2009) Natural alternatives to in-feed antibiotics in pig production: can immunomodulators play a role? Animal 3, 1644–1661

Gallotti, F., Lavelli, V., & Turchiuli, C. (2020). Application of Pleurotus ostreatus β-glucans for oil–in–water emulsions encapsulation in powder. *Food Hydrocolloids*, *105*, 105841.

Giavasis I (2014) Bioactive fungal polysaccharides as potential functional ingredients in food and nutraceuticals. Current Opinion in Biotechnology 26:162–173

Giavasis, I. 2013. Production of microbial polysaccharides for use in food. In Microbial Production of Food Ingredients, Enzymes and Nutraceuticals, ed. B. McNeil, D. Archer, I. Giavasis, and L. M. Harvey, pp. 413–468. Cambridge: Woodhead Publishing

Giavasis, I., and C.G. Biliaderis, (2006). Microbial Polysaccharides. In C.G. Biliaderis, & M.S. Izydorczyk (Eds.), Functional Food Carbohydrates (pp. 167-214), CRC Press: Boca Raton

Gounga, M.E., S.Y. Xu, Z. Wang, and W.G. Yang, (2008), 'Effect of whey protein isolate–pullulan edible coatings on the quality and shelf life of freshly roasted and freezedried Chinese chestnut', Journal of food and Science technology, 73, E155–E161.

Guo, A. W. Mao, Y Li, J, Tian and J., Xu, 2013. Structural elucidation of the exopolysaccharide produced by fungus *Fusarium oxysporum* Y24-2, Carbohydrate research"365 9–13.

Guo, J., C. Yuan, M. Huang, Y. Liu, Y. Chen, C., Liu, and Y. Chen, (2018). Ganoderma lucidum-derived polysaccharide enhances coix oil-based microemulsion on stability and lung cancer-targeted therapy. *Drug delivery*, *25*(1), 1802-1810.

Halleck FE (1967). Polysaccharides and methods for production thereof, Chem. Abstr, 66, 84772

Halleck FE (1972). Cosmetic composition employing water-soluble polysaccharide. U.S. Patent 3,659,025

Halleck FE. 1970 Wave set composition containing a polysaccharides. US Patent 3507290..

Hamed SB, M. Belhadri, 2009. Rheological properties of biopolymers drilling fluids. Journal of Petroleum Science and Engineering; 67:84–90.

Harikrishnan, R. et al. (2011) Diet enriched with mushroom *Phellinus linteus* extract enhances the growth, innate immune response, and disease resistance of kelp grouper, *Epinephelus bruneus* against vibriosis. Fish Shellfish Immunology. 30, 128–134

Heleno, S. A., L. Barros, A. Martins, M. J. R. P. Queiroz, C. Santos-Buelga, and I. C. F. R. Ferreira. 2012. Fruiting body, spores and in vitro produced mycelium of *Ganoderma lucidum* from Northeast Portugal: A comparative study of the antioxidant potential of phenolic and polysaccharidic extracts. Food Research International 46:135–140.

Higashi, D. et al. (2012). The effect of lentinan combination therapy for unresectable advanced gastric cancer. Anticancer Research 32, 2365–2368

Holzwarth G.(1985) Xanthan and scleroglucan: structure and use in enhanced oil recovery. Developments in industrial microbiology; 26(): 271–80

Hsieh C-W, Huang Y-S, Lai C-H, Ko W-C (2014) Removal of higher fatty acid esters from Taiwanese rice-spirits by nanofiltration. Food and Bioprocess Technology 7:525–531

Hu DJ, KL Cheong, J Zhao, and SP Li (2013) Chromatography in characterization of polysaccharides from medicinal plants and fungi. Journal of separation science 36(1):1–19

Hwang, H.J., S.W. Kim, J.W. Choi, J.W. Yun, 2003. Production and characterization of exopolysaccharides from submerged culture of *Phellinus linteus* KCTC 6190, Enzyme and Microbial Technology. 33 309–319.

Jesenak, M. et al. (2013) Immunomodulatory effect of pleuran (bglucan from *Pleurotus ostreatus*) in children with recurrent respiratory tract infections. International Immunopharmacology. 15, 395–399

Johnson. M, (1996) Fluid systems for controlling fluid losses during hydrocarbon recovery operations. United States Patent 5228524

Karinaga R, K Koumoto, M Mizu, T Anada, S Shinkai and K Sakurai (2005). PEG-appended â-(1'!3)-D-glucan schizophyllan to deliver antisense-oligonucleotides with avoiding lysosomal degradation, Biomaterials, 26(23), 4866-4873.

Kim SP, MY Kang, YH Choi, JH Kim, SH Nam, and M Friedman. (2011) Mechanism of *Hericium erinaceus* (Yamabushitake) mushroom-induced apoptosis of U937 human monocytic leukemia cells Food and Function;2:348–56.

Kim, J., S. Lee, I. Y. Bae, H. G. Park, H. G. Lee, and S. Lee. 2011. (1–3)(1–6)-β-Glucan enriched materials from *Lentinus edodes* mushroom as a high-fibre and low-calorie flour substitute for baked foods. Journal of the Science of Food and Agriculture 91:1915–1919.

Kim, S. Y., H. J. Song, Y. Y. Lee, K. H. Cho, and Y. K. Roh. 2006. Biomedical issues of dietary fibre β-glucan. Journal of Korean Medical Science 21:781–789.

Kim, S. Y., S. I. Chung, S. H. Nam, and M. Y. Kang. 2009. Cholesterol lowering action and antioxidant status improving efficacy of noodles made from unmarketable Oak Mushroom (Lentinus edodes) in high cholesterol fed rats. Journal of Korean Society for applied Biological Chemistry 52:207–212.

Kirkwood S (1974) Unusual polysaccharides. Annual Review of Biochemistry 43:401–417

Kobayashi, H., K. Matsunaga, and Y. Oguchi. 1995. Antimetastatic effects of PSK (Krestin), a protein-bound polysaccharide obtained from basidiomycetes: An overview. Cancer Epidemiology Biomarkers Prevention 4:275–281.

Kotra, L.P. and S. Mobashery, 1998. $-lactam antibiotics, $-lactamases and bacterial resistance., Bulletin de l'Institut Pasteur 96: 139-150

Lakhanpal, T. N. and M. Rana. 2005. Medicinal and nutraceutical genetic resources of mushrooms. Plant Genet Resource 3:288–303

Leal-Serrano, G., Ruperez, P., and Leal, J. A., 1980. Acidic polysaccharide from *Aureobasidium pullulans*, Transactions of the British Mycological Society ., 75, 57,

Leathers. td (2003), 'Biotechnological production and applications of pullulan', Applied microbiology and biotechnology., 62, 468–73.

LeDuy, A., J. E. Zajic, and J. H. Luong, PulMan, 1988 in Encyclopedia of Polymer Science and Engineering, Vol. 13, 2nd ed., Mark, H. F., Bikales, N. M., Overberger, G. C., and Mengcs, G., Eds., John Wiley & Sons, New York, , 650

Lee JS, KM Min, JY Cho, and EK Hong. Study of macrophage activation and structural characteristics of purified polysaccharides from the fruiting body of *Hericium*

erinaceus. Journal of Microbiology and Biotechnology 2009;19:951–9.

Lee, B. C., J. T. Bae, H. B. Pyo, T. B. Choe, S. W. Kim, and H. J. Hwang, et al. (2003). Biological activities of the exopolysaccharides produced from submerged culture of the edible basidiomycete *Grifola frondosa*. Enzyme and Microbial Technology, 32, 574–581.

Lee, J. H., S. M. Cho, H. M. Kim, N. D. Hong, and I. D. Yoo, (1996). Immunostimulating activity of polysaccharides from mycelia of *Phellinus linteus* grown under different culture conditions. Journal of Microbial Biotechnology, 6, 52–55.

Lee, S.H. et al. (2010) In vitro effects of plant and mushroom extracts on immunological function of chicken lymphocytes and macrophages. British Poultry Science. 51, 213–221

Li, P., Mou, Y., Shan, T., Xu, J., Li, Y., Lu, S., et al. (2011). Effects of polysaccharide elicitors from endophytic *Fusarium oxysporium* Dzf17 on growth and diosgenin production in cell suspension culture of *Dioscorea zingiberensis*. Molecules, 16, 9003–9016

Lindequist, U., T. H. Niedermeyer, and W. D. Jülich. 2005. The pharmacological potential of mushrooms. Evidence-based complementary and alternative medicine 2:285–299.

Lu, H., Y. Yang, E. Gad et al. 2011. Polysaccharide Krestin is a novel TLR2 agonist that mediates inhibition of tumor growth via stimulation of CD8 T cells and NK cells. Clinical Cancer Research 17:67–76.

Maeda, Y.Y., S.T. Watanabe, C. Chihara, and M. Rokutanda, (1988). Denaturation and renaturation of a β-1,6:1,3-glucan, lentinan associated with expression of T-cell mediated responses. Cancer Research, 48(3), 671-675.

Mahajna J., N. Dotan, B. Z. Zaidman, R. D. Petrova, and S. P. Wasser. 2009. Pharmacological values of medicinal mushrooms for prostate cancer therapy: The case of *Ganoderma lucidum.* Nutrition and Cancer 61:16–26.

Mahapatra S, and D. Banerjee. Structural elucidation and bioactivity of a novel exopolysaccharide from endophytic *Fusarium solani* SD5. Carbohydrate Polymers 2012; 90(1):683–9.

Mahapatra, S., and D. Banerjee, (2013) Fungal exopolysaccharide: production, composition and applications, Microbiology Insights 6 1–16.

Manzi P, L. Pizzoferrato. Beta-glucans in edible mushrooms. Food Chemistry. 2000; 68(3):315–8.

Markova, N., V. Kussovski, T. Radoucheva, K. Dilova, and N. Georgieva. 2002. Effects of intraperitoneal and intranasal application of Lentinan on cellular response in rats, International Immunopharmacology 2:1641–1645.

Mastromarino P, Petruzziello R, Macchia S, Rieti S, Nicoletti R & Orsi N (1997). Antiviral activity of natural and semisynthetic polysaccharides on early steps of rubella virus infection, Journal of Antimicrobial Chemotherapy, 39, 339.

Mattila, P., K. Suonpaa, and V. Piironen. 2000. Functional properties of edible mushrooms. Nutrition 16:694–696.

Mello BCBS, Petrus JCC, Hubinger MD (2010) Concentration of flavonoids and phenolic compounds in aqueous and ethanolic propolis extracts through nanofiltration. journal of the International Society of Food Engineering 96:533–539

Mishra, A., Jha, B., 2013 Microbial exopolysaccharides, in: E. Rosenberg, E.F. DeLong, F. Thompson, S. Lory, E. Stackebrandt (Eds.), Theprokaryotes: Applied Bacteriology and Biotechnology, Springer, Berlin, Heidelberg, pp. 179–192.

Mizuno, M. and Y. Nishitani. 2013. Immunomodulating compounds in basidiomycetes Journal of Clinical Biochemistry and Nutrition 52:202–207.

Moon SH, Park CS, Kim YJ, Park YI. 2006 Biosorption isotherms of Pb (II) and Zn (II) on Pestan, an extracellular polysaccharide, of *Pestalotiopsis* sp. KCTC 8637P. Process Biochemistry;41(2):312–6

Moresi M, Lo Presti S, Mancini M, (2001) Rheology of scleroglucan dispersions. journal of the International Society of Food Engineering 50(4):235–245

Morschhäuser, J., G. Köhler, W. Ziebuhr, G. Blum-Oehler, U. Dobrindt and J. Hacker, 2000. Evolution of microbial pathogens. Philosophical transactions of the Royal Society of London. Series B,355: 695-704

Muzzarelli, R. R. A., Boudrant, J., Meyer, D., Manno, N., DeMarchis, M., & Paoletti, M. G. (2012). Current views on fungal

chitin/chitosan, human chitinases, food preservation, glucans,pectins and inulin: Atribute to Henri Braconnot,precursor of the carbohydrate polymers science, on the chitin bicentennial. Carbohydrate Polymers, 87, 995–1012.

Oba, K., M. Kobauashi, T. Matsui, Y. Kodera, and J. Sakamoto. 2009. Individual patient based meta-analysis of lentinan for unresectable/recurrent gastric cancer. Anticancer Research 29:2739–2746.

Okada k, yoneyama m, mandai t, aga h, sakai s and ichikawa. t (1990), 'Digestion and fermentation of pullulan', Journal of Japan Society of Nutrition and Food Science, 43, 23–9.

Okamura-Matsui, T., K. Takemura, M. Sera et al. 2001. Characteristics of a cheese like food produced by fermentation of the mushroom *Schizophyllum commune*. Journal of Bioscience and Bioengineering 92:30–32.

Orlandelli, R.C., Vasconcelos, A.F.D., Azevedo, J.L., Silva, L.M.C., Pamphile, J.A. (2016) Screening of endophytic sources of exopolysaccharides: preliminary characterization of crude exopolysaccharide produced by submerged culture of *Diaporthe* sp. JF766998 under different cultivation time, Biochimica Open 2 33–40.

Palframan, R., G.R. Gibson, and R.A. Rastall, (2003). Development of a quantitative tool for comparison of the prebiotic effect of dietary oligosaccharides. Letters in Applied Microbiology, 37(4), 281-284.

Palleschi A, Bocchinfuso G, Coviello T, Alhaique F (2005) Molecular dynamics investigations of the polysaccharide scleroglucan: first study on the triple helix structure. Carbohydrate Research 340(13):2154–2162

Parab, D. N., J. R. Dhalagade, A. K. Sahoo, and R. C. Ranvee. 2012. Effect of incorporation of mushroom (*Pleurotus* sajor-caju) powder on quality characteristics of Papad (Indian snack food). Journal of food Composition and Analysis 63:866–870

Paul F, Morin A, Monsan P. 1986 Microbial polysaccharides with actual potential industrial applications. Biotechnol Advances; 4(2):245–59

Paulsen BS (2002) Biologically active polysaccharides as possible lead compounds. Phytochemistry Reviews 1(3):379–387

Pirri RG (1996) Scleroglucan gel applied in the oil industry. France Patent 5,555,936

Pochanavanich, P., Suntornsuk, W. (2002) Fungal chitosan production and its characterization, Letters in applied microbiology 35 17–21.

Podkolzin, A. A., Dontsov, V. I., Sychev, I. A., Kobeleva, G., and Yu Kharchenko, O. N. (1996). Immunomodulating, antianemic, and adaptogenic effects of polysaccharides from plaster clover (Melilotus officinalis). Bulletin of Experimental Biology and Medicine, 121, 597–599.

polysaccharide from the mycelium of liquid-cultured *Agaricus blazei* Mill. Biochemistry and Molecular Biology International 47(4):707–714

Prets H, Eusley H, McNamee R, Jones E, Browder I and D Williams (1991). Isolation, physicochemical characterisation and pre-clinical efficiacy evaluation of a soluble Scleroglucan, Journal of Pharmacology and Experimental Therapeutics, 257, 500

Regulation (EC) N. 1831/2003 of the European Parliament and of the Council of 22 september 2003 on Additives for Use in Animal Nutrition (http://irmm.jrc.ec. europa.eu/SiteCollectionDocuments/EC-1831- 2003.pdf)

Roller S, Dea ICM. 1992. Biotechnology in the production and modification of biopolymers for foods. Critical Reviews in Biotechnology.;12(3):261–77.

Sandford PA, (1979) Exocellular, microbial polysaccharides. Advances in Carbohydrate Chemistry and Biochemistry 36:265–313

Sandven, P., 2000. Epidemiology of canidemia. Revista Iberoamericana de Micología, 17: 73-81.

Santos, F.L., G.M. DeAmorim, Biotechnological challenges and perspectives of using exopolysaccharides, Journal of Analytical & Pharmaceutical Research 7 (3) (2018) 264–266.

Sasidhara, R. and T. Thirunalasundari. 2012. Antimicrobial activity of mushrooms. Biomedicine 32:455–459.

Seviour RJ, SJ Stasinopoulos, DPF Auer, and PA Gibbs. Production of pullulan and other exopolysaccharides by filamentous fungi. Critical Review in Biotechnology. 1992; 12(3):279–98.

Sheppard. D.C., P.L. Howell, (2016) Biofilm exopolysaccharides of pathogenic fungi: lessons from bacteria, Journal of Biological Chemistry. 291 (24) 12529–12537

Singh P, R Wisler, R Tokuzen and W Nakahara (1974). Scleroglucan, an antitumor polysaccharide from *Sclerotium glucanicum*, Carbohydrate Research, 37, 245

Singh.rs, gaganpreet. ks and kennedy. j (2008), 'Pullulan: Microbial sources, production and applications', Carbohydrate Polymer, 73, 515–31.

Singla, R., M. Ghosh, and A. Ganguli. 2009. Phenolics and antioxidant activity of a ready-to-eat snack food prepared from the edible mushroom (*Agaricus bisporous).* Nutr Food Sci 39:227–234.

Smiderle, F.R., Olsen, L.M., Ruthes, A.C., Czelusniak, P.A., Santana Filho, A.P., Sassaki, G.L., Gorin, P.A.J., Iacomini, M. Exopolysaccharides, proteins and lipids in *Pleurotus pulmonarius* submerged culture using different carbon sources, Carbohydrate Polymers. 87 (2012) 368–376.

Sood, G., G. Sharma, S. Kapoor, and P.K. Khanna, 2013. Optimization of extraction and characterization of polysaccharides from medicinal mushroom *Ganoderma lucidum* using response surface methodology, The Journal of Medicinal Plants Research. 7 2323–2329.

Stachowiak, B. and J. Reguła. 2012. Health-promoting potential of edible macromycetes under special consideration of polysaccharides: A review. European Food Research Technology 234:369–380.

Steluti, R.M., E.C. Giese, M.M. Piggato, A.F.G. Sumiya, L.G. Covizzi, A.E. Job, M.S., Cardoso, M.L. Corradi da Silva, R.F.H. Dekker, A.M. Barbosa, (2004) Comparison of botryosphaeran production by the ascomyceteous fungus *Botryosphaeria* sp., grown on different carbohydrate carbon sources, and their partial structural features, Journal of Basic Microbiology. 44 480–486.

Suga, T., Shiio, T., Maeda, Y.Y., & Chihara, G. (1984). Antitumor activity of lentinan in murine syngeneic and autochthonous hosts and its suppressive effect on 3-methylcholanthrene-induced carcinogenesis. Cancer Research, 44(11), 5132- 5137.

Sutherland IW. 1994 Structure-function relationships in microbial exopolysaccharides. Biotechnological Advances; 12(2):393–448

Sutherland IW. Extracellular polysaccharides. 1996 In: Rhem HJ, Reed G, editors. Biotechnology Vol. 6. VCH, Weinheim;:615–57

Suzuki, I., T. Sakurai, K. Hashimoto, S. Oikawa, A. Masuda, M. Ohsawa, and T. Yadomae, (1991). Inhibition of experimental pulmonary metastasis of Lewis lung carcinoma by orally administered β-glucan in mice. Chemical and Pharmaceutical Bulletin (Tokyo), 39(6), 1606-1608.

Suzuki, M., T. Kikuchi, F. Takatsuki, and J. Hamuro (1994). Curative effects of combination therapy with lentinan and interleukin-2 against established murine tumors, and the role of CD8-positive T cells. Cancer Immunology, Immunotherapy, 38(1), 1-8.

Thomson, K.S. and E.S. Moland, 2000. The new blactamases of Gram-negative bacteria at the dawn of the new millennium. Microbes and Infection, 2: 1225-1235

Tseng, Y. H., J. H. Yang, and J. L. Mau. 2008. Antioxidant properties of polysaccharides from *Ganoderma tsugae*. Food Chemistry 107:732–738.

U.U. Nwodo, E. Green, A.I. Okoh, Bacterial exopolysaccharides:Functionality sand prospect, International Journal of Molecular Sciences 13 (11) (2012) 14002–14015.

Vandamme EJ, Bruggeman G, De Baets S & Vanhooren PT (1996). Useful polymers of microbial origin, AgroFood-Industry Hi-Tech, 5, 21-25

Vaningelgem, F., M. Zamfir, T. Adriany, and L. De Vuyst, (2004) Fermentation conditions affecting the bacterial growth and exopolysaccharide production by *Streptococcus thermophilus* ST111 in Milk-based medium, Journal of applied microbiology. 97 (6) 1257–1273.

Vannucci, L., J. Krizan, and P. Sima et al. 2013. Immunostimulatory properties and antitumor activities of glucans. International Journal of Oncology 43:357–364.

Veverka, M., T. Dubaj, E., Veverková, and P. Šimon, (2018). Natural oil emulsions stabilized by β-glucan gel. *Colloids and Surfaces a: Physicochemical and Engineering Aspects*, *537*, 390-398.

Villares, A., L. Mateo-Vivaracho, and E. Guillamon, (2012). Structural features and healthy properties of polysaccharides occurring in mushrooms. Agriculture, 2(4), 452-471.

Wang Y, McNeil B. Scleroglucan. Critical Reviews in Biotechnology. 1996;16(3): 185–215

Wang, H.X. and T.B. Ng, 2000. Quinqueginsin, a novel protein with anti-human immunodeficiency virus, antifungal, ribonuclease and cell-free translation inhibitory activities from American ginseng roots. Biochemical and biophysical research communications., 269: 155-159.

wasser .sp (2002), 'Medicinal mushrooms as a source of antitumor and immunomodulating polysaccharides', Applied Microbiology Biotechnology, 60, 258–74

Wasser SP, Weis AL (1999) Medicinal properties of substances occurring in Higher Basidiomycetes mushrooms: current perspectives. International Journal of Medicinal Mushrooms 1:31–62

Wasser, S. P. 2002. Medicinal mushrooms as a source of antitumor and immunomodulating polysaccharides. Applied Microbiology and Biotechnology 60:258–274.

Wasser, S.P. (2002). Medicinal mushrooms as a source of antitumor and immunomodulating polysaccharides. Applied Microbiology and Biotechnology, 60(3), 258-274.

Wasser, S.P. and A.L. Weis, 1999. Medicinal properties of substances occurring in higher Basidiomycetes mushrooms: Current perspectives (Review). Interational Journal of Medicinal Mushroom., 1: 31-62.

Wasser, S.P., 2002. Medicinal mushrooms as a source of antitumor and immunomodulating polysaccharides (minireview). Applied Microbiology and Biotechnology., 60: 258-274

Weng BBC, Lin YC, Hu CW, et al. Toxicological and immunomodulatory assessments of botryosphaeran (β-glucan) produced by *Botryosphaeria rhodina* RCYU 30101. Food and Chemical Toxicology. 2011; 49(4):910–6.

Willis, W.L. et al. (2009) Administration of mushroom extract to broiler chickens for bifidobacteria enhancement and Salmonella reduction. Journal of Applied Poultry Research. 18, 658–664

Wolff, E.R.S.E., Wisbeck, M.L.L. Silveira, R.M.M. Gern, M.S.L. Pinho and S.A. Furlan, 2008. Antimicrobial and antineoplasic activity of *Pleurotus ostreatus*. Applied Biochemistry and Biotechnology., 151: 402-412

Wu, F., H. Yan, X. Ma et al. 2011. Structural characterization and antioxidant activity of purified polysaccharide from cultured *Cordyceps militaris*. African Journal of Microbiology Research 5:2743–2751.

Xiang, Y., Xu, X., Li, J. 2012 Chemical properties and antioxidant activity of exopolysaccharides fractions from mycelial culture of *Inonotus obliquus* in a ground corn stover medium, Food Chemistry. 134 1899–1905.

Xiao Y, Hongmei L, Hong Y, Rugang Z (2007) Extraction immunocompetent sections of *Agaricus blazei* Murill polysaccharides by membranes technology. In: International conference on complex medical engineering, Beijing, China, 23-27 May 2007, pp 1734–1737. doi:10.1109/ICCME. 2007.4382044

XiaoPing, C., C. Yan, L. ShuiBing, C. YouGuo, L. JianYun, and L. LanPing. 2009. Free radical scavenging of *Ganoderma lucidum* polysaccharides and its effect on antioxidant enzymes and immunity activities in cervical carcinoma rats. Carbohydrate Polymers 77:389–393.

Xu L, S Wang (2005) The Ginkgo biloba extract concentrated by nanofiltration. Desalination 184:305–313

Xu, Y. 2001. Perspectives on the 21st century development of functional foods: Bridging Chinese medicated diet and functional foods. International Journal of Food Science and Technology 36:229–242.

Yamanaka, D., Y. Liu, M. Motoi, and N. Ohno. 2013. Royal Sun medicinal mushroom, Agaricus brasiliensis Ka21 (Higher

Basidiomycetes), as a functional food in humans. International Journal of Medicinal Mushroom 15:335–343.

Yanaki T, Kojima T, Norisuye T (1981) Triple helix of scleroglucan in dilute aqueous sodiumhydroxide. Polymer journal 153:1135–1143

Yanaki T, T Norisuye (1983) Triple helix and random coil of scleroglucan in dilute solution. Polymer Journal 15:187–396

Yang H, G He. 2008 Influence of nutritional conditions on exopolysaccharide production by submerged cultivation of the medicinal fungus *Shiraia bambusicola*. World Journal of Microbiology and Biotechnology.;24(12):2903–7

Yi HA, JC Panepinto, and A Jacobs. 2012 Inhibition of HIV entry by extracellular glucuronoxylomannan of *Cryptococcus neoformans*. Microbial Pathogenesis.;52(1):25–30

Yin Y, Y Hu, and F Xiong. 2011 Sorption of Cu(II) and Cd(II) by extracellular polymeric substances (EPS) from *Aspergillus fumigatus*. International Biodeterioration and Biodegradation.; 65(7): 1012–8.

Yuen, J. W. M. and M. D. I. Gohel. 2005. Anticancer effects of *Ganoderma lucidum*: A review of scientific evidence. Nutrition and Cancer 53:11–17.

Zakany, J., G. Chihara, and J. Fachet, (1980). Effects of lentinan on tumor growth in murine allogenic and syngenic hosts. International Journal of Cancer, 25(3), 371-376.

Zeman, M., V. Nosalova, P. Bobek, M. Zakálová, and S. Černá (2001). Changes of endogenous melatonin and protective effect of diet containing pleuran and extract of black elder in colonic inflammation in rats. Biologia, 56(6), 659- 701.

Zhang B, P Yan, H Chen, and J He. 2012 Optimization of production conditions for mushroom polysaccharides with high yield and antitumor activity. Carbohydrates Polymer; 87(4):2569–75.

Zhang, Y., H. Kong, Y. Fang, K. Nishinari, and G.O. Phillips, 2013. Schizophyllan: a review on its structure, properties, bioactivities and recent developments, Bioactive Carbohydrates. Dietary Fibre 1 53–71

Zhang, Y., X. Xu, and L. Zhang, (2008b). Gel formation and low-temperature intramolecular conformation transition of a triple-helical polysaccharide lentinan in water. Biopolymers, 89, 852e861.

Zhou, B.-L., Q. Liang, Y. Zou, J. Ming, and G.-H. Zhao, (2011). Research progress in prebiotic properties of edible mushroom. Food Science, 32(15), 303-307.

Zhu. H., S. Su., and S. Zhang, 2016. Enhanced production of total flavones and exopolysaccharides via Vitreo scilla hemoglobin biosysnthesis in *Phellinus igniarius*, Bioresource technology. 102 1747–1751

Zhu.d (1987), 'Recent advances on the active components in Chinese medicines', Abstr Chin Med, 1, 251–86.

EXPLORING THE CHEMICAL SPACE OF TUBULIN AND VARIOUS BINDING POCKETS: A DOCKING AND COMPUTATIONAL STUDY

Radhika Rani, Reetika Sahore, Avneet Saini*

Department of Biophysics, Panjab University, Chandigarh – 160 014 (India)

**Department of Biophysics, Panjab University, Chandigarh – 160 014, India*

ABSTRACT

Microtubules are important cellular targets in anticancer therapy. Microtubule inhibiting agents (MIAs) stabilize or destabilize microtubules, thereby suppressing microtubule dynamics requisite for appropriate mitotic function, efficiently blocking cell cycle progression and resulting in apoptosis. In spite of this significance, innate or acquired drug resistance to MIAs hampers their overall clinical usefulness. In the present study, virtual screening, docking and molecular dynamic studies (in NPT ensemble for 1ns at 300K) have been performed to shortlist desired ligands. Out of these, ligands 2, 7, 9, 13(3), 14 and 15 occupied the binding pocket near the taxol binding domain and five ligands, i.e. ligand 10, 11, 12, 13(1) and 17 lay near the colchicine binding domain. β-tubulin-ligand 7 complex was found to be most stable in taxol binding domain and β-tubulin-ligand 11 complex attained maximum stability in the colchicine binding domain even with respect to their corresponding β-tubulin complexes.

Keywords: Tubulin, Microtubule inhibiting agents (MIAs), Docking, Molecular Dynamics (MD)

INTRODUCTION

Tubulin is a highly conserved αβ dimeric protein present and is essential for all eukaryotes. αβ-Tubulin dimers assemble into microtubules, dynamic polymers important in a variety of functions, most noticeably, mitosis. Microtubule-inhibiting agents (MIA) currently used in clinic therapies work through the suppression of the microtubule dynamics by misdirecting the formation of a functional mitotic spindle in fast-dividing tumor cells. This arrests the cells in G2–M phase, thereby leading to apoptosis of the tumor cells, which is in contrast to those drugs acting on DNA for cancer chemotherapy. Based on their mechanism of action, MIAs are classified into two broad categories: microtubule stabilizing agents and destabilizing agents. Mechanistically all of these drugs bind to tubulin and prevent its polymerization into microtubules (e.g. vinca alkaloids) or cause excessive polymerization (e.g. taxanes) resulting in altered microtubule polymer mass and indiscriminate cell death in normal and tumor cells. These agents, most notably colchicine, colcemid, nocodazole, paclitaxel and the vinca alkaloids have played seminal roles in probing the basic mechanisms of mitosis, inhibit cell proliferation and induce cell death. Some of these compounds have been useful clinically in the management of a variety of neoplasms including, breast cancer, lung cancer, neuroblastoma, rhabdomyosarcoma, acute leukemia, Hodgkin‘s disease, and non-Hodgkin‘s lymphoma. In the last years, different mitotic regulators have been proposed as drug candidates for antitumor therapies. In particular, inhibitors of Cdks, Chks, Aurora kinase and Polo-like kinase have been synthesized and evaluated in vitro and in animal models and some of them have reached clinical trials. However, to date, none of these inhibitors has been approved for use in chemotherapy regimes. Despite the robust rate of discovery and the development of new mitosis-selective inhibitors, the unpredictable complexities of the human body‘s response to these drugs still herald the substantial limitations such as high systemic toxicity, poor water solubility and bioavailability, as well as complex synthesis and isolation procedures. Also, anticancer drugs have poor and highly variable oral bioavailability (Rowinsky, 1997). Another significant concern about anti-microtubule agents (MTA) is that these compounds cause significant side effects such as neutropenia and neurotoxicity. Even though the mechanism by which MTIs promote mitotic arrest is well understood, relatively little is known about how MTIs act in the context of a tumor and why drug sensitivity varies amongst different cancers, i.e. why taxol is effective against ovarian and mammary tumors but is ineffective against other solid tumors such as kidney and colon carcinomas. In addition, once a tumor becomes insensitive to a certain drug it will also show resistance to drugs whose structure and mechanism of action may be completely different (a phenomenon known as multi-drug resistance or MDR (Baguley, 2010). Drug sensitivity (inherent resistance) and the development of resistance during treatment are thought to be mediated by multiple mechanisms such as increased drug efflux, drug inactivation, mutations in the target protein and evasion of drug-induced damage or apoptosis (Fojo and Menefee, 2007; Perez, 2009). For all these

*Corresponding author: avneet@pu.ac.in

Received: May 20, 2021, Accepted: June 30, 2021

reasons, there is a constant demand for novel anti-cancer agents that could provide new treatment options by overcoming resistance mechanisms and, therefore, extending survival duration while minimizing toxicity and maintaining high quality of life. Despite numerous studies on antimitotic drugs, there is significant structural diversity amongst the large number of small molecules that have been reported as tubulin polymerization inhibitors. Thus, there is a need to explore the chemical space of tubulin and various binding pockets efficiently. The drug designing approach is extensive and thorough in its chemical space. Such studies aid the better understanding of unsolved problems of secondary toxicity and even multiple drug resistance.

METHODOLOGY

The 3-D structure of tubulin was obtained from protein data bank (PDB id- 1TUB).

LOCALIZATION OF BINDING SITE

CASTp: The CASTp web server aims to provide a comprehensive and detailed quantitative characterization of interior voids and surface pockets of proteins, which are prominent concave regions of proteins that are frequently associated with binding events. CASTp is based on the alpha shape and the pocket algorithm developed in computational geometry (Liang *et al*., 1998b).

Coach: COACH is a consensus approach to binding site prediction that combines the multiple prediction results of algorithms from TM-SITE, S-SITE, COFACTOR, FINDSITE and ConCavity. To generate a prediction, the query sequence along with the structure are provided as input and fed into the individual programs. The top-scoring predictions from each of the programs are combined using a linear SVM as implemented by the software SVM-light (Joachims, 2006). The results predicted by Coach are ranked according to their C-score. C-score is a confidence score for estimating the quality of predicted models by Coach. It is calculated based on the significance of threading template alignments and the convergence parameters of the structure assembly simulations (Yang *et al*., 2013).

VIRTUAL SCREENING

Molecular Docking: More than 40,000 binding poses were generated and the compounds were scored on the basis of their binding affinity. Binding energy is the sum of intermolecular energy and torsional free-energy (Batool*et al.*, 2013). All the heteroatoms of the tubulin PDB (1TUB) were removed. In the Vina Wizard of the PyRx software, the macromolecule (tubulin) and ligands (compounds) were selected. In the next step, search space was defined. The entire surface of protein was selected to perform blind docking. Once the calculations were done, results were displayed in a table with the binding affinity (kcal mol^{-1}) values. More negative the binding affinity, better the orientation of the ligand in the binding site. The maximum binding affinity with tubulin for any drug like compound from the library was -20.3 kcal mol^{-1}. All the ligands within 3 kcal mol^{-1} of the maximum binding affinity i.e. -20.3 kcal mol^{-1} to -17.3 kcal mol^{-1} were selected for further analysis.

MD SIMULATIONS

The system was constructed by placing the complex in the centre of the simulation box maintaining a distance of 1 nm from the wall of the box. The system was solvated with water and simple point charge (SPC) water model was used. Energy minimization using steepest descent algorithm was performed. Solvation was carried out by performing the position restrain for 20 ps. The Lennard-Jones interactions cut off was at 1.0 nm. Interaction parameters within the design sequence are taken from GROMOS-96 force field (Van Gunsteren *et al.*, 1996). MD simulation at 300 K for 1 ns, without any restrictions was carried out in a simple cubic periodic box under NPT with a time step of 2 fs using the leapfrog algorithm (Hockney and Eastwood, 1981). Temperature was controlled through weak coupling to a bath of constant temperature (Berendsen *et al.*, 1984) using a coupling time; τp of 0.1 ps. LINCS algorithm (Hess *et al.*, 1997) was used to restrict all bonds to their equilibrium lengths. The long range electrostatic interactions were calculated using a particle mesh Ewald summation (Essmann *et al.*, 1995) and updated every 10 fs during generation of the neighbor list. Initial velocities of all atoms were taken from a Maxwellian distribution at the desired initial temperature.

RESULTS AND DISCUSSION

Active sites of the target protein were predicted by Coach active site prediction tool. The feasible active sites predicted by the tool are as follows.

Binding Site Prediction

CASTp: All the annotated residues predicted by CASTp are given in Table 1 and also displayed in Figure 1. This table reports information about the position of the annotation on the sequence of the PDB structure, the three letter amino acid code of the annotated residue. The area of the pocket predicted by CASTp was 1177.2 $Å^2$ and the volume was 1330.4 $Å^3$. Thus, indicating that these residues offer larger area for the ligands to bind to them.

Table 1: CASTp results

Chain	Residue	Amino acid
A	142	Gly
	143	Gly
	144	Gly
	145	Thr
	146	Gly
	147	Ser
	148	Gly
B	142	Gly
	143	Gly
	144	Gly
	145	Thr
	146	Gly
	147	Ser
	148	Gly

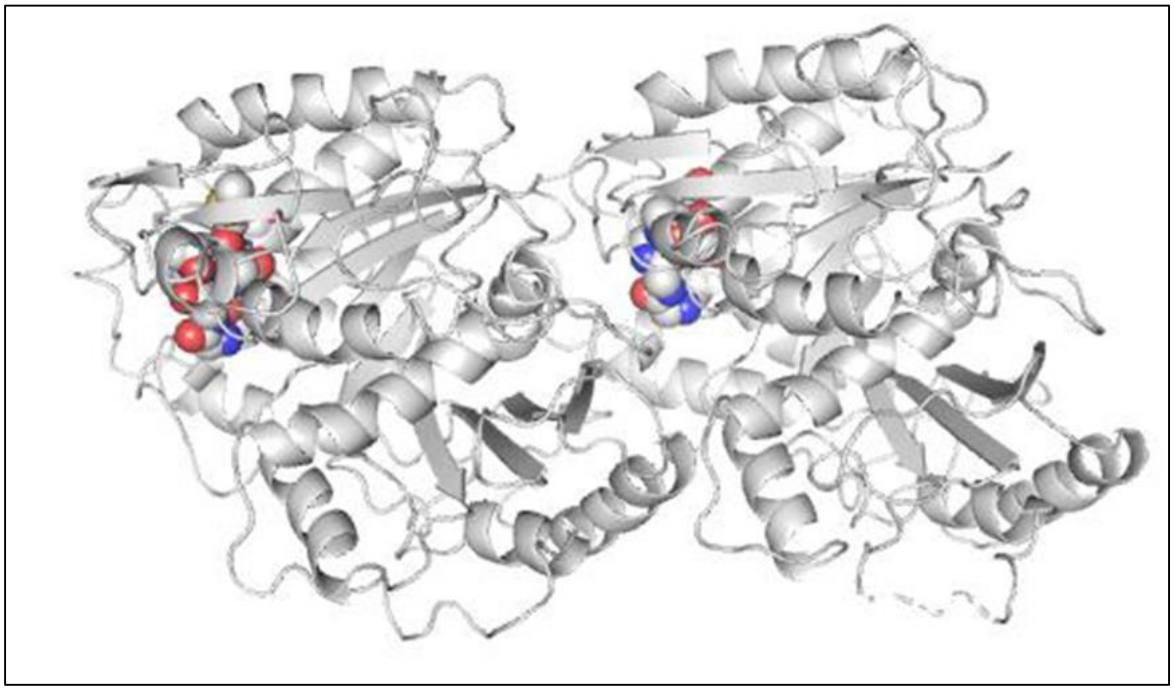

Figure 1: CASTp results (residues forming binding pocket are shown as spheres)

Coach: All the residues predicted by Coach were in A chain of tubulin. C-score is typically in the range of -5 to +2 where a C-score of higher value signifies a model with a high confidence and vice-versa. In total ten binding sites were predicted by Coach having C-score of 0.98, 0.07, 0.06, 0.05, 0.05, 0.04, 0.04, 0.03, 0.02 and 0.02. The pocket having highest c-score i.e. 0.98 (having highest confidence) was selected and the cluster size was predicted to be 310. All the residues were predicted to be present on A chain.

Table 2: Predicted residues by Coach

Residue No.	Amino Acid	Residue No.	Amino Acid
10	Gly	146	Gly
11	Gln	171	Ile
12	Ala	173	Pro
15	Gln	177	Val
16	Ile	178	Ser
100	Ala	182	Val
101	Asn	206	Asn
140	Ser	224	Tyr
143	Gly	227	Leu
144	Gly	228	Asn
145	Thr	231	Ile

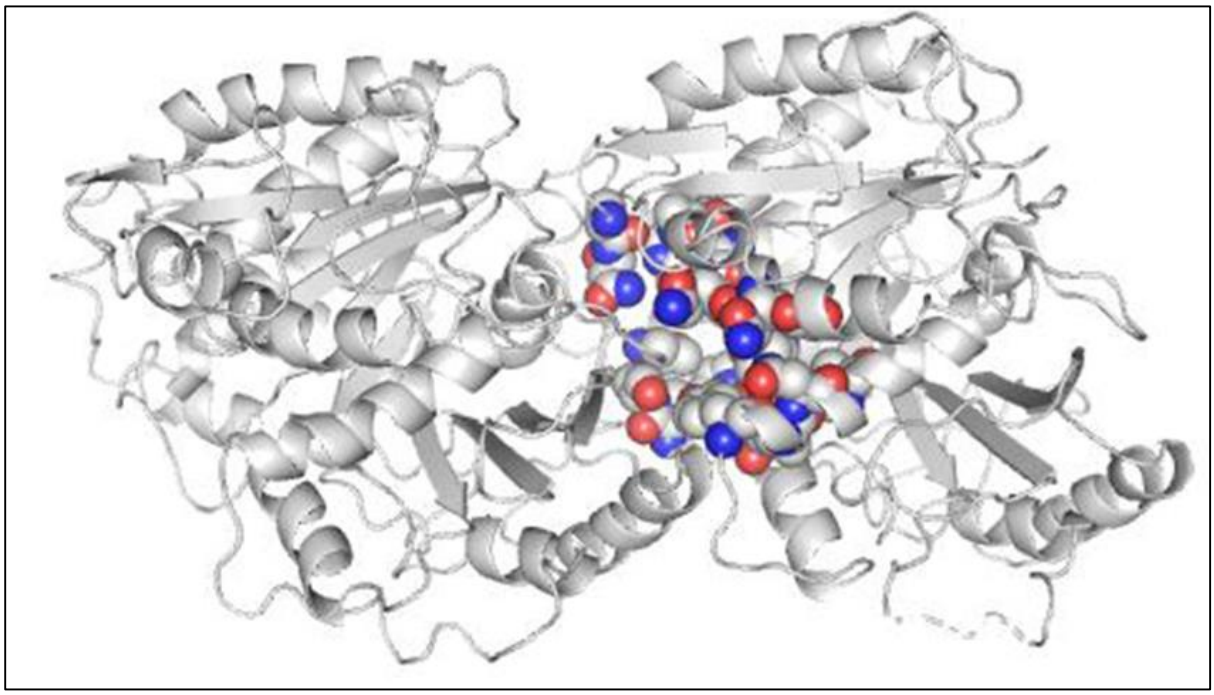

Figure 2: Coach results (residues forming binding pocket are shown as spheres)

Virtual Screening

Molecular Docking: The ChemDiv antimitotic library (ChemDiv, 2015) containing 10,665 diverse drug like compounds was screened against tubulin using AutoDockVina (Trott and Olson, 2010) in PyRx (Dallakyan and Olson, 2015). More than 40,000 binding poses were generated and the compounds were scored on the basis of their binding affinity (In publication). Multiple modes of binding were predicted for some compounds while for others only one mode was predicted. This is due to the use of blind docking technique that does not limit the docking site to one small area, but instead gives the possibility of finding the best binding site for the ligand on the entire surface of tubulin (Hetenyi and van der Spoel, 2002). All the binding modes of the selected ligands were analysed and the mode with the maximum affinity on the basis of binding energy values, was selected for a particular ligand. Further, the results of binding site and binding mode thus generated by AutoDockVina were then compared using PyMol. Wherever ligands bound to the same binding site but with different modes having comparable energy, the mode with maximum binding affinity was selected for further studies. On the basis of this screening, 30 ligands were selected (In publication).

The ligands (1-30) that showed a strong binding affinity with tubulin are a part of the ChemDiv antimitotic library (ChemDiv, 2015). The library was synthesized via high-throughput synthesis with multiple parallel library validations to design novel potential mitotic kinases-targeted ligands, particularly aurora kinase, polo- like kinase (plk1) and cyclin dependent kinase (Cdk). Therefore, the binding affinities of the ligands (1-30) against these kinases namely, aurora kinase A (pdb id- 1MQ4), polo-like kinase 1(pdb id- 2OU7) and cyclin-dependent kinases (pdb id- 1HCL) were also and clearly show that the binding affinity of these ligands with kinases is less than their binding affinity with tubulin by 3 kcal mol^{-1}. This implies that these drugs may act on multiple antimitotic sites in a synergistic manner or even be better suited as ligands against tubulin.

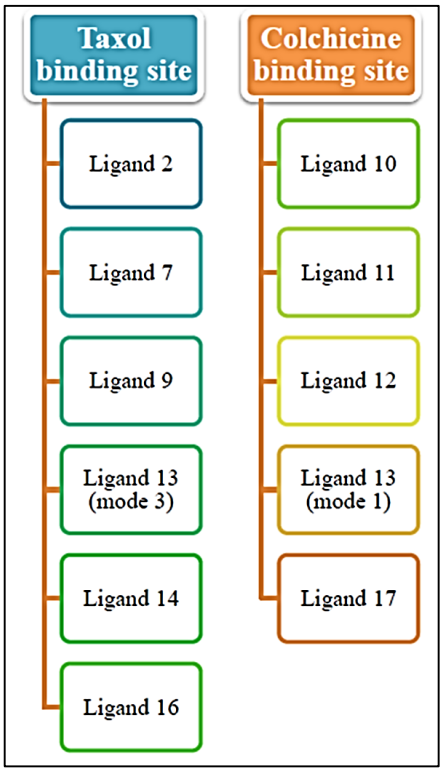

Figure 3: Classification of predicted binding site of the selected ligands

Non-Covalent Interactions

Analysis of the binding site of various shortlisted ligands (i.e. ligands 2, 7, 9, 10, 11, 12, 13, 14, 16 and ligand 17) revealed that ligands 2, 7, 9, 13 (mode 3), 14 and 15 bind to the taxane binding domain and ligands 10, 11, 12, 13 (mode1) and 17 bind to the colchicine binding domain (**Figure 3**).

Ligands binding to taxane binding site

The ligands bind to the taxol binding domain of β-tubulin with binding affinity in the range of -19.7 kcal mol^{-1} to -18.7 kcal mol^{-1}. Upon binding with tubulin, all the ligands occupy a residue basin situated between α helix H9 and M loop of β tubulin. The M loop in of β-tubulin is made up of residues Pro- 274, Leu- 275, Thr- 276, Ser- 277, Tyr- 278, Arg- 284. Unlike paclitaxel, these ligands do not form any strong contacts with β strands B8 and B9 of tubulin but some of them contact strand B7 with a distance of 3.5 Å. The side chains of residues lying in close proximity of these ligands are Leu- 275, Serine- 277, Arg- 278, Gln-282, Tyr- 283, Thr- 276 and Asp- 292 with a distance ranging from 2.4 Å to 4 Å.

Ligand 2 and β-tubulin complex is stabilized largely by lone pair-π interactions. The carbonyl oxygen of Thr- 276 (M loop) is involved in strong lone pair-π interactions with the 3, 4-dihydropyrido ring system of ligand 2 (dlp…π = 3.7 Å). Similarly, carbonyl oxygen of the Gln- 281 (M loop) is interacting strongly with the π electron cloud of the trimethylbenzene ring (dlp…π = 3.3 Å). It is interesting to mention here that trimethylphenyl cyclohexane carboxamide ring systems of ligand 2 are found to be mutually perpendicular to each other in the binding domain of the tubulin (**Figure 4**). Such an orientation is stabilized by another lone pair-π interaction involving carbonyl oxygen of the side chain of Glu 290 (helix H9) and lone pair of electrons of the same trimethylbenzene ring system (dlp…π 3.8 Å), thus holding the trimethylbenzene ring from the opposite site of Thr-276 (M loop).

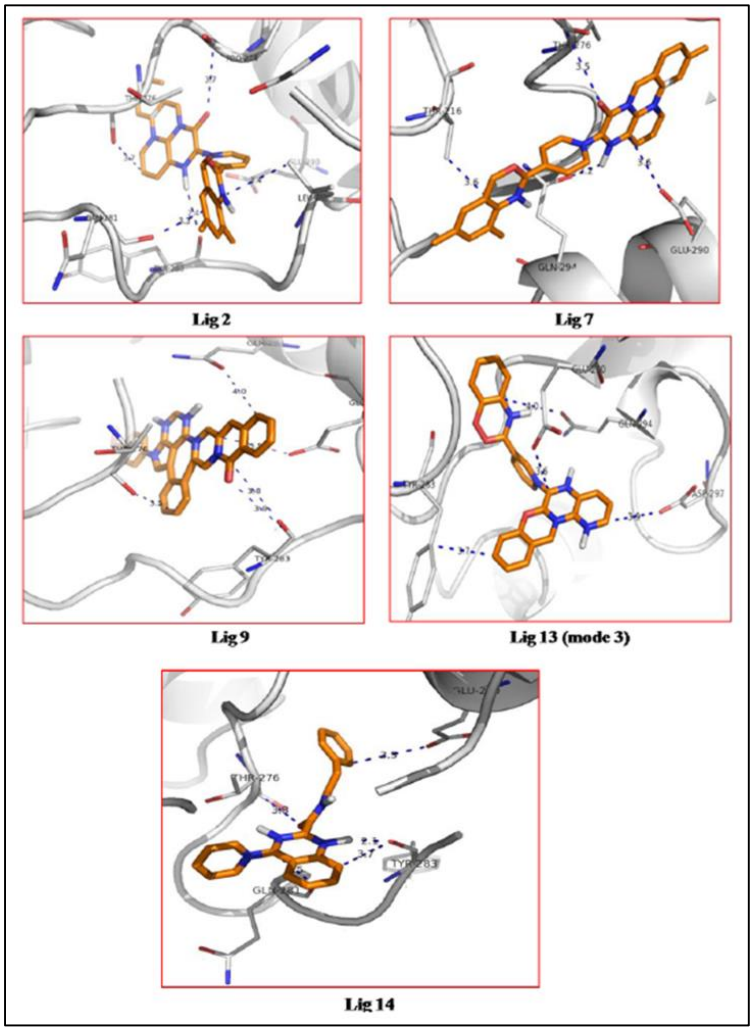

Figure 4: Lone pair-π interactions of ligands binding to taxol binding domain

Noncovalent interactions form the backbone of supramolecular chemistry and include hydrogen bonds (H-bonds), stacking, electrostatic, hydrophobic, and charge-transfer interactions as well as metal ion coordination (Lehn *et al.,* 1996). H…π interactions are expected simply from electrostatic arguments, a stabilizing effect of the interaction between a lone pair of electrons and the face of the π system (lp...π interaction) appears counterintuitive. Ab initio calculations (counterpoise-corrected, cc, MP2 (full)/ 6-31G**) revealed that for the water-hexafluorobenzene system the magnitude of the lp…π interaction (-2.1 kcal mol^{-1}) is comparable to that of the H,,,π interaction between water and benzene (-1.8 kcal mol^{-1}) (Lehn *et al.,* 1996). A more recent report using the cc-LMP2/6- 31+G* level of theory compared the H…π and lp…π interactions for the water-benzene complex; the energies are -2.7 and -0.6 kcal mol^{-1}, respectively (Reyes *et al.,* 2005). Clearly, the higher stability of the lp…π interaction between water and hexafluorobenzene as compared to the water-benzene system is due to the presence of electron-withdrawing fluorine atoms. These lone pair-π interactions have a great effect in stabilizing the structure of the protein.

Similar interactions were observed in case of ligand 7 which binds to β-tubulin with the binding affinity of -18.9 kcal mol^{-1}. The former is made up of seven ring system. Four of these rings sit in M loop of β-tubulin molecule and are in close proximity to residues Thr- 276, Ser- 277, Tyr- 283, Gln- 282 and Ala- 285 (at a distance ranging from 2.5 Å to 4 Å (**Figure 4**). The other three rings of ligand 7 are projected towards the H6 helix, so that both the subring systems lie in horizontal plane to each other.

In depth analysis reveals that β-tubulin and ligand 9 complex is stabilized largely by lone pair-π interactions. On close examination of this complex it is observed that the carbonyl oxygen of side chain of Glu- 290 (H9 helix) interacts with lone pair electrons of the piperazine ring of methylbenzoyl piperazine ring system ($d_{lp...\pi}$ = 3.5 Å). Also, the side chain carbonyl oxygen of Gln- 294 (H9 helix) interacts with the lone pair electrons of benzene ring of the same ring system ($d_{lp...\pi}$ = 3.5 Å). Lone pair-π interactions are observed in the case of β-tubulin and ligand 13 & of β-tubulin and ligand 14 complex also. the quinazoline ring of ligand 14 interacts with the carbonyl oxygen of the side chain of Tyr- 283 ($d_{lp...\pi}$ = 3.7 Å) and also the carbonyl oxygen of Gln- 281 ($d_{lp...\pi}$ = 3.5 Å) (**Figure 4**). The carbonyl oxygen of the side chain of Glu- 290 also interacts with the phenyl ring of ligand 14 ($d_{lp...\pi}$ = 3.5 Å) imparting stability to the ligand in the residue basin of β-tubulin.

Besides these lone pair-π interactions, carbonyl…carbonyl interactions and hydrogen bonds also imparts stability to the protein-ligand complex. The oxygen atom of piperidine carboxamide group of the ligand 2 is stabilizing itself through weak carbonyl-carbonyl interactions with the carbonyl carbon of Pro- 274 (M loop) ($d_{CO...CO}$ = 3.7 Å). Besides this, the carbonyl oxygen of Tyr- 283 (M loop) is involved in a weak hydrogen bond formation with amide hydrogen of 3, 4 dihydropyrido ring system ($d_{NH...OC}$ = 2.4 Å) and also with the lone pair-π with pyridine ring ($d_{lp...\pi}$ = 3.6 Å)

The importance of coulombic interactions between the backbone carbonyls in the proteins as a stabilizing factor in α-helices and β-strands is well documented (Maccallum *et al.,* 1995a; 1995b). These interactions also stabilize the partially allowed Ramachandran formations of asparagines and aspartic acids (Deane *et al.,* 1999). Helical structures without hydrogen bonds have been shown to stabilized by carbonyl…carbonyl interactions for peptides constructed from achiral and unusual amino acids like Aib and Δ^zPhe (Nandel *et al.,* 2001; 2003; 2005). The magnitude of these interactions is 4.4 kcal mol^{-1}; depending on the approach of carbonyl groups and is competitive with hydrogen bond, in terms of their stabilization energy (Nandel *et al.,* 2003; 2005).

Conformational analysis of the ligands binding to the taxol binding domain reveals that these ligands make contacts to Thr- 274, Thr- 276 and Gln- 281. Thus, it is concluded that ligands binds to the taxol binding domain but occupy a conformation different from the taxols.

Ligands binding near colchicine binding domain

Ligands bind to colchicine binding domain with the binding affinity ranging from -18.7 kcal mol^{-1} to -18.4 kcal mol^{-1}. These ligands occupy a cartesian space located between the B9 loop, B10 loop and H7 helix of β-tubulin and make close contacts with residues Gly- 237, Ala- 317, Cys- 356 and Lys- 254 with a distance ranging from 2.5 Å to 4.1 Å.

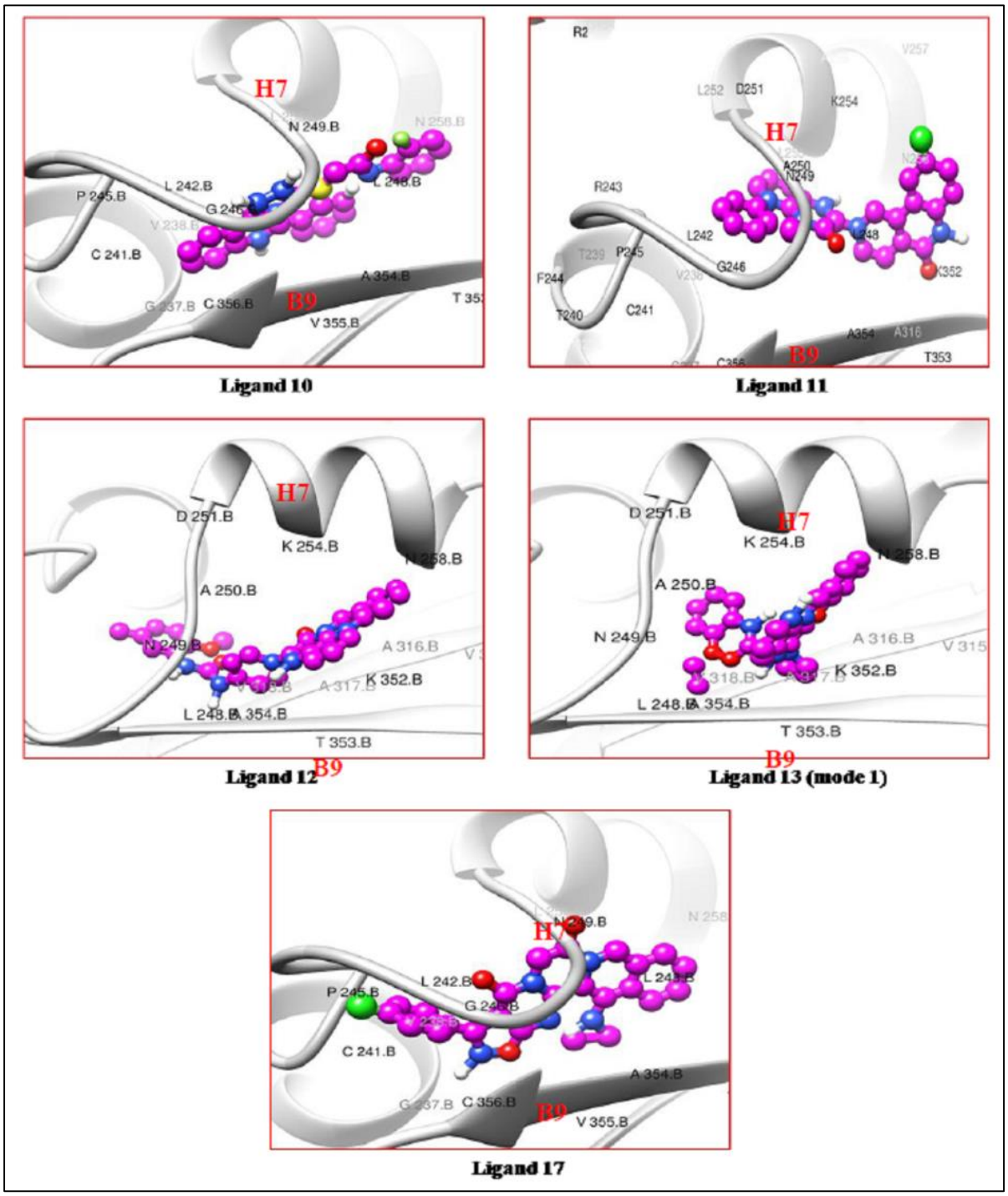

Figure 5: Binding of ligands to colchicine binding domain

The complexes of various ligands with β-tubulin are stabilized by number of interactions including lone pair-π interactions, stacking interactions, carbonyl…carbonyl interactions and hydrogen bonds. Ligands binding to the colchicine binding domain of β-tubulin include ligand 10, 11, 12, 13 (mode 1) and ligand 17. Lone pair interactions also impart stability to the ligands binding to the site near the colchicines binding domain and β-tubulin. In depth analysis of β-tubulin and ligand 10 complex reveals that this complex is stabilized by CH-π interactions, methyl moiety of Ala- 250 interacts with the lone pair electrons of the pyrimidine ring of ligand 10 ($d_{CH...\pi}$ = 4.1 Å), also methyl group of Ala- 354 interacts with the localized electrons of the pyrazine ring of ligand 11 ($d_{CH...\pi}$ = 2.6 Å). Apart from CH-π interactions, two carbonyl…carbonyl interactions impart stability to this complex (**Figure 6**).

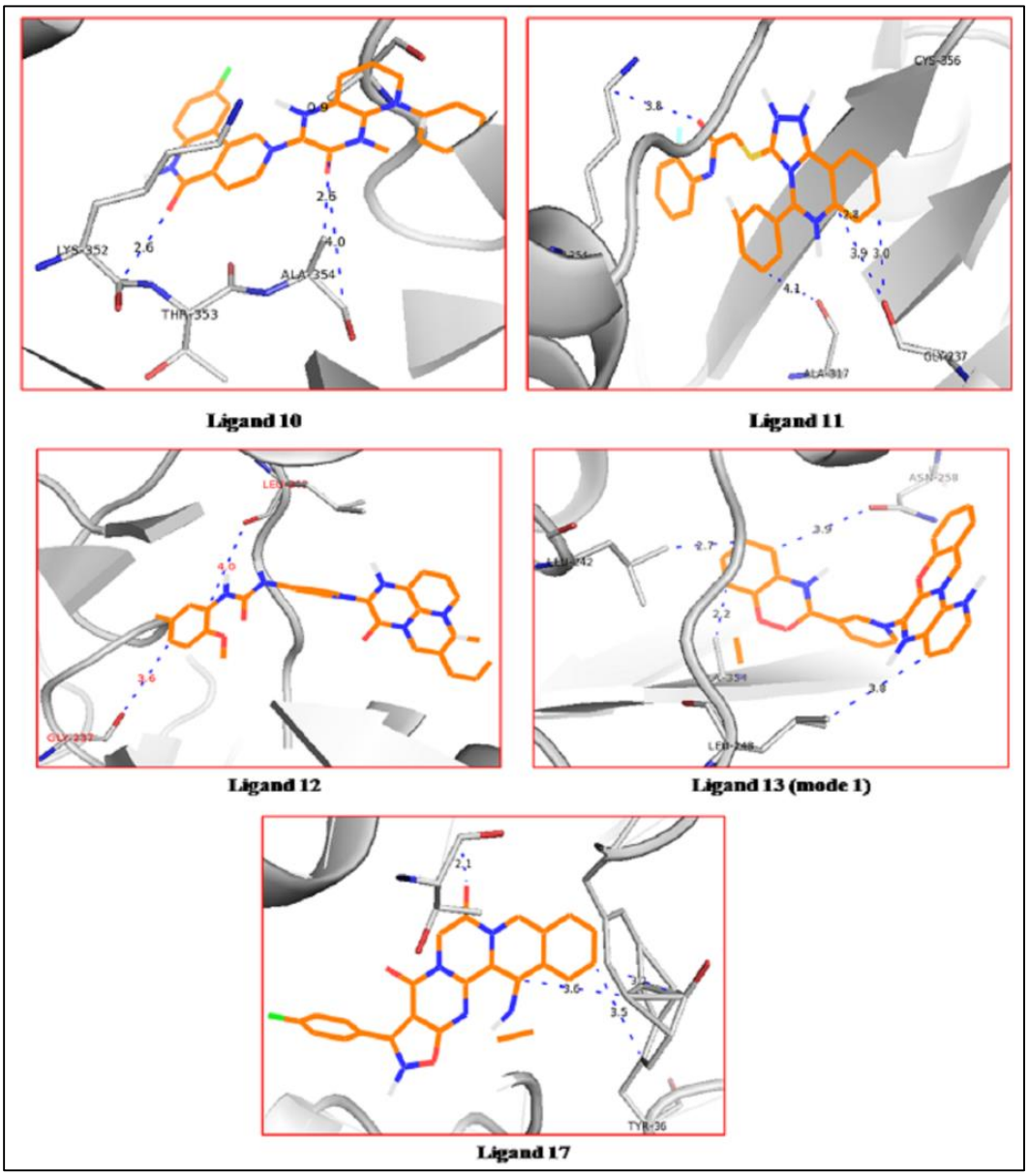

Figure 6: Interactions of ligands with the residues of colchicine binding domain

Similarly, thorough analysis of ligand 10 and β-tubulin complex reveal that it is stabilized by three lone pair interactions involving the quinazoline ring and phenyl rings of ligand 10 (**Figure 6).** It is observed that the backbone carbonyl oxygen of Gly-237 interacts with the lone pair electrons of both rings of quinazoline ring ($d_{lp...\pi}$ = 3 Å and 3.9 Å). The carbonyl oxygen of Ala- 317 stabilizes the delocalized electrons of the phenyl ring of ligand 10 ($d_{lp...\pi}$ = 4.1 Å) as shown in **Figure 6** and thus accounting for the greater stability of this ligand in the cartisian space of β-tubulin.

In case of β-tubulin and ligand 12 complex it is observed that the carbonyl oxygen of the side chain of residue Gln- 237 of β subunit of tubulin interacts with the delocalized electrons of the methoxyphenyl ring of ligand 12 ($d_{lp...\pi}$ = 3.6 Å). Ligand 13 binds both to tubulin binding domain as well as colchicine domain with comparable energy. Strong lone pair- π interactions play a major role in stabilizing the ligand 13 in the colchicine binding domain as shown in **Figure 6**.

Ligand 17 also stabilizes itself in β subunit of tubulin by the means of lone pair-π interactions. In depth analysis of β-tubulin and ligand 17 complex reveals that the carbonyl oxygen of side chain of Thr- 240 interacts with the lone pair electrons of the chlorophenyl ring of the ligand and thus stabilizing it in the cartisian space of β-tubulin. Also the benzene ring of ligand stabilizes itself by means of two strong stacking interactions, one with the phenyl

ring of Phe- 244 and other with the phenyl ring of the residue Tyr- 36 (d= 2.1 Å and 3.5 Å respectively).

MD SIMULATIONS

The aim of molecular docking is to achieve an optimized conformation for both the protein and ligand and relative orientation between protein and ligand so that the free energy of the overall system is minimized. To study various electrostatic interactions of water with different ligands in their respective binding domain, MD simulations were carried out under NPT conditions for 1ns. Plot of total energy vs. time (in ps) of ligands 2, 7 and ligands 10, 11 is shown in **Figure 7** and **Figure 8** respectively.

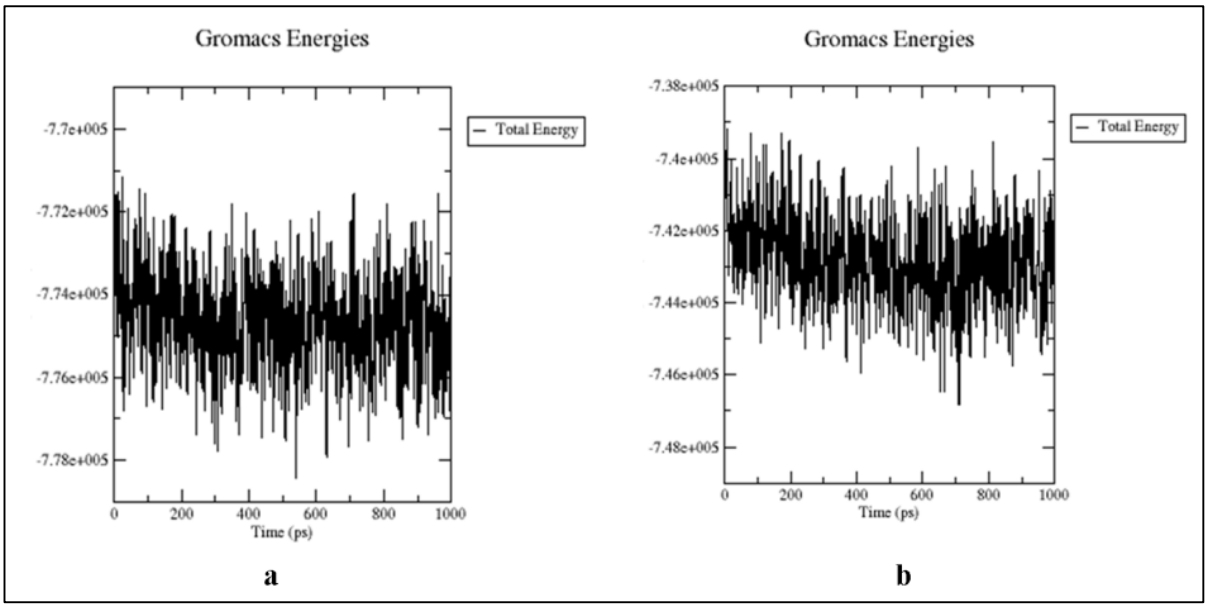

Figure 7: Energy of (a) ligand 2 and (b) ligand 7 in taxol binding domain

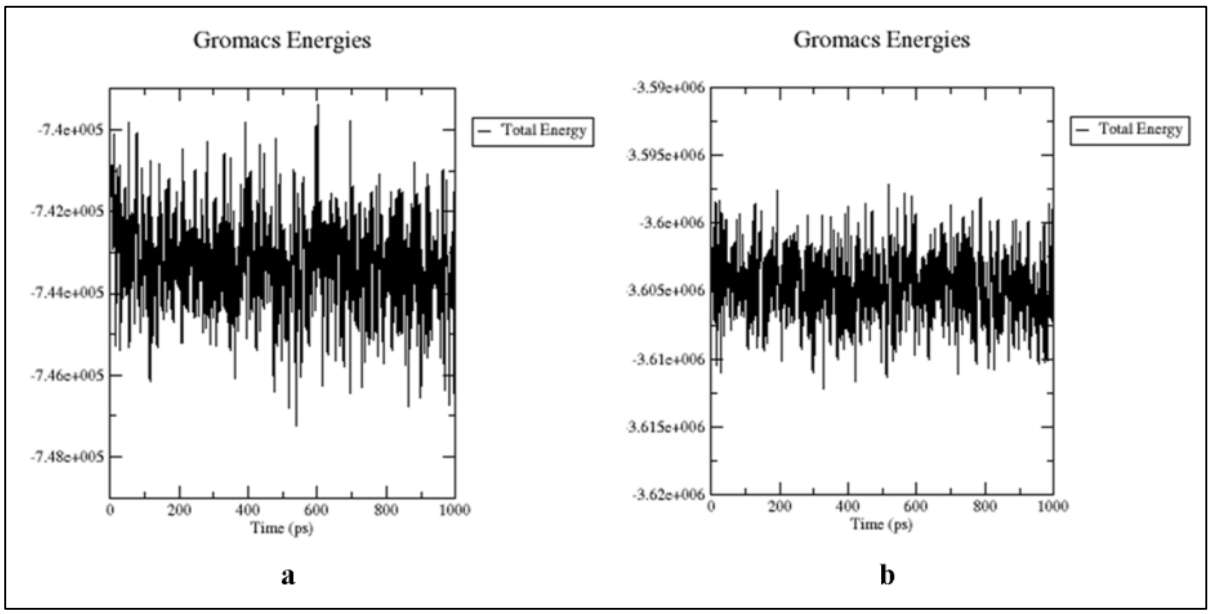

Figure 8: Energy of (a) ligand 10 and (b) ligand 11 in colchicine binding domain

It is evident that the protein-ligand complex has attained equilibrium and is more or less stable from 500 ps to 1000 ps of the simulation run. Therefore, the average structures were calculated. For the complexes 2, 7, 9, 13 (both modes), 14 and 15 the average structure was calculated over the last 350 ns of the trajectory and for complexes 10, 11, 12 and 17 it was calculated for the last 200 ns of the trajectory and total energy was computed and is shown in **Table 3**. It is evident that in the taxol binding domain, the β-tubulin-ligand 7 complex stands out of the group in terms of energy. Also, this complex is more stable than the β-tubulin-taxane complex.

Table 3: Total energy (kcal mol^{-1}) of ligands after simulation in water

Lig	Taxol Binding domain β -tubulin-tax complex	β-tubulin lig complex	Lig	Colchicine binding domain β-tubulin-col complex	β-tubulin lig complex
2	-2447.6	-2473.4	**10**	-2473.8	-2191.5
7	-3464.2		**11**	-2751.5	
9	-2241.8		**12**	-2651.8	
13(3)	-3016.1		**13(1)**	-2245.3	
14	-2307.1		**17**	-2311.6	
15	-2567.9				

Similarly, in the colchicine binding domain, the β-tubulin-ligand 11 complex attains maximum stability which is greater than the β-tubulin-col complex as well. The molecular view of the most stable protein-ligand complex in taxane and colchicine binding domains is shown in **Figure 9a** and **b**, respectively.

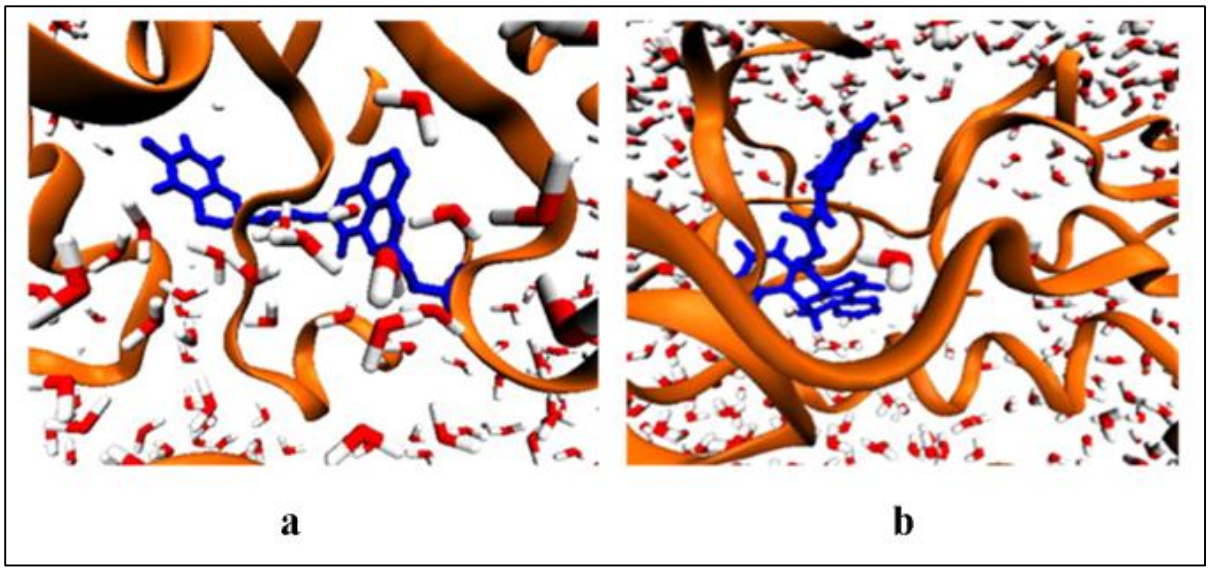

Figure 9: Molecular view of complex of (a) ligand 7 and (b) ligand 11 with β-tubulin complex in water after 1ns simulation studies.

Root-mean Square deviation (RMSD) calculation

RMSD plot indicates stablility a ligand is with respect to the protein and its binding pocket. Monitoring the RMSD of the protein gives insights into its structural conformation throughout the simulation. In order to monitor the conformational changes and stability of secondary structure elements, the backbone root mean square deviation (RMSD) scores are calculated. RMSD analysis indicates if the simulation has equilibrated- its fluctuations towards the end of the simulation are around some thermal average structure. As evident from **Figure 10**, the stabilities of the interactions were achieved in the atom positional RMSD with the values between 0.12 nm and 0.3 nm. During the first 600 ps of the simulation, the RMSD values of all ligands 7 and 11 increase up to 0.16 nm and the RMSD values of ligands 12 and 13 increase up to 0.2 nm.

After this time, the values of RMSD were maintained until the end of the simulation time, indicating greater stability till the end of simulation. It is suggested that changes of the order of 1-3 Å are perfectly acceptable for globular proteins (Baig *et al.*, 2014). Changes much larger than that, however, indicate that the protein is undergoing a large conformational change during the simulation. It is also important that the simulation converges- the RMSD values stabilize around a fixed value. If the RMSD of the protein is still increasing or decreasing on average at the end of the simulation, then the system has not equilibrated, and the simulation may not be long enough for rigorous analysis (Baig *et al.*, 2014). Thus, from RMSD analysis we can conclude that the complex of β-tubulin with both the ligands were stable in the simulation environment during the simulation time.

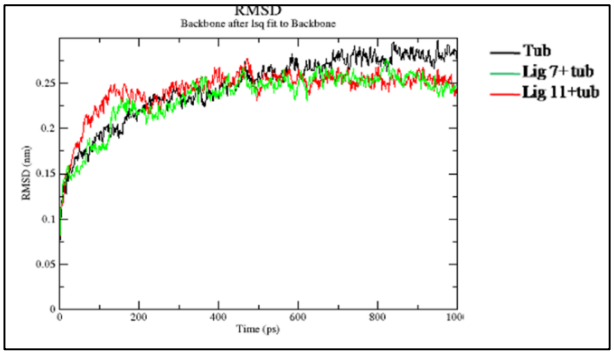

Figure 10: RMSD of different ligands with protein

Root Mean Square Fluctuation

RMSF essentially calculates the degree of movement of each Cα around its average position, implying regions of the protein that are highly flexible will show a large RMSF value while regions that are constrained will show up a low RMSF (Natarajan and Senapati, 2012). To examine the local structural transformations of β-tubulin when bound to the ligands in greater detail, the RMSF of each residue was calculated. The results were plotted against residue numbers based on the 1ns trajectory data and are shown in **Figure 11**.

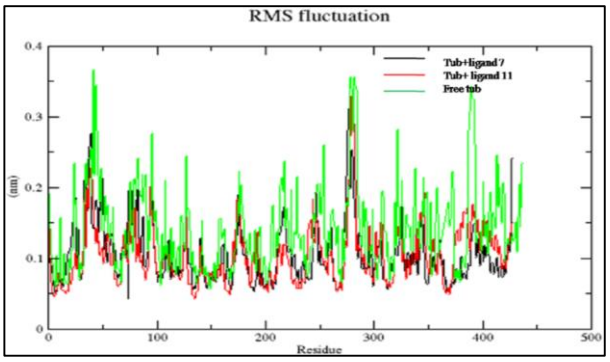

Figure 11: Root Mean Square fluctuation of free residues and tubulin-ligand complexes

It is observed that the fluctuation of 90% of the residues is in the range of 0.1nm - 0.15nm. It is also evident from **Figure 11** that the RMSF plots have shown similar flexibilities in all ligand complexes. In addition, the focused RMSF plots for four important amino acids in their active sites showed their potential flexibilities. These amino acids namely, Asn- 91, Gly- 95, Glu- 127 and Ile- 347 which have shown small flexibilities, which indicate their vital roles in active site. The RMSF values of Gly- 279 and Asp- 39 indicates the more flexibility of these residues.

The analysis of root mean square fluctuations (RMSF) of backbone atoms of β-tubulin in the absence and presence of inhibitors can be used as a reference to evaluate mobility of the residues. The results of the RMSF analysis of β- tubulin indicated that the main fluctuations (> 0.2 nm) correspond to residues belonging to mobile loops of the protein that are far from the ligand binding pocket. In contrast, residues that were found to interact with the ligands 7 in binding site of αβ-tubulin (Glu- 294, Asp- 297, Glu- 290, Thr- 216, Gln- 294, Thr- 276) are among one of the most stable residues of this protein (RMSF < 0.2 nm). Thus, it indicates that the binding to the ligand decreases the fluctuation of amino acids with critical roles in the ligand–protein interactions.

CONCLUSION

Based on virtual screening results, thirty compounds were selected and ADMET analysis was performed to obtain novel tubulin inhibitors having suitable pharmacokinetic properties (In publication). Eleven ligands that followed the Lipinski‘s rule of five were selected and their binding mode on tubulin heterodimer was evaluated. Out of these, six ligands, i.e. ligands 2, 7, 9, 13(3), 14 and 15 occupied the binding pocket near the taxol binding domain and five ligands, i.e. ligand 10, 11, 12, 13(1) and 17 lay near the colchicine binding domain. Further molecular dynamics simulations were carried out to have knowledge about the dynamic structure, interactions and stability of different protein ligand complexes in aqueous environment. The various complexes of β-tubulin and ligands obtained after energy minimization were simulated in NPT ensemble for 1ns at 300K and average structure was computed.

Based on energy calculations of the average structure of all the complexes, the most stable ligands for the taxol binding domain and for colchicine binding domain were selected. It was observed that ligand 7 and β-tubulin complex was the most stable in the taxol binding domain while the ligand 11 and β-tubulin was most stable in colchicine binding domain. On the basis of energy these complexes were found to be even more stable than the β-tubulin-taxol complex and β-tubulin-colchicine complexes respectively.

REFERENCES

Baguley, B.C. 2010. Multiple drug resistance mechanisms in cancer. Mol. Biotechnol., 46: 308-316.

Baig, T., H. Sheikh, and P.K. Tripathi. 2014. In-Silico Studies of Oncogene Protein with Anti-Cancer Drugs. Global J. Biotech. & Biochem., 9: 65-75.

Batool, S., S. Ferdous, M.A. Kamal, H. Iftikhar, and S. Rashid. 2013. In silico screening for Identification of Novel Aurora Kinase Inhibitors by Molecular Docking, Dynamics Simulations and Ligand-Based Hypothesis Approaches. Enzeng., 2 : 1-12.

Ben-Naim, A. 2002. Molecular recognition–viewed through the eyes of the solvent. Biophys. Chem., 101: 309–319.

Berendsen, H.J.C., J.P.M. Postma, A. DiNola, and J.R. Haak. 1984. Molecular dynamics with coupling to an external bath. J. Chem. Phys., 81: 3684–3690.

ChemDiv Antimitotic Library. http://www.chemdiv.com

Cheung, M., A. Garcia, and J. Onuchic. 2002. Protein folding mediated by solvation: water expulsion and formation of the hydrophobic core occur after the structural collapse. Proc. Natl. Acad. Sci., 99: 685–690.

Dallakyan, S. and A. Olson. 2015. Small-molecule library screening by docking with PyRx. Methods MolBiol., 1263: 243-250.

Deane, C., F. Allen, R. Taylor, and T. Blundell. 1999. Carbonyl-carbonyl interactions stabilize the partially allowed Ramachandran conformations of asparagine and aspartic acid. Prot. Eng., 12: 1025-1028.

Dunn, R.V. and R.M. Daniel. 2004. The use of gas-phase substrates to study enzyme catalysis at low hydration. Philos. Trans. R. Soc. Lond. B., 359: 1309-1320.

Essmann, U., L. Perera, and M.L. Berkowitz, et al. 1995. A smooth particle mesh Ewald method. J. Chem. Phys., 103: 8577–8592.

Fojo, T. and M. Menefee. 2007. Mechanisms of multidrug resistance: the potential role of microtubule-stabilizing agents. Ann. Oncol., 18: 3-8.

Halle, B. 2004. Protein hydration dynamics in solution: a critical survey. Philos. Trans. R. Soc. Lond. B., 359: 1207-1224.

Hess, B., H. Bekker, H.J.C. Berendsen, and J.G.E.M. Fraaije. 1997. LINCS: a linear constraint solver for molecular simulations. J. Comp. Chem., 13: 1463–1472.

Hetenyi, C. and D. Van Der Spoel. 2002. Efficient docking of peptides to proteins without prior knowledge of the binding site. Protein Sci., 11: 1729-1737.

Hockney, R.W. and J.W. Eastwood. 1981. Computer simulation using particles. McGraw-Hill, New York.

Lehn, J.M., J.L. Atwood, J.E.D. Davies, D.D. MacNicol, and F. Vogtle. 1996. Comprehensive Supramolecular Chemistry; Pergamon: Oxford, UK.

Li, Z. and T. Lazaridis. 2007. Water at biomolecular binding interfaces. Phys. Chem. Chem. Phys., 9: 573-581.

Maccallum, P.H., R. Poet, and E.J. Milner-White. 1995a. Coulombic interactions between partially charged main-chain atoms not hydrogen-bonded to each other influence the conformations of alpha-helices and anti-parallel beta-sheet. A new method for analyzing the forces between hydrogen bonding groups in proteins includes all the Coulombic interactions. J. Mol. Biol., 248: 361-373.

Maccallum, P.H., R. Poet, and E.J. Milner-White. 1995b. Coulombic attractions between partially charged main-chain atoms stabilize the right-handed twist found in most betastrands. J. Mol. Biol., 248: 374-384.

Nandel, F.S. and B. Khare. 2005. Conformation of peptides constructed from achiral amino acid residues Aib and Δ^zPhe: Computational study of the effect of L/D- Leu at terminal positions. Biopolymers, 77 : 63-73.

Nandel, F.S. and H. Kaur. 2003. Effect of terminal achiral and chiral residues on the conformational behaviour of poly Δ^zPhe and analysis of various interactions. Indian J. Biochem. Biophys., 40: 265-273.

Nandel, F.S., H. Kaur, N. Malik, N. Shankar, and D.V.S. Jain. 2001. Conformational study of peptides containing dehydrophenylalanine: Helical structures without hydrogen bonds. Indian J. Biochem. Biophys., 38: 417-425.

Natarajan, K. and S. Senapati. 2012. Understanding the Basis of Drug Resistance of the Mutants of αβ-Tubulin Dimer via Molecular Dynamics Simulations. Plos One, 7: 1-13.

Perez, E.A. 2009. Microtubule inhibitors: Differentiating tubulin-inhibiting agents based on mechanisms of action, clinical activity, and resistance. Mol. Cancer Ther., 8: 2086-2095.

Reyes, A., L. Fomina, L. Rumsh, and S. Fomine. 2005. Are water-aromatic complexes always stabilized due to π-H interactions? LMP2 study. Int. J. Quantum Chem., 104: 335-341.

Rowinsky, E.K. 1997. The development and clinical utility of the taxane class of antimicrotubule chemotherapy agents. Annu. Rev. Med., 48: 353-74.

Trott, O. and A.J. Olson. 2010. AutoDockVina: improving the speed and accuracy of docking with a new scoring function, efficient optimization and multithreading. J. Comput. Chem., 31: 455-461.

Van Gunsteren, W.F., S.R. Billeter, and A.A. Eising, et al. 1996. Biomolecular simulation: the GROMOS96 manual and user guide. Vdf Hochschulverlag AG an der ETH Zürich, Zürich, Switzerland, pp 1–1042.

Yang, J., A. Roy, and Y. Zhang. 2013. Protein-ligand binding site recognition using complementary binding-specific substructure comparison and sequence profile alignment. Bioinformatics, 29: 2588-2595.

EFFECTIVE OPTIMIZATION APPROACH FOR PREDICTING THE NUCLEOPHILICITIES OF ORGANIC MOLECULES: A MACHINE LEARNING APPROACH

Vaneet Saini,[a*] Aditya Sharma[a] and Dhruv Nivatia[b]

[a] *Department of Chemistry & Centre for Advanced Studies in Chemistry*
Panjab University, Chandigarh-160014, India
[b] *IT Department, University Institute of Engineering & Technology,*
Panjab University, Chandigarh 160014, India

ABSTRACT

Nucleophilicity of organic molecules is an important parameter for predicting reactivity and selectivity of organic reactions. Since experimental determination of nucleophilicity requires expensive resources, a machine learning approach can be an alternate way for accurate prediction of nucleophilicity. We have recently shown that this is possible with the aid of quantum mechanical descriptors trained on a neural network and tree-based algorithms. However, the hyperparameters associated with these algorithms need to be optimized to achieve the best accuracy. This can generally be achieved manually which is not always the best approach, and there is a possibility of missing out on the best parameters. Also, unbalanced distribution of the data and presence of anomalies can often lead to low accuracy. In this paper, we propose an effective data optimization techniques involving genetic algorithm, Isolation Forest, GridSearchCV which when applied to Random Forest model can help us achieve the optimal data set without compromising the accuracy.

Keywords: Nucleophilicity, Genetic Algorithm, IForest, GridSearchCV

INTRODUCTION

Predicting chemical properties of organic molecules is at the forefront of Al-guided cheminformatics approaches as intuition gained from these properties can help the organic chemist better understand the mechanism of organic reactions (Varnek & Baskin, 2012). These techniques have gaining popularity because of their ability to learn complex patterns and predict the trend with high accuracy at reasonable computational cost (Iype & Urolagin, 2019). A recent advancement in the field of data science is offering potential alternative to computationally expensive quantum chemical methods. However, the benefits of these Al-enabled approaches come at the cost of big data production as the algorithm requires huge amount of machine readable data in the form of features and observations in order to learn. Since, data availability is still a huge challenge and sometimes, we do need the help of these quantum chemical methods to generate enough data so as to efficiently train the machine learning (ML) model. These techniques provide significant advancement over the traditional methods as the trained model takes only fraction of a second to compute the properties of molecules (Faber, Lindmaa, von Lilienfeld, & Armiento, 2016).

Lately, ML has been widely used for predicting yields and enantioselectivities(Zahrt et al., 2019) of organic reactions. For example, Doyle's group has successfully deployed machine learning algorithm for predicting yields and reaction performance in deoxyfluorination reaction (Nielsen, Ahneman, Riera, & Doyle, 2018) and Buchwald-Hartwig cross-coupling reaction (Ahneman, Estrada, Lin, Dreher, & Doyle, 2018). The ML models were trained on the data obtained through high-throughput screening, which were then used for performance predictions. Additionally, feasibility prediction of an organic reaction has also been achieved using ML models trained on literature databases.(Schwaller et al., 2019). Moreover, ML has emerged as a predictive tool in plethora of fields such as drug discovery and design (Lipinski, Maltarollo, Oliveira, da Silva, & Honorio, 2019), material discovery (Butler, Davies, Cartwright, Isayev, & Walsh, 2018; Ryan, Lengyel, & Shatruk, 2018) and organic synthesis(Granda, Donina, Dragone, Long, & Cronin, 2018; Segler, Preuss, & Waller, 2018). Inspired by the latest achievement in the ML field for prediction of various chemical and physicochemical properties of organic molecules, we have recently published a neural network model for predicting the nucleophilicities of organic molecules(Saini, Sharma, & Nivatia, 2022). The experimental nucleophilicity N values were obtained from Mayr's database and quantum-mechanical and thermodynamic descriptors were computationally calculated (Phan, Breugst, & Mayr, 2006). Data was generated for 752 organic molecules which included 69 electronic, thermodynamic and steric descriptors. The nucleophiles were from diverse categories, for example, C-nucleophiles, H-nucleophiles, N-nucleophiles,

*Corresponding author: vsaini@pu.ac.in
Received: October 22, 2021, Accepted: December 21, 2021

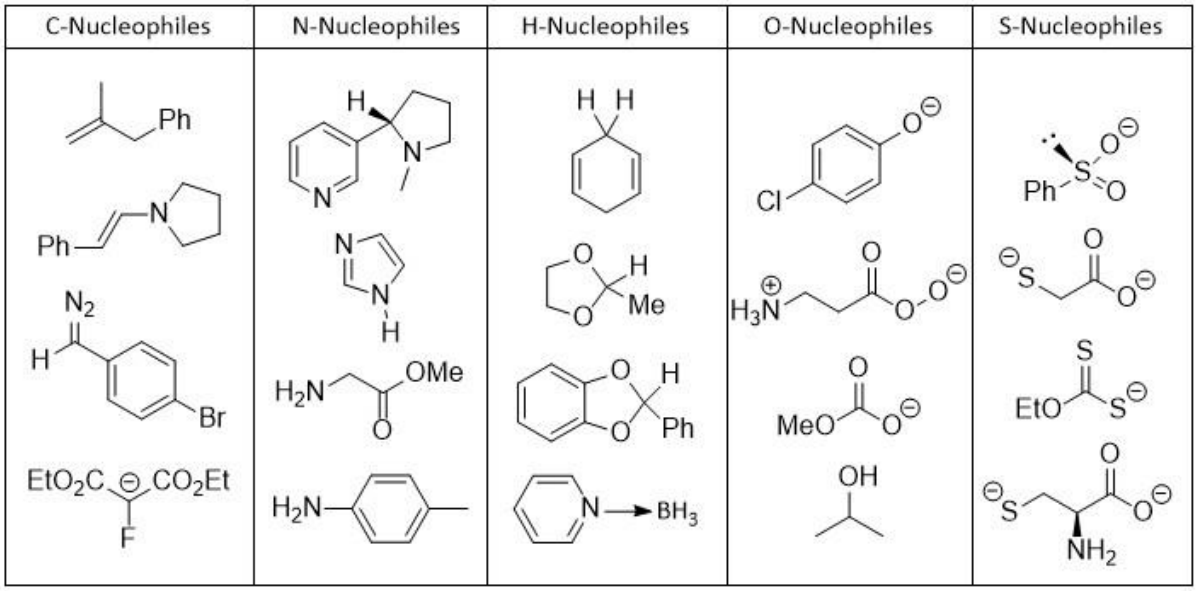

Fig. 1: Representative examples of different types of nucleophiles employed in this study.

O-nucleophiles and S-nucleophiles as shown in Figure 1. The nucleophilicity values for these nucleophiles are typically in the range of -9 to 31. Several machine learning algorithms were tested for this study such as multiple linear regression, support vector machines, K-nearest neighbors, random forest, extra tree, neural network, etc. Tree based models namely random forest and extra tree as well as neural network model were the best performing model which gave robust predictive power and accuracy.

In this report we showed the advantages of non-linear machine learning models over traditional linear regression models in predicting nucleophilicity of organic molecules. Selection of best model is practical rather than intuitive as all the available algorithms need to be tried and tested to identify the best performing model. This is a straightforward approach as there are only limited ML models which can be evaluated and initial guess can be obtained as to which model can be taken forward for further tuning. However, the challenge lies in fine tuning the model obtained from trial and error approach as it involves a variety of parameters, generally known as 'hyperparameters'. The approach for searching the optimal model parameters is known as 'hyperparameter tuning'. Manual hyperparameter tuning can be cumbersome and computationally expensive process as manual adjustments need to be applied over the course of many training runs to arrive at the optimal value. Therefore, in this report we present few efficient automated techniques, namely genetic algorithm, Isolation Forest (iForest) and GridSearchCV which would help analyze the optimal model architecture without manually exploring a range of possibilities. In brief the study is aimed at the use of optimization protocols to either increase the predictive power compared to the non-optimized methods or decrease the computational time as well increase the interpretability of the model.

Methodology

A)

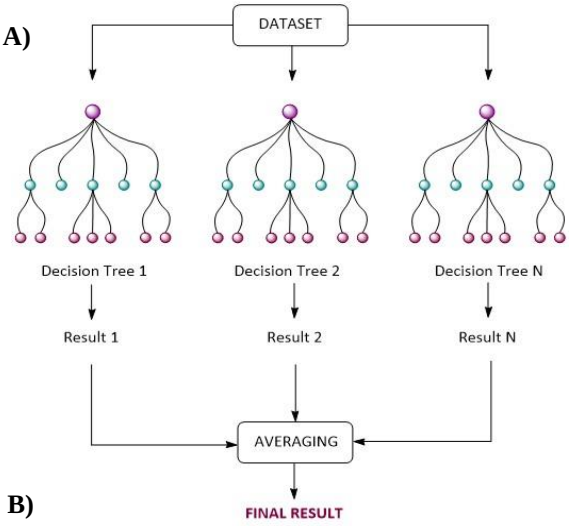

B)

Parameter	Description
ntree	The number of trees in the forest.
Mtry (max_features)	The maximum features in the forest when looking for the best split.
Max depth	Represents the depth of each tree in the forest.
Minimum sample split	Represents the minimum number of samples required to split an internal
Node size (Minimum sample leaf)	The minimum number of samples required to be at a leaf node.
Sample size (max_samples)	The maximum number of samples.

Fig. 2: A) General workflow of Random Forest Algorithm. B) Various Parameters of Random Forest Algorithm.

The dataset employed in our previous study was used for data sampling and hyper parameter tuning (Saini, Sharma, & Nivatia, 2022). This dataset consists of 752 data points and 69 quantum chemical descriptors. Random forest regressor (Breiman, 2001) was shortlisted for hyperparameter tuning as it was one of the best models for nucleophilicity predictions. Random forest uses stumps of decision trees and averages the results obtained from these trees in evaluating the final output (Figure 2). It contains a wide variety of hyperparameters that provides the opportunity to fine-tune many aspects of the model to reach the optimal value. Genetic algorithm(Whitley, 1994) is one of the powerful computational techniques for creating subsets of data, which can be fed to iForest algorithm (Liu, Ting, & Zhou, 2008) for the purpose of outlier detection or identification of best features. Genetic algorithm is inspired by human evolution, where the concept of genetics and natural selection is used to solve a problem. The general workflow of genetic algorithm is shown in Figure 3. Genetic algorithm generally starts with an initial random population of individuals which are binary strings of a particular length. Each string is referred to as a chromosome. Fitness function is used to evaluate each chromosome. The design of the genetic algorithm consists of three operators; selection, crossover and mutation. Selection is performed on the initial population after fitness scores of each chromosomes are evaluated. The chromosomes which represent better solution to a particular task are allowed to reproduce, whereas others are discarded. New population is generated with the aid of crossover and mutation. In crossover, two parent chromosomes are cut in half and swapped as shown in Figure 4. After crossover, mutation induces randomness in the new population.

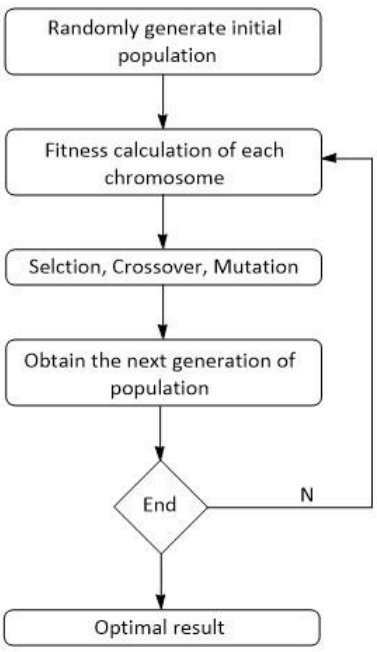

Fig. 3: General Workflow of Genetic Algorithm.

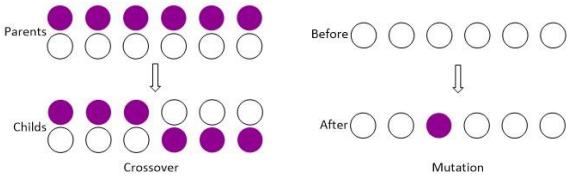

Fig. 4: Crossover and Mutation

RESULTS AND DISCUSSION

Data Sampling

Any data point which deviates significantly from other data points is known as an anomaly or an outlier. In this report the outliers are eliminated using Isolation Forest (iForest) algorithm(Liu et al., 2008) and the truncated dataset was evaluated using Random Forest (RF) regressor to obtain the optimal training set. IForest algorithm is a tree-based anomaly detection system with linear time complexity and high precision making it suitable to handle complex data. It is a type of unsupervised ML model which is based on the assumption that anomalies are "few and different". In this approach the dataset is divided into subsets and processed in a decision tree based on randomly selected features. The observations that have penetrated deep into the tree are less likely to be outliers, whereas samples that can traverse less distance and are confined to shorter trees are considered as anomalies. In this regression problem, coefficient of determination R^2 is used as criterial to determine the accuracy of the regressor.

Initial dataset which constituted 752 observations was split into training and test set, where test set constituted 10% of the observations. Before applying iForest training set was subjected to 10 fold cross-validation using RF model which gave R^2 score of 0.92. This was followed by model evaluation on test set which gave R^2 score of 0.91. After the application of iForest algorithm, 163 outliers were removed and we were left with 589 data points. The RF model was built using the truncated dataset and evaluated on the same test set which gave similar test score of 0.92.

Feature Selection

Initial dataset consisted of 69 independent features. Since there are 5 different types of nucleophiles and in order to include the impact of different types of nucleophiles on the nucleophilicity index values, label encoding was performed which converted these categorical features into numerical values. Therefore initial feature count was increased to 70. It is obvious that not all the features are significant in predicting

the nucleophilicity, therefore it is necessary to identify the best features. The identification of the best features or features which impact N values the most is crucial because it not only decreases the computational cost associated with model development but also increases the interpretability of the model. Therefore, in order to shortlist the best features GA(Elyan & Gaber, 2017) was used in combination with iForest algorithm which eliminated 34 features leaving us with 36 features, which were taken forward for model training and testing. Interestingly, the use of only 36 features gave similar test accuracy as suggested by the R^2 score of 0.91.

Hyperparameter Tuning

As already discussed RF provides the user with plenty of hyperparameters which can be fine-tuned to achieve the optimal accuracy. However, dealing with such a large number of parameters can be challenging especially if this task is performed manually. Nevertheless, there are plenty of automated techniques, which can be used to screen a variety of different parameters via permutation-combination in one go and sort out the best hyperparameters for the model. GridSearchCV is one such automated techniques which can be utilized for this purpose. The prerequisite is the initial specification of parameter values in the form of grid and all the possible combinations of parameter values are evaluated by GridSearchCV and the best combination is retained.

Table 1: Default, input and output hyperparameters used for GridSearchCV.

Entry	Parameters	Default values	Input grid	Output parameters
1.	Bootstrap	True	True	True
2.	Max_depth	None	[7,10,12,15,True]	12
3.	Max_features	auto	[auto, log2]	auto
4.	n_estimators	100	[100,150,120]	150
5.	min_sample_leaf	1	[1,2]	1
6.	min_sample_split	2	[2,1]	2

The range of hyperparametes which are tested using GridSearchCV along with default and output values are listed in Table 1. Random forest is a powerful ensemble machine learning technique which utilized bootstrap aggregation(Breiman, 1996) method for predictive analysis and provides more accurate predictions by avoiding overfitting/underfitting problem. Therefore, the "bootstrap" parameter is always turned on in the default and the search space provided. The parameter named "max_depth" captures the depth of each tree. Generally, greater the depth of the tree, better is the accuracy achieved by the model due to more information gained by the system. However, more depth also means more computational time and after a certain value the improvement remains unchanged. Considering both the computational time and accuracy in mind values between 7 to 15 were fed as input, and optimal depth came out to be 12. Maximum features allowed to be used at a time is represented by "max_features". The default value is *n*, no of features available. It means there are no restrictions imposed on the availability of features to the individual trees.

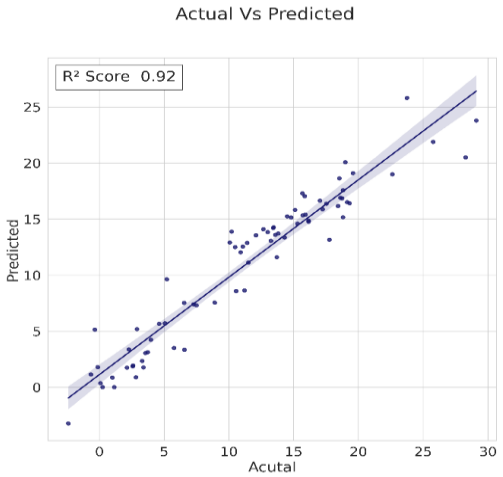

Fig. 5: Plot of experimental (actual) vs predicted nucleophilicities.

Resultant optimal feature length came out to be equal to the default value. Since, the output of random forest is based on average of the predictions made by individual trees, "n_estimators" deals with the number of trees need to be built before the averaging process. The parameters "min_sample_leaf" and "min_sample_split" represents minimum number of observations required to split an internal node and leaf node, respectively. The coefficient of determination R^2 for the test set on the random forest model trained using new hyperparametes came out to be 0.92 as shown in Figure 5. Of note, there is not much difference in the R^2 values for the random forest model built on tuned parameters compared to the default parameters ($R^2 = 0.91$) because the accuracy is already high for this dataset and there is marginal chance of improvement.

Table 2: List of nucleophiles with least error (1-4) and maximum error (5-8) between experimental and predicted nucleophilicity values.

Entry	Compound (Type of nuc.)	Experimental (N)	Predicted (N)	Residue
1.	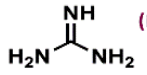 (N)	13.58	13.59	0.01
2.	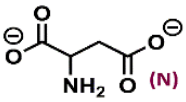 (N)	13.81	13.73	0.08
3.	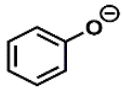 (O)	18.53	18.64	0.11
4.	 (C)	1	0.87	0.13
5.	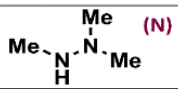 (N)	17.75	13.17	4.58
6.	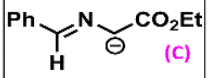 (C)	29.1	23.79	5.31
7.	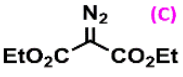 (C)	-0.35	5.15	5.5
8.	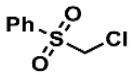 (C)	28.27	20.51	7.76

Analysis of the results reveal that the model has shown excellent predictive power with N-nucleophiles such as guanidine and aspartate ion (Table 2, Entry 1,2) with absolute error of 0.01 and 0.08, respectively. Whereas nucleophilicity of C-nucleophiles were difficult to predict as shown in Table 2 (Entry 6-8). For example, the predicted nucleophilicity values of chlro(phenylsulfonyl) methanide and diethyl diazomalonate were way off the actual experimental values as the absolute error values are 7.76 and 5.5 respectively. The average error for all the 76 predicted values is 1.58 which is excellent considering the diversity of nucleophiles used in this study.

CONCLUSION

In this report, we have described a data optimization approach for a chemistry based regression problem. First step of the optimization procedure consist of data sampling, where we initially started with 752 observations and obtained an R^2 of 0.91 on the test set after training the model on random forest. After applying iForest algorithm, we eliminated 163 observations and model trained on fewer data points provided similar predictive power without any deterioration of accuracy. For selecting relevant features, Genetic algorithm and iForest was used and total number of features were reduced to 36 from 70. Again, similar accuracy was achieved as suggested by R^2 value of 0.91. GridSearchCV was employed in the end to identify the best hyperparameters. It involved permutation -combination approach on all the input values and provides us with most optimal parameters. Infact, slight enhancement in the accuracy shows the importance of GridSearchCV for its potential application in obtaining optimized parameters for random forest model.

Data Availability

Dataset, code, predicted values are available at https://github.com/v-saini/Data-Optimization.

ACKNOWLEDGEMENTS

V. S. thanks Department of Science and Technology for DST-Inspire Faculty grant (DST/INSPIRE/04/ 2017/ 002529).

REFERENCES

Ahneman, D. T., J. G. Estrada, S. Lin, S. D. Dreher, and A. G. Doyle, (2018). Predicting reaction performance in C– N cross-coupling using machine learning. *Science*, *360*(6385), 186-190. doi:doi:10.1126/ science.aar5169

Breiman, L. (1996). Bagging Predictors. *Machine Learning*, *24*(2), 123-140. doi:10.1023/ A:1018054314350

Breiman, L. (2001). Random Forests. *Machine Learning*, *45*(1), 5-32. doi:10.1023/A:101 0933404324

Butler, K. T., D. W. Davies, H. Cartwright, O. Isayev, and A. Walsh, (2018). Machine learning for molecular and materials science. *Nature*, *559*(7715), 547-555. doi:10.1038/s41586-018-0337-2

Elyan, E., and M. M. Gaber, (2017). A genetic algorithm approach to optimising random forests applied to class engineered data. *Information Sciences*, *384*, 220-234. doi:https://doi.org/10.1016/j.ins.2016.08.007

Faber, F. A., A. Lindmaa, O. A. von Lilienfeld, and R. Armiento, (2016). Machine Learning Energies of 2 Million Elpasolite $(AB{C}_{2}{D}_{6})$ Crystals. *Phys.*

Rev. Lett., *117*(13), 135502. doi:10.1103/ PhysRevLett.117.135502

Granda, J. M., L. Donina, V. Dragone, D.-L. Long, and L. Cronin, (2018). Controlling an organic synthesis robot with machine learning to search for new reactivity. *Nature*, *559* (7714), 377-381. doi:10.1038/s41586-018-0307-8

Iype, E., and S. Urolagin, (2019). Machine learning model for non-equilibrium structures and energies of simple molecules. *J. Chem. Phys.*, *150*(2), 024307. doi:10.1063/1.5054968

Lipinski, C. F., V. G. Maltarollo, P. R. Oliveira, A. B. F. da Silva, and K. M. Honorio, (2019). Advances and Perspectives in Applying Deep Learning for Drug Design and Discovery. *Front. Robot. AI*, *6*. doi:10.3389/ frobt.2019.00108

Liu, F. T., K. M. Ting, and Z. Zhou, (2008, 15-19 Dec. 2008). *Isolation Forest.* Paper presented at the 2008 Eighth IEEE International Conference on Data Mining.

Nielsen, M. K., D. T. Ahneman, O. Riera, and A. G. Doyle, (2018). Deoxyfluorination with Sulfonyl Fluorides: Navigating Reaction Space with Machine Learning. *J. Am. Chem. Soc.*, *140*(15), 5004-5008. doi:10.1021/jacs. 8b01523

Phan, T. B., M. Breugst, and H. Mayr (2006). Towards a General Scale of Nucleophilicity? *Angew. Chem., Int. Ed.*, *45*(23), 3869-3874. doi:https://doi.org/ 10.1002/anie.200600542

Ryan, K., J. Lengyel, and M. Shatruk, (2018). Crystal Structure Prediction via Deep Learning. *J. Am. Chem. Soc.*, *140*(32), 10158-10168. doi:10.1021/ jacs.8b03913

Saini, V., A. Sharma, and D. Nivatia (2022). A machine learning approach for predicting the nucleophilicity of organic molecules. *Phys. Chem. Chem. Phys.*, *24*(3), 1821-1829. doi:10.1039/D1CP05072A

Schwaller, P., T. Laino, T. Gaudin, P. Bolgar, C. A. Hunter, C. Bekas, and A. A. Lee, (2019). Molecular Transformer: A Model for Uncertainty-Calibrated Chemical Reaction Prediction. *ACS Cent. Sci.*, *5*(9), 1572-1583. doi:10.1021/acscentsci.9b00576

Segler, M. H. S., M. Preuss, and M. P. Waller, (2018). Planning chemical syntheses with deep neural networks and symbolic AI. *Nature*, *555*(7698), 604-610. doi:10.1038/nature 25978

Varnek, A., and I. Baskin, (2012). Machine Learning Methods for Property Prediction in Chemoinformatics: Quo Vadis? *J. Chem. Inf. Model.*, *52*(6), 1413-1437. doi:10.1021/ ci200409x

Whitley, D. (1994). A genetic algorithm tutorial. *Statistics and Computing*, *4*(2), 65-85. doi:10.1007/BF00175354

Zahrt, A. F., J. J. Henle, B. T. Rose, Y. Wang, W. T. Darrow, and S. E. Denmark, (2019). Prediction of higher-selectivity catalysts by computer-driven workflow and machine learning. *Science*, *363*(6424), eaau5631. doi:doi:10.1126/science.aau5631

ESSENTIAL OIL BASED NANOEMULSIONS AS POTENT NANOWAGONS FOR DELIVERY OF HERBICIDES

Khushwinder Kaur[1,*] and Pervinder Kaur[2]

[1]*Department of Chemistry, Panjab University, Chandigarh, Punjab, India*

[2]*Department of Agronomy, Punjab Agricultural University, Ludhiana, Punjab, India*

ABSTRACT

Weeds are the major constraint to crop production. In addition to direct competition with crops for sunlight and nutrients, weeds also result in indirect damage by harboring pests and other pathogens. Globally 30% to 80 % loss of agriculture production is attributed to weeds and pests. Plant-derived substances, particularly essential oils have been an increasing interest in safe and environmentally-friendly application to crops as a powerful substitute to agrochemicals. Nanoemulsions formulated with essential oil can be used as herbicidal/pesticide formulations, however, the information available is scarce. They can contribute to the development of alternative tools for sustainable weed management by reducing the toxic effect and environmental pollution caused by man-made herbicides.

Key-words: Essential oil, Nanoemulsion, Herbicidal/pesticide formulations

INTRODUCTION

Essential oil (EOs) obtained from plants are of significant curiosity to food as well as agriculture scientists occupied in investigating and describing novel compounds and their functionalities. EOs and their components are natural molecules extracted from aromatic plants. Essential oils are usually produced by plant families such as *Araceae, Zingiberaceae, Pinaceae, Piperaceae, Lauraceae, Myrtaceae, Lamiaceae, Asteraceae, Rutaceae, Poaceae, and Cupressaceae*. The multi component nature of EOs enables them to act on numerous target sites, thus enabling them to work against otherwise resistant microorganisms. They process the inherent ability to inhibit the activity of various pathogens thus finding application in food, drug and agriculture industry. The properties of EOs depend on chemical composition, relative amounts and interactions of their constituents. They are GRAS (Generally Recognized As Safe). Despite of their significant potential they find restricted use in food and agriculture industry. This is due to volatilization, strong aroma and chemical instability (Raveau *et al*. 2020; Hancock *et al.* 2015; Bassole *et al.* 2012; Koul *et al.* 2018; Ravensberg 2015; Khater 2012; Mossa 2016). Therefore, agriculture and food scientists are at work to find solutions to harness the properties of EOs to the maximum extent.

To maximise the agriculture efficiency pathogens such as insects, fungi and particularly weeds need to be controlled. Weeds are the unwanted and undesirable plants growing with the main crop competing for food and light which adversely affects the natural farming. They account for almost 30 % of the total loss of crops in organic farming as they contaminate the plant with their seeds thereby causing problem for the next season. The use of chemical herbicides is an effective solution but is now being limited due to increased public concern on human health and environment. These problems have shifted attention to the development of alternative weed control technologies that are based on natural products. This involves allelopathy *i.e.* use of herbicides obtained from natural products such as bialaphos and phosphonthricin, use of triketones, terpenoids, *etc* (Vyyaan 2002). One of the best natural herbicides are EOs. They are recently being exploited as natural bioherbicides due to low toxicity, non-groundwater pollution and non-persistence in the soil (Isman 2000). Although research is being carried out to study the herbicidal potential of EOs but it is limited. Only a few studies have focused on evaluating the herbicidal prospects of plant extracts and EOs. This includes the work of (Bari *et al.* 2017; Campiglia *et al.* 2007; Hazrati *et al.* 2018; Frabboni *et al.* 2019; Nikolova *et al.* 2018; Synowiec *et al.* 2017). Further the mechanism of action of EOs is unclear and is still being widely explored by scientists. It is believed that some components of EOs – such as carvacrol, thymol, α- and β-pinene, 1,8-cineole, borneol, limonene, and camphor have strong inhibitory activity on seed germination which is found to be dependent on specific species (Abd-ElGawad *et al.* 2021). Further, in many cases the chemical constituents of EOs work synergistically to improve effectiveness and improve pollination. The advantage of using EOs for weed control is that they are environmentally safe and human friendly. They show low toxicity to non-target organisms and degrade rapidly in the environment.

*Corresponding author: makkarkhushi@gmail.com

Received: November 15, 2021, Accepted: December 25, 2021

Since every coin has two sides, there are some the disadvantages of applying EOs in crop protection. This is because EOs of one species has great variability in its composition due to climatic conditions, geographic and genetic factors. The method of extraction and stage of harvest has significant effects. They sometimes have pungent odour and usually degrade rapidly. They are highly volatility which makes them safe for the environment, is at the same time a disadvantage (Harley *et al.* 2004). Therefore, the area needs focus and recent studies have been depicts that most of the problems associated with EOs can be solved through the application of nanotechnology.

Nanotechnology is one of the pre-eminent ways to increase the stability and bioavailability of EOs. This includes spray drying, coacervation, solid lipid nanoparticles and nanoemulsions (NEm) to potentially improve the stability and biological activity of EOs. Since colloidal dispersions are heterogeneous systems where inner phase is dispersed into continuous phase; they are referred to as are the versatile tools for encapsulating and stabilizing EOs (Prakash *et al.* 2018). The present mini review will focus on the encapsulation of EOs in NEms and exploring the herbicidal potential.

NEms are defined as oil-in-water (o/w) emulsions with mean droplet diameters ranging from 50 to 1000 nm (Sneha *et al.* 2022; Batish *et al.* 2004). They are transparent/translucent systems that can't be formed spontaneously by simple mixing. They are kinetically stable non-equilibrium systems having high solubilisation capacity for lipophillic components. They offer better resistance to droplet collisions induced by Brownian movement. Simple mixing, grinding, colloidal mills, static mixers, etc. are some of the conventional methodologies that were practiced to generate emulsions. Since NEms not formed spontaneously, they are thermodynamically unstable and unfavourable systems. This is attributed to positive free energy change associated with forming the oil–water interface. They have the tendency to break down over a period of time due to gravitational separation, flocculation, coalescence, and Ostwald ripening (McClements *et al.* 2007). This is also observed in case of conventional emulsions obtained by mixing. However, the rates at which these processes occur are often considerably different in NEms than in conventional emulsions because of particle size and curvature effects. NEms are often more stable to gravitational separation, flocculation and coalescence, but are less stable to Ostwald ripening. A major focus of emulsion scientists, therefore, is to create NEms that have a sufficiently long kinetic stability suitable for commercial applications. The kinetic stability of NEms can be improved by controlling their composition (e.g., oil, surfactant and water phase) and microstructure (e.g., particle size distribution), or by incorporating additives known as stabilizers such as emulsifiers, texture modifiers, weighting agents or ripening retarders (Kabalnov *et al.* 2021; Guzey *et al.* 2006).

Various physicochemical properties of the droplets such as droplet size, size distribution, morphology and viscosity greatly impact the agricultural characteristics of NEms and thus, the formulation of extremely fine emulsion droplets continues to be a challenge. The fabrication of a formulation with uniform droplet size along with the selection of its preparation method plays a pivotal role in the agriculture industry (McClements 2005). NEms are usually fabricated by means of low or high energy emulsification approaches. Low energy emulsification method relies upon the alteration in the chemical or environmental conditions of the system resulting in spontaneous formation of tiny oil droplets. These include spontaneous emulsification, phase inversion temperature (PIT), phase inversion composition (PIC), and emulsion inversion point (EIP) methodologies. High energy emulsification method requires input of energy to produce disruptive forces that mechanically breakup large oil droplets into fine droplets suspended within the aqueous phase. Commonly used high energy techniques for the preparation of NEms include high pressure homogenization, microfluidization and probe ultrasonication (McClement 2004).

Both high and low energy methods are used to design agrochemical formulations. However, when the common emphasis is laid on a low energy emulsification method where chemical potential is generated through the use of surfactants. There are certain limitations that accompany this method. This involves the use of a large quantity of surfactant, high polydispersity index (PDI), which brings about instability after long term storage. The other method reported in literature is high energy homogenization method which basically involves two steps. In the first step, a high speed blender prepares a coarse emulsion by homogenizing the aqueous and organic phases for two minutes. Secondly, the prepared coarse emulsion is instantly passed through a high pressure homogenizer. Recently, ultrasonication has gained popularity since homogenization method is quite expensive and sensitive. The ultrasonication

cavitation method allows us to obtain a more stable NEms with reduced rate of Ostwald ripening than those prepared using PIT method. The high energy input generated from the micro-turbulent implosions of cavitation bubbles provides enormous forces to deform and break-off the droplets into nanometer scale (provided the Laplace pressure is overcome). It has been found that the ultrasonically-generated NEms have much smaller droplets with improved physical stability than the ones prepared by homogenizer. Though microfluidizer can be employed to obtain NEms with much smaller droplet sizes, a comparative study unfolded that microfluidization is not as convenient as ultrasound probe sonication (Hu *et al.* 2017). The use is much easier as it is free of line blockage and is easy to clean while the contamination of materials poses a limitation in case of microfluidizer. All the above facts stand in favour of ultrasonic cavitation as the most effectual and propitious methodology for the production of agrochemical NEms (Mcclements McClements 2012).

NEms have therefore become a promising tool in handling storing and stabilising EOs within the oil phase and exploiting the effect of these on plants as crop protecting agents.

Literature reports on EOs having herbicidal activities

This section provides a short overview of the latest studies that have been carried out to investigate the efficiency and efficacy of EOs in weed control and management. Table 1 reports the EO that have been investigated for herbicidal potential.

Table 1: Examples of EOs acting against weeds

S. No.	Essential oil	Active component	Weeds	Reference
1	Asteraceae	Aertemisia ketone	*Amaranthus retroflexus, Setariaviridis*	Weeds for weed control: Asteraceae essential oils as natural herbicides, 2017
2	Moldavian dragonhead	Geranyl acetate	*Bromus tectorum*	Phytotoxic activity of Moldavian dragonhead (*Dracocephalummoldavica* L.) essential oil and its possible use as bio-herbicide, 2022
3	Denaei Thyme	thymol (20.8-60.5 %) and carvacrol (20.1-63.4 %) a	*Amaranthus retroflexus, Avenafatua, Datura stramonium and Lepidium sativum*	Essential Oil Compositions and Natural Herbicide Activity of Four Denaei Thyme (Thymus daenensis Celak.) Ecotypes, 2014
4	clove (*Eugenia caryophyllus* (Spreng.) Bullock & S.G. Harrison) and pine (*Pinus sylvestris* L.)	Eugenol, then eugenyl acetate and β-caryophyllene	*Winter oilseed rape and maize*	Effect of selected essential oils on the efficacy of volunteer oilseed rape control and phytotoxicity in maize plants, 2022
5	Thymol Chemotype *Origanum vulgare L.*	Thymol (76%)	*Triticum aestivum and Hordeum vulgare*	Thymol Chemotype Origanum vulgare L. Essential Oil as a Potential Selective Bio-Based Herbicide on Monocot Plant Species, 2020
6	Anise (*Pimpinella anisum L.*)	Anethole<trans>	*Anagalis arvensis and Malva parviflora*	Using Anise (Pimpinella anisum L.) Essential Oils As Natural Herbicide, 2020
7	*Carum carvi L.* essential oil	Carvone and Limonene	*Echinochloa crus-galli*	Carum carvi L. essential oil: A promising candidate for botanical herbicide against Echinochloa crus-galli (L.) P. Beauv. in maize cultivation, 2019
8	*Satureja hortensis L*	Carvacrol	*tomato (Lycopersicon*	A natural post-emergence herbicide

		(52.55%), γTerpinene (30.21%)	*esculentum Mill.) and amaranth weed (Amaranthus retroflexus L.)*	based on essential oil encapsulation by cross-linked biopolymers: characterization and herbicidal activity, 2020
9	Oregano and Rosemary	Carvacrol (57.01), γ-Terpinene (8.77%) and 1.8-Cineole (21.45%), Camphor (19.70%),	*Chamomile (Matricaria chamomilla L.)*	Bio-Herbicidal Effects of Oregano and Rosemary Essential Oils on Chamomile (Matricaria chamomilla L.) Crop in Organic Farming System, 2019
10	Eucalyptus citriodora	Citronellal and citronellol	*Sonchus arvensis, S. oleraceus, Xanthiumstrumarium, A. fatua*	Allelopathic Effect of Eucalyptus citriodora Essential Oil and its Potential Use as Bioherbicide, 2018
11	*Eucalyptus gunnii* and *E. pulverulenta*	1,8-cineole (75%)	*Lolium multiflorum, Portulaca oleracea*	Eucalyptus gunnii and Eucalyptus pulverulenta 'Baby Blue' Essential Oils as Potential Natural Herbicides, 2021
12	Savory	Carvacrol (52.55%)and γ-terpinene (30.21%)	*Amaranth and tomato*	Development of pre-emergence herbicide based on Arabic gum-gelatin, apple pectin and savory essential oil nano-particles: A potential green alternative to metribuzin, 2021
13	*Cuminum cyminum, Mentha longifolia* and *Allium sativum*	α pinene, limonene and trans-piperitone epoxide, piperitenone oxide and diallyl trisulfide, diallyl disulfide	*Rumex crispus L. and Convolvulus arvensis L.*	Herbicidal and Fungicidal Effects of Cuminum cyminum, Mentha longifolia and Allium sativum Essential Oils on Some Weeds and Fungi, 2018
14	*Foeniculum vulgare* Mill.	α-pinene	*Portulaca oleracea L. and Amaranthus retroflexus L.*	Weed management by allelopathic activity of *Foeniculum vulgare* essential oil, 2022
15	*Artemisia fragrans*	α-thujone (30.4 %), camphor (26.4 %), 1,8-cineole (12.6 %) and β-thujone (10.0 %)	*Convolvulus arvensis L.*	Exploring the bio-control efficacy of Artemisia fragrans essential oil on the perennial weed Convolvulus arvensis: Inhibitory effects on the photosynthetic machinery and induction of oxidative stress, 2020
16	*Thymbra capitata, Mentha piperita, Eucalyptus camaldulensis,* and *Santolina chamaecyparissus*		*Erigeron bonariensis*	Control of Erigeron bonariensis with Thymbra capitata, Mentha piperita, Eucalyptus camaldulensis, and Santolina chamaecyparissus Essential Oils, 2020
17	*Eucalyptus globulus*	1,8-Cineole (86.94%)	*Lactucasativa ,Avenafatua andAmaranthus hybridus*	Chemical composition and phytotoxic potential of Eucalyptus globulus essential oil against Lactuca sativa and two herbicide-resistant weeds: Avenafatua and Amaranthus hybridus, 2022

18	*Piper nigrum L.*	Linalool (21.73 %)	*Solanumlycopersicum, Zea mays* L. and *Vigna unguiculata*	hytotoxicity of essential oil from Piper nigrum on some selected food crops as a potential herbicide in Africa, 2021

Also studies have been carried out under both lab and field conditions but very limited number of these EOs are formulated to NEm. Table 2 enlists nanoformulations of herbicides with EOs. Oil/ water NEms containing *Satureja hortensis* (garden savory) EOs was evaluated for its herbicidal activity against *Amaranthus retroflexus* and *C. album*. The NEms were prepared by low energy method and have low polydispersity and the mean droplet. The reported size was 130 nm even after 30 days of storage. NE at 1000 µL L^{-1} completely suppressed all the growth features of *Amaranthus retroflexus* under laboratory conditions; however, at the mentioned concentration, *C. album* was significantly inhibited. The NEm reported herbicidal properties as it has high phytotoxic effect, and interferes with the germination, growth and physiological processes of the weeds (Hossein *et al*. 2017).

EOs of *Thymus capitatus* and *Majorana hortensis* have also been evaluated for herbicidal activity against *Convolvulus arvensis* and *Setaria viridis* (Balah 2016). The inhibitor effects of *Majorana hortensis* was more as compared to *Thymus capitatus*. The nano formulation exhibits better efficiency and faster release of active ingredients after application on weed leave surface and weed seeds due to pronounced surface properties. Allelopathic effects of Eucalypt, Lawson Cypress, Rosemary and White ceda have been studied by Ramezani *et al*. (Ramezani *et al* 2008). The germination of herbicides was potentially inhibited by EOs particularly Eucalypt when used at 300 ppm. The authors reported that there were differences in the sensitivity of the various weed species and herbicidal potency of the EOs. Monoterpene and sesquiterpenes present in EOs affects physiological process of weeds like chlorophyll synthesis, photosynthesis, and cellular disruption which can implicate the accumulation of lipid globule in cytoplasm or reduction on organelles.

Recently, Kaur *et al* (Kaur *et al.* 2021) has reported the herbicidal potential of NEms fabricated with fennel (*Foeniculum vulgare* Mill.) EOs. They were formulated by ultrasonic emulsification method and evaluated for herbicidal potential against *P. minor, A. ludoviciana, R. dentatus and M. denticulata* through Petri dish bioassay. The authors reported that the germination of *P. minor, A. ludoviciana, R. dentatus* and *M. denticulata* was totally inhibited at concentrations 0.4, 0.3, 0.3 and 0.05 wt%. major Major constituents of *F. vulgare* essential oilEOs, estragole, anethole and binary mixture did not completely inhibit the germination of the tested weed species even at highest concentrations. NEms having 0.05 and 0.01 wt% EOs were spherical in nature with average size below 130 nm and have good stability to centrifugation and dilution. The formulated NEms were clear and transparent even after 30 days of storage at ambient temperature. NEms were more effective and completely inhibited the germination of *P. minor, A. ludoviciana, R. dentatus and M. denticulata* even at low dose of 0.05 wt% by adversely affecting the physiological processes like membrane leakage and reactive oxygen species mediated cellular damage.

Table 2: NEms of EO having herbicidal potential

Species	**Active ingredients**	**LC_{50} /EC_{50}/IC_{50}**	**Active against**	**Reference**
Vitex negundo L.	β-Caryophyllene (27.80%)	-	*Avenafatua* L. *Echinochloa cru-galli* L.	(Issa *et al*. 2020)
Satureja hortensis L.	Carvacrol (55.6%), ϒ-terpiene (31.9%)	800 µl/L	*Amaranthus retrofexus*	(Hazrati *et al* 2017)
Leptospernumpetersonii *Eucalyptus gumii*	Geranyl acetate (31.4%) ϒ-terpinene (12.3%) Terpinolene (9.3%)	-	*Raphanussativus* *Lolium multiflorum* *Lepidium sativum* L.	(Caputo *et al.* 2020)
Thymus capitatus L. *Majorana hortensis* L.	Thymol (34.4%), α-terpiene, thymol, o-cymene	5-10 µg/ml	*Convolvulus arvensis* *Setariaviridis*	(Balah *et al.*2016)

Herbicidal activity

Commercial products containing essential oils used for weed control:

A few commercial products for weed control based on essential oil are available in the market. One of the most commonly used is GreenMatch EX®. It is based on lemongrass Oil (*Cymbopogon flexuosus*) and is a non-selective, post-emergent weed killer. (Quarles, 2010; Dayan *et al.,* 2009). The best efficacy is achieved at 10 to 15 % dilution (v/v). Another product GreenMatch TMO contains 70 % d-limonene (monoterpene of orange peels) and provides control of broadleaved and grass weeds at dilution 1:3 or as 18 %. (Koivunen *et al*., 2008). Another product Matran II contains up to 50 % clove oil (*Syzygium aromaticum*) and it is applied as 5-8 % solution. A commercialized mixture of cinnamon and clove oil is branded under the name Weed Zap TM (Dayan *et al.,* 2009). However, it is a long way to go until new and more bioavailable formulations reach the market.

References

Abd-ElGawad AM, A EI-Gendy, AM Assaeed, Al-Rowaily SL, AS Alharthi, TA Mohamed, MI Nassar, YH Dewir, and AI Elshamy (2021) Phytotoxic effects of plants essential oils: A systematic review and structure-activity relationship based on Chemometric analyses. Plants (Basel) 10(1):36

Araniti F, M Landi, A Lupini, F Sunseri, L Guidi, and MR Abenavoli (2018) Origanum vulgare essential oils inhibit glutamate and aspartate metabolism altering the photorespiratory pathway in Arabidopsis thaliana seedlings. J Plant Physiol 231:297-309

Awojide SH, KA Oyewole, OO Abiona, and AW Agbaje (2021) Phytotoxicity of essential oil from Piper nigrum L. on some selected food crops as a potential herbicide in Africa. Afr J Pure Appl Sci 2(2): 93-99.

Balah, MA, and WM Abd-ElAzim (2016) Emulsions and Nanoemulsions Formation from Wild and Cultivated Thyme and Marjoram Essential Oils for Weeds Control. J Plant Prot and Path 7(10): 641-648

Bari IN, H Kato-Noguchi (2017) Phytotoxic effects of *cerebera manghas* L.leaf extract seedling elongation of four monocot and four dicot test species. Act Agrpbotanica 70(3): 1720

Bassole IHN HR Juliani (2012) Essential oils in combination and their antimicrobial properties. Molecules 17(4):3989-4006

Batish D, HP Singh, R Kohli, and N Setia (2004) Phytotoxicity of lemon –scented eucalypt oil and its potential use as a bioherbicide. Crop Prot 23(12):1209-1214

Benchaa S, M Hazzit, and H Abdelkrim (2018) Allelopathic effect of Eucalyptus citriodora essential oil and its potential use as bioherbicide. Chem Biodivers 15(8):e1800202.

Benvenuti S, PL Coni, G Famine, and A Pardossi (2017) Weeds for weed control: Asteraceae essential oils as natural herbicides. Int J Weed Biol, Ecol and Veget Manag 57(5): 342-53.

Campiglia E, R Mancinelli, A Cavalieri, and F Caporali (2007) Use of essential oils of Cinnamon, Lavender and Peppermint for weed control. Ital J Agron 2(2): 171-178

Caputo L, A Smeriglio, D Trombetta, L Cornara, G Trevena, M Valussi, F Fratianni, V D Feo, and F Nazzaro (2020) Chemical composition and biological activities of the essential oil of Leptospermum petersoniiand Eucalyptus gunni. Food Microbiol 11(409): 1-15

Danna C, L Cornara, A Smeriglio, D Trombetta, G Amato, P Aicardi, LD Martino, VD Feo, and L Caputo (2021) Eucalyptus gunnii and Eucalyptus pulverulenta 'Baby Blue' essential oils as potential natural herbicides. Molecules 26(21): 6749

El-Rokiek KG, ME Ibrahim, SA Saad El-Din, SA El-Sawi (2020) Using Anise (Pimpinella anisum L.) essential oils as natural herbicide. J Mater Environ Sci 11(10): 1689-98

Flores-Macias A, GG Reyes-Zarate, CCA Gomes, R Lopez-Ordaz, GJ Compos and MA Ramos-López (2021) Chemical composition and phytotoxic potential of Eucalyptus globulus essential oil against

Lactuca sativa and two herbicide-resistant weeds: Avenafatua and Amaranthus hybridus. Tip Rev EspCienc Quim Biol 24**:** 1-8

Frabboni L, A Tarantino, F Petruzzi, and G Disciglio (2019) Bio-herbicidal effects of oregano and rosemary essential oils on chamomile (Matricaria chamomilla L.) crop in organic farming system. Agronomy 9(9):475

Gharibvandi A, H Karimmojeni, P Ehsanzadeh, M Rahimmalek and A Mastinu (2022) Weed management by allelopathic activity of Foeniculum vulgare essential oil. Plant Biosyst 11(7):975

Grulova D, L Caputo, HS Elshafie, B Baranova, LD Martino, V Sedlak, Z Gogalova, J Poracova, I Camele and VD Feo (2020) Thymol Chemotype Origanum vulgare L. essential oil as a potential selective bio-based herbicide on monocot plant species. Molecules 25(3): 595.

Guzey D, DJ MccClements (2006) Influence of Environmental Stresses on O/W Emulsions Stabilized by β-Lactoglobulin–Pectin and β-Lactoglobulin– Pectin–Chitosan Membranes Produced by the Electrostatic Layer-by-Layer Deposition Technique. Food Biophys 1:30-40.

Hancock RD, S Hogenhout, and CH Foyer (2015) Mechanism of plant-insect interaction. J Exp Bot 66:421-424

Harley RM, S Atkins, AL Budantsev, PD Cantino, BJ Conn, R Grayer, MM Harley, RD DeKoK, TD Krestovskaja, R Morales, and Labiatae. (2004) In Flowering Plants Dicotyledons, Springer: Berlin/Heidelberg Germany 167–275

Hazrati H, M Mahmoodreza, MJ Saharkhiz, and H Khoshghalb (2018) Phytotoxic effects of several essential oils on two weed species and Tomato. Biocatal Agric Biotechnol 13:204-212

Hazrati H, MJ Saharkhiz, M Niakousari, and M Moien (2017) Natural herbicide activity of Satureja hortensis L. essential oil nanoemulsion on the seed germination and morphophysiological features of two important weed species. Ecotox Environ Saf 142:423-30

Hossein H, MJ Saharkhiz, M Niakousari, and M Moein (2017) Natural herbicide activity of *Satureja hortensis* L. essential oil nanoemulsion on the seed germination and morphophysiological features of two important weed species. Ecotoxicol Environ Saf 142:423-430

Hu YT, Y Ting, JY Hu, and SC Hsieh (2017) Techniues and methods to study functional characteristics of emulsion system. J Food Drug Anal 25(1):16-26

Isman MB (2000) Plant essential oils for pest and disease management. Crop Prot 19(8-10):603-608

Issa M, S Chandel, HP Singh, DR Batish, RK Kohli, SS Yadav, and A Kumari (2020) Appraisal of phytotoxic, cytotoxic and genotoxic potential of essential oil of a medicinal plant Vitex negundo. Indus Crops Prod 145:112083

Kabalnov A (2001) Ostwald ripening phenomena. J Dispers Sci Technol 22:1-12

Kashkooli AB and MJ Saharkhiz (2014) Essential oil compositions and natural herbicide activity of four Denaei Thyme (Thymus daenensisCelak.) ecotypes. J Essent Oil Bear Plants 17(5):859-74

Kaur P, S Gupta, K Kaur, N Kaur, R Kumar, and MS Bhullar (2021) Nanoemulsion of *Foeniculum vulgare* essential oil: A propitious striver against weeds of *Triticum aestivum. Ind Crops Prod 168:113601*

Khater HF (2012) Prospects of Botanical Biopesticides in Insect Pest Management. Pharmacologia 3:641–656.

Koul O, S Walia, and GS Dhaliwal (2008) Essential oils as green pesticides: Potential and constraints. Biopestic Int 4:63–84

McClement DJ (2004) Emulsion Formation. Food Emulsions:CRC Press

McClements DJ (2007) Critical review of techniques and methodologies for characterization of emulsion stability. Crit Rev Food Sci Nutr 47(7): 611-49

Mcclements DJ (2012) Advances in fabrication of emulsions with enhanced functionality using structural design principles. Curr Opin Colloid Interface Sci 17(5): 25-245

McClemts DJ (2005) Food Emulsions: Principles, Practices and Techniques. Boca Ration: CRC Press.

Mossa ATH (2016) Green Pesticides: Essential Oils as Biopesticides in Insect-pest Management. J Environ Sci Technol 9(5):354-378

Nikolova M, and S Berkov (2018) Use of essential oils as natural herbicides. Ecol 10(2):259-265

Pouresmaeila M, MS Nojadehb, A Movafeghia, and F Maggi (2020) Exploring the bio-control efficacy of Artemisia fragrans essential oil on the perennial weed Convolvulus arvensis: Inhibitory effects on the photosynthetic machinery and induction of oxidative stress. Inds Crop Prod 155: 112785.

Prakash A, R Bakaran, N Paramasivam, and V Vadivel (2018) Essential oil based nanoemulsions to improve the microbial quality of minimally processed fruits and vegetables: A review. Food Res Int 111:509-523

Ramezani S, MJ Saharkhiz, F Ramezani, and MH Fotokian (2008) Use of Essential Oils as Bioherbicides. J Esssent Oil-Bear Plants 11(3):319-327

Raveau R, Fontaine J, Sahraoui AL (2020) Essential oils as potential alternative biocontrol products against plant pathogens and weeds: A review. Foods 9(3):365

Ravensberg W (2015) Crop protection in 2030: Towards a natural, efficient, safe and sustainable approach; Proceedings of the IBMA International Symposium, Swansea University; Swansea, Wales

Sneha K, and A Kumar (2022) Nanoemulsions: Techniques for the preparation and the recent advances in their food applications. Innov Food Sci Emerg Technol 76: 102914

Synowiec A, D Kalemba, E Drozdek, and J Bocianowski (2017) Phytotoxic potential of essential oils from temperate climate plants against the germination of selected weeds and crops. Journal of Pest Science 90(1): 407–419.

Synowiec A, K Mozdzen, A Krajewska, M Landi, and F Araniti (2019) Carum carvi L. essential oil: A promising candidate for botanical herbicide against Echinochloa crus-galli (L.) P. Beauv. in maize cultivation. Inds Crops Prod 140: 111652.

Taban A, M J Saharkhiz and R Naderi (2020) A natural post-emergence herbicide based on essential oil encapsulation by cross-linked biopolymers: characterization and herbicidal activity. Environ Sci Pollut Res Int 27(36):45844-45858

Taban A, MJ Saharkhiz and G Kavoosi (2021) Development of pre-emergence herbicide based on Arabic gum-gelatin, apple pectin and savory essential oil nano-particles: A potential green alternative to metribuzin. Int J Bioll Macromol 167: 756-65.

Ustuner T, S Kordali, and AU Bozhuyuk (2018) Herbicidal and fungicidal effects of Cuminum cyminum, Mentha longifolia and Allium sativum essential oils on some weeds and fungi. Rec Nat Prod 12(6): 619-29

Verdeguer M, LG Castaneda, N Torres-Pagan, JA Llorens-Molina, and A Carrubba (2020) Control of Erigeron bonariensis with Thymbra capitata, Mentha piperita, Eucalyptus camaldulensis and Santolina chamaecyparissus essential oils. Molecules 25(3): 562

Vyyaan JR (2002) Allelochemicals as leads for new herbicides and agrochemicals. Tetrahedron 58(9):1631-1646

MARINE MICROBIAL SLICK GEMS

Bhagwan Rekadwad*

Division of Microbiology and Biotechnology, Yenepoya Research Centre, Yenepoya (Deemed to be University), University Road, Deralakatte, Mangalore 575018, Karnataka, India

ABSTRACT

Marine bacteria produce Exopolysaccharides (EPS) as a stratagem for progression, adhesion to solid surfaces, and survival in harsh environments. The EPSs form a protective barrier around the cell, guarding it from extremes in temperature and salinity. These produced EPS by marine bacteria possesses diverse structure-physicochemical properties, which can be exploited as immune-modulatory and anti-viral agents, for bone-regeneration and therapy, as cicatrizing molecules, in foodstuff and bakery as thickening and gelling soup. Apart from these biotechnological application, most unique EPS are monosaccharide and linear polysaccharide from marine origin have potential application in sustainable agriculture; specifically as suppressing agent for soil-borne plant diseases, promoting plant growth, and acting as a phytopathogen, biocontrol agent, manufacturing bio-waste, waste-water treatment and as chelating agent for elimination of heavy metals.

Keywords: Exopolysaccharides; Marine bacteria; Sustainable development; Heavy metal; Oil recovery and mining

INTRODUCTION

Marine bacteria such as *Falsibacillus albus* GY10110, *Paenibacillus oceani* IB182363, *Salinimonas sediminis* N102, *Alteromonas spp.*, *Sclerotium rolfsii*, *Schizophyllum commune*, *Halomonas maura*, *Haloferax mediterranei*, *Halomonas ventosae*, *Halomonas alkaliantarctica*, *Hahella chejuensis*, *Sinorhizobium meliloti*, *Alcaligenes faecalis* and *Aureobasidium pullulans* are famous for their proven ability to produce various exopolysaccharides. For instance, *Thiobacimonas profunda* JLT2016 had a number of transporter systems that were involved in the export of carbohydrates, carboxylic acids, amino acids, peptides, metals, and other nutrients. JLT2016 has a lot of exporters that are involved in polysaccharide, heavy metal, and metabolite efflux outside of their cells (Torres et al., 2019).

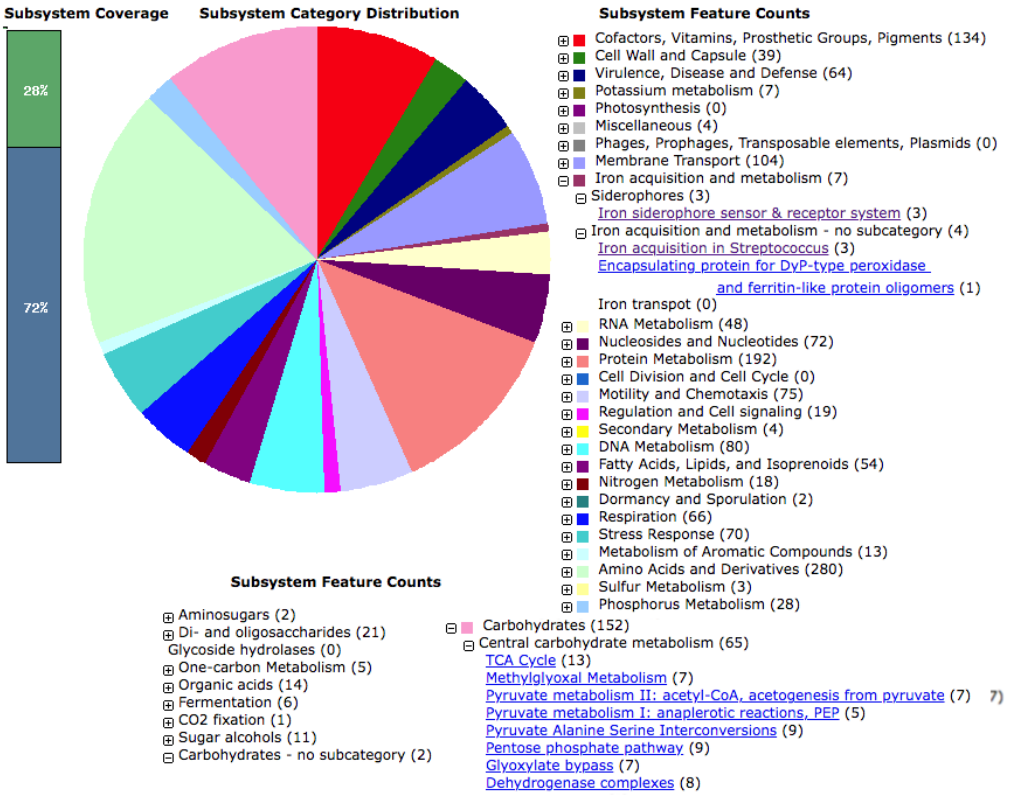

Figure 1. RAST-Genome analysis of *Salinimonas sediminis* N102 (CP031769) shows various polysaccharide transporter, receptor and metabolic systems

*Corresponding author: rekadwad@gmail.com
Received: November 3, 2021, Accepted: December 27, 2021

Similarly, oxidase- and catalase-positive bacterium *Salinimonas sediminis* N102 has been isolated from deep-sea sediment capable of optimal growth at 28 °C (temperature range, 4–40 °C), pH 7.0–7.5 (pH range, 6.0–9.0), 3–4% (w/v) NaCl (salt tolerance range, 2–15%), optimum pressure for growth 10 MPa (pressure tolerance up to 70 MPa). Like *Thiobacimonas profunda* JLT2016, strain N102 possess various metabolism and systems involved activities such as iron-siderophore sensory and receptor system, iron acquisition and various carbohydrate metabolism systems (**Figure 1**). Process optimization at laboratory scale generates potent exopolysaccharide for applications in food (as gels, thickening agent, food, preserver, and food stabilizing agent) and in agriculture (as an absorber for removal and accumulation of heavy metal ions, formation of metallic complexes, agents helps in quorum sensing and as a flocculating agent for municipal sludge treatment/removal of pollutants) (Korcz and Varga, 2021; Berninger et al., 2021).

Uses of microbial potential in industries and for sustainable development

Marine microorganisms are well known for their potential biotechnological applications. Process optimization at laboratory scale generates potent exopolysaccharide for applications in food (as gels, thickening agent, food preservation, and food stabilizing agent) and in agriculture (absorber for removal and accumulation of heavy metal ions, formation of metallic complexes, helps in quorum sensing and flocculating agents for municipal sludge treatment/ removal of pollutants). Halophiles - piezohalopsychrophiles and piezoacidohyperthermophiles - such as *Micromonospora, Streptomyces, Rhodococcus marinonascens, Bathymodiolus septemdierum, Thermococcus* sp., *Methanococcus janaschii, Halomonas* sp., *Calyptogen asoyoae, Thermovibrio ammonificans,* and others are capable of producing numerous bioactive polymers. Archaeal sterols, glycerol ethers, loihichelins, amphiphilic and ammonificins siderophores are among the metabolites produced by these polyextremophiles (Thornburg et al., 2010; Corinaldesi, 2015). These produce industrially important microbial metabolites especially exopolysaccharides (EPS) and siderophores those are useful in solubilization of trace elements. Production of these polymers by microorganisms may be initiated by quorum sensing. The variety of marine microorganisms capable of making EPS is an area that has received little attention of scientific community. In-depth investigation will shed a limelight for the discovery of biocatalytic molecules, which may find ranges of applications in sustainable agriculture, preventing plant pest, increased crop production, removal of hazardous molecules from waste water and sewage, in therapeutics etc.

Capsular polymers are secreted by the marine EPS producer in their surroundings. The released EPS remain connected to the cell membrane via lipo-polysaccharides (LPS), giving the producer colonies a slimy feel. The sluggish LPS may slowly make its way into the environment. Marine EPS is combined with other polysaccharides (chitosan, alginate) of bacterial origin to create host disease resistance. Moreover, it improves cell integrity, surface adhesion, nutrient trapping, and protects host cells from toxic compounds and detrimental bone-freezing conditions (Rekadwad and Khobragade, 2017). Therefore, exopolysaccharide producing bacteria (e.g. *Pseudomonas*) found in glacial ice have an ability to produce cryoprotective exopolysaccharide (Ali et al., 2020).

Such cold adapted marine microorganisms would have offering protection to marine chlorophyll producing cold-adapted flora in Antarctica. Additionally, many novel strains polysaccharide-secreting bacteria have been isolated from marine habitat (Table 1). As a result, researchers are increasingly focused on finding new marine bacteria in marine-environments, particularly in extremes such as marine habitats (Zhenming and Yan, 2004). The EPS proportion obviously varies between phytoplankton and bacteria, which may reflect the destiny of the ocean. Uronic acid, which makes up 20–50% of the total polysaccharide fraction in bacterial EPS, is a key component. Phytoplankton, on the other hand, has an EPS that is deficient in uronic acid. The negative (-) charge associated with COOH-groups of $C_6H_{10}O_7$ (uronic acid) in marine exopolysaccharide has been associated as the crucial factor of the complexified macromolecules with transition metals viz. Copper, Iron, Nickel, Zinc, Chromium, Gold, Cobalt, Manganese, Silver, Scandium, Mercury, Titanium, Vanadium, Platinum, Cadmium, Yttrium, Molybdenum, Rhodium, Tungsten, Ruthenium, Palladium, Niobium, Zirconium, Iridium, Osmium, Technetium, Hafnium, Copernicium, Roentgenium, Rhenium, Tantalum, Rutherfordium, Meitnerium, Seaborgium, Bohrium, Hassium, Darmstadtium and Dubnium. This property may have a substantial outcome on the long-term fortune and dilapidation of EPS in the ocean. Due to the difficulty in degrading bacterial

EPS as compared to eukaryotic EPS, it collects in marine environments (Zhang et al., 2015). It's still not clear what factors influence how readily bacterial extracellular polysaccharides (EPS) chelate heavy metal and their impact on various pathogens. Hence, isolation and characterization of both marine EPS-producing bacteria and their exo- mono- & polysaccharides using modern techniques will help to understand the mechanism of exopolysaccharide action. Thus, this would offer for their use in agriculture as a suppressor of soil-borne plant pathogens, a tool for promoting plant growth, and a biocontrol agent against phytopathogens.

Table 1: Polysaccharide producing novel marine bacteria isolated between 2017-2021

Taxonomically valid name and strain number	Habitat	GenBank/ EMBL/DDBJ accession number	Characteristics	Reference
Alteromonas indica IO390401	Surface seawater, Indian Ocean	MG852173, PYVY00000000	4.4 Mb chromosome, G+C content = 48.2 mol%	Lin et al., 2018
Alteromonas oceani S35	Deep sediment of hydrothermal vent	MF687202, NZ_RCUA00000000	Optimal growth at 28 °C, at pH 7.0–8.0 in media contaning 2.0% (w/v) NaCl, GC Content 51.3 mol%	Jin et al., 2018
Alteromonas lipolytica JW12	Surface seawater	KX14648, MJIC00000000	Poly-bhydroxybutyrate producer, DNA GC Content 48.4 mol%	Shi et al., 2017
Salinimonas sediminis N102	Deep-sea sediment sample	MH816968, CP031769	oxidase- and catalase-positive, optimal growth at 28 °C (range, 4–40 °C), pH 7.0–7.5 (range, 6.0–9.0), 3–4%(w/v) NaCl (range, 2–15%), optimum pressure for growth 10 MPa, pressure tolerance up to 70 MPa	Cao et al., 2018
Alteromonas aestuariivivens JDTF-113	Tidal flat	NR_157790 / KY497472	Optimum growth at 30 ºC, at pH 7.0–8.0, 2.0 % (w/v) NaCl	Park et al., 2017
Alteromonas pelagimontana 5.12	Southwest Indian Ridge	LT593862, CP052766	Oxidase- and catalase-positive, optimum growth at 35 C, at pH 6.0, salt requirement 3.5 % (w/v) NaCl, DNA G+C content 46.1 mol%	Sinha et al., 2017
Alteromonas alba 190	Seawater of the West Pacific Ocean	MG856904, PVNP00000000	Optimum temperature 30 °C, range 4–40 °C, optimum pH 6.5, pH range 5.5–10.5, optimum salt concentration, 2%, salt tolerance limit between 0.5–12.5% (w/v) NaCl, DNA–DNA hybridization value 53.8%, DNA G+C content 48.7 mol%	Sun et al., 2019
Falsibacillus albus GY10110	Mangrove soil	MH13531, RCVZ00000000	Temperature 15–37 C (optimum, 28 C), Salt tolerance at 0–3 %(w/v) (Optimum, 1 %) NaCl, pH range 6.0–9.0 (optimum, pH 7.0), DNA G+C content 42.3 mol%	Shi et al., 2019
Paenibacillus oceani IB182363	Surface seawater	MN911320, NZ_JACXJA000000000	pH 5.0–9.5 (optimum, pH 7-8), 20–40 °C (optimum, 30 °C), NaCl tolerance 1–8% (w/v with optimum, 2–4%, DNA G+C content 54.5mol%	Chen et al., 2021

CONCLUSION

Salt-loving marine exopolysaccharide producing bacteria are mostly belonging the mesophilic to the psychrophilic range of temperature tolerance with some exceptions such as thermophiles/ hyperthermophiles inhabiting hydrothermal vents and hot springs. These bacteria possess the inherent ability to produce exopolysaccharides either in response to hostile conditions or in response to signalling molecules.

The later response suggests that polysaccharides secreted by marine bacteria would have offered benefits to signalling flora and nourishes its surrounding. Therefore, exploitation of these real microbial slick gems will offer benefits in various sectors for sustainable developments in agriculture, the environment and in health sectors.

REFERENCES

Ali P, AA Shah, F Hasan, N Hertkorn, M Gonsior, W Sajjad, and F Chen (2020) A Glacier bacterium produces high yield of cryoprotective exopolysaccharide. Frontiers in Microbiology, 10: 3096. https://doi.org/10.3389/fmicb.2019.03096

Berninger T, N Dietz, and OG López (2021) Water-soluble polymers in agriculture: xanthan gum as eco-friendly alternative to synthetics. Microbial Biotechnology, 14: 1881-1896. https://doi.org/10.1111/1751-7915.13867

Corinaldesi, C. (2015). Newperspectivesinbenthicdeep-seamicrobialecology, 2, 17

Donot. F., A. Fontana, J.C. Baccou, and S. Schorr-Galindo, (2012). Microbial exopolysaccharides: main examples of synthesis, excretion, genetics and extraction. Carbohydrate Polymers, 87, 951-962

Finore, I., P. Didonato, V. Mastascusa, B. Nicolaus, and A. Poli, (2014). Fermentation technologies for the optimization of marine microbial exopolysaccharide production. Marine Drugs, 12, 3005-3024

Korcz E, and L Varga (2021) Exopolysaccharides from lactic acid bacteria: techno-functional application in the food industry. Trends in Food Science & Technology, 110: 375-384. https://doi.org/10. 1016/j.tifs.2021.02.014

Rekadwad BN, and CN Khobragade (2017) Marine polyextremophiles and their biotechnological applications, In: VC Kalia (ed) & P. Kumar (ed), Microbial Applications Vol.2 - Biomedicine, Agriculture and Industry, Springer Nature, Switzerland, pp.319-331. https://doi.org/10.1007/978-3-319-52666-9_15

Thornburg, C.C., T.M. Zabriskie, and K.L. McPhail, (2010). Deep-sea hydrothermal vents: potential hot spots for natural products discovery? Journal of Natural Products, 73, 489–499

Zhang, Z., Y. Chen, R. Wang, R. Cai, Y. Fu, and N. Jiao, (2015). The Fate of marine bacterial exopolysaccharide in natural marine microbial communities. PLoS ONE, 10(11), e0142690

Zhenming, C., and F. Yan, (2005). Exopolysaccharides from marine bacteria. Ocean University China, 4: 67.

Lin D, Y Chen, S Zhu, J Yang, and J Chen (2018) *Alteromonas indica* sp. nov., isolated from surface seawater from the Indian Ocean. International Journal of Systematic and Evolutionary Microbiology, 68: 3881-3885. doi: 10.1099/ijsem.0.0030

Jin QA, YH Hu, and Li Sun (2018) *Alteromonas oceani* sp. nov., isolated from deep-sea sediment of a hydrothermal field. International Journal of Systematic and Evolutionary Microbiology, 68: 657–662. doi: 10.1099/ijsem.0.002560

Shi XL, YH Wu, XB Jin, CS Wang, and XW Xu (2017) *Alteromonas lipolytica* sp. nov., a poly-beta-hydroxybutyrate-producing bacterium isolated from surface seawater. International Journal of Systematic and Evolutionary Microbiology,67:237–242. doi: 10.1099/ijsem.0.001604

Cao J, Q Lai, Y Was, L Wang, R Liu, and J Fang (2018) *Salinimonas sediminis* sp. nov., a piezophilic bacterium isolated from a deep-sea sediment sample from the New Britain Trench. International Journal of Systematic and Evolutionary Microbiology, 68: 3766–3771. doi: 10.1099/ijsem.0.003055

Park S, SJ Choi, JM Park, and JH Yoon (2017) *Alteromonas aestuariivivens* sp. nov., isolated from a tidal flat. International Journal of Systematic and Evolutionary Microbiology, 67: 2791–2797. doi: 10.1099/ijsem.0.002023

Sinha RP, KP Krishan, A Singh, FA Thomas, A Jain, and PJ Kurian (2017) *Alteromonas pelagimontana* sp. nov., a marine exopolysaccharide-producing bacterium isolated from the Southwest Indian Ridge. International Journal of Systematic and

Evolutionary Microbiology, 67: 4032–4038. doi: 10.1099/ijsem.0.0022

Sun C, M Xamxidin, YH Wu, H Cheng, CS Wang, and XW Xu (2019) Alteromonas alba sp. nov., a marine bacterium isolated from seawater of the West Pacific Ocean. International Journal of Systematic and Evolutionary Microbiology, 69:278–284. doi: 10.1099/ijsem.0.003151

Shi SB, C Liu, MG Jiang, GD Li, LF Yang, JF Wu, LQ Jiang, K Zhang, NK Shen, CL Jian, and Y Jiang (2019) *Falsibacillus albus* sp. nov., isolated from mangrove soil. International Journal of Systematic and Evolutionary Microbiology, 69:1411–1416. doi: 10.1099/ijsem.0.003328

Chen YF, L Ye, HQ Huang, MG Jiang, YH Hu, DM Sun, and KL Mo (2021) *Paenibacillus oceani* sp. nov., isolated from surface seawater. International Journal of Systematic and Evolutionary Microbiology, 71: 005024. doi: 10.1099/ijsem.0.005024

Torres M, KW Hong, TM Chong, JC Reina, KG Chan, Y Dessaux, and I Llamas (2019) Genomic, physiologic, and proteomic insights into metabolic versatility in Roseobacter clade bacteria isolated from deep-sea water. Scientific Reports, 9: 1215. https://doi.org/10.1038/s41598-018-37720-2.

ETHNO-MEDICINAL FORMULATIONS FOR MUSCULOSKELETAL CONDITIONS

Sumiksha Gupta[1],* M. C. Sidhu[2] and Amrik Singh Ahluwalia[3]

[1]Department of Botany, Government Post Graduate College, Una-174303, (H.P.)

[2]Department of Botany, Panjab University, Chandigarh-160014

[3]Department of Botany, Eternal University, Baru Sahib-173101, Sirmour, (H.P.).

ABSTRACT

A survey was conducted to study the use of medicinal plants by the people in district Una of Himachal Pradesh to manage various musculoskeletal problems. A total of 500 respondents were contacted and they have suggested the use of 113 plant species belonging to 58 families to take care of musculoskeletal conditions. The enlisted plant species were mainly herbs (46), followed by trees (32). Leaves, fruits and seeds were most commonly used in remedial preparations. Most of the species (48) were used as fresh followed by powdered form (40). These plants were utilized through a variety of local preparations including '*morabba', 'panjiri', 'kheer', 'halwa', 'gulkand', 'chutney', 'laddoos', 'sherbat', 'tea' etc*. The mode of applications depends upon the ailments. Maximum plants (62) were used for arthritis followed by (37) for general swellings and (35) for joint pains. The documented plants include both wild, cultivated species and also procured from the market.

Keywords: Cultivated, Medicinal, Musculoskeletal, Remedy, Traditional, Wild

INTRODUCTION

Plants have been in use for food and medicine since the advent of civilization. The healing and medicinal properties of all the plants, especially the angiosperms, have contributed immensely for improving human health and welfare. The wild plants are in great demand as raw materials for drug manufacturing, phytoremedies and traditional healing practices. After China, India is the second largest exporter of raw herbal drugs, mainly from the Himalayan region (Lange, 1997). Recently, there has been an upsurge in the production and use of plant based medicines, health tonics and body toning agents.

Ethnomedicine is the totality of health, knowledge, values, beliefs, skills and practices of members of a society including all the clinical and nonclinical activities which relate to their health needs (Foster and Anderson, 1978). Traditional plant based medicines are used by the locals either directly or after necessary processing for the treatment of various diseases (Tilburt and Kaptchuk, 2008). This traditional knowledge related to medicinal plants has survived till today due to unquestioned patronage and respect from different sections of the society.

India has also witnessed this increase in ayurvedic and other traditional systems of medicine. As per World Health Organization (2013), the primary health care of nearly 80% of the developing societies is satisfied through traditional plant medicines. Thus, plants of medicinal interest have the advantage to be grown, protected and even worshipped for their use. In developing world, traditional health care practices still hold a centre stage in spite of the advent of modern medical facilities because of their affordable price and deep cultural and spiritual faith of people (Timothy and Craig, 2007; Vishwakarma *et al*., 2013). Because of their cost-effectiveness and safety, these medicines are popularly used by the rural folk in countries like India, China and other parts of the world (Katewa *et al*., 2004).

India has a rich repository of plant diversity occurring at different altitudes and latitudes to provide medicinal plant resources. More than 70% of rural population in India is dependent on traditional plant medicines (Seth and Sharma, 2004) with 15% geographical area inhabited by about 5000 tribal villages having rich ethnobotanical knowledge (Chowdhuri, 2000). The significance of ethno-medicine becomes more pronounced in a country like India where most of the population is residing in villages and far-flung or remote hilly terrains, often making them solely dependent on native plants for immediate relief. There has been a decline in the expertise and usage of medicinal plants may be because of the establishment of primary health care centres, dispensaries, government and private hospitals. Further, due to connectivity of rural areas with the cities, people prefer to visit cities for their health care requirements. The problem arising in the correct identification of plant species in the field has further reduced the use of these medicines. Present study is an attempt to compile the plant based remedies practiced by the natives to take care of the musculoskeletal ailments.

*Corresponding author: sumiksha666@gmail.com

Received: November 27, 2021, Accepted: December 16, 2021

MATERIALS AND METHODS

The present study has been conducted in district 'Una', Himachal Pradesh, India. Regular field visits were undertaken to document the ethnomedicinal knowledge in general and ethnomedicines for musculoskeletal ailments in particular. A total of around 170 sites were visited for the present documentation. The respondents were selected at random (irrespective of their sex, education and occupation) and subject to their availability and willingness to share knowledge. The interviews were exchanged in an informal and participative atmosphere. To facilitate this, local dialect was used along with extending an affirmative response and patience hearing to the respondents.

A semi-structured questionnaire and informal talks through frequent visits in the study area were employed to elicit the information on medicinal uses of plants by the natives. The questionnaire included items on various aspects such as local name, medicinal use, plant part(s) used, modes of preparation and administration of formulations to treat diseases or health conditions.

The personal comments of the respondents on the present scenario, efficacy and future prospects of traditional plant remedies were also recorded. They were also asked as to how they first felt the importance of the plant in a particular ailment. The medicinal plants of common occurrence were easily identifiable whereas others were collected as specimens with notable features. The natives helped in identification of species in their natural habitat. The plants cited by at least two persons independently for their medicinal uses only were recorded.

RESULTS AND DISCUSSION

A total of 113 plant species belonging to 58 families were reported for treating various musculoskeletal ailments, including those used in traditional body massages for pre-and postpartum maternal care (Table 1). There were 11 species of family Fabaceae followed by Solanaceae (6), Zingiberaceae (5) and Asteraceae (5) used in traditional herbal preparations. Apocynaceae, Combretaceae and Euphorbiaceae were represented by 4 species each. As many as 35 families were represented each by single species (Table 2).

Table 1: Plant species used in the treatment of musculoskeletal ailments

S. No.	Botanical Name (Family)		GH	AS	PPU	Mode of preparation	Mode of administration	Ethnomedicinal use
1.	*Achyranthes aspera* L. (Amaranthaceae)	Puthkanda, chirchitta, latjira	H	W	Rt	powder	Oral	Root powder is given to treat internal injuries and fractures.
2.	*Acorus calamus* L. (Acoraceae)	Vach, bach-barya	H	W	Rz	paste	Topical	Paste of (rhizome) is applied on arthritic joints
3.	*Aegle marmelos* (L.) Correa (Rutaceae)	Bael, bilpatri, bilva	T	W, Cv	Rt, Lf and Ft	as such, decoction, powder, local recipe	Oral	Root and leaf (powder or decoction) in arthritis; ripe fruit, powder, marmalade or *morabba* and 'panjiri' in joint pains.
4.	*Allium sativum* L. (Amaryllidaceae)	Lahsun	H	Cv	Bl	as such, cooked, infusion, pickle, roasted and local recipe	Oral, topical	Bulblets taken fresh, roasted, cooked, as pickle or '*chutney*' in rheumatism, as '*kheer*' in arthritis; oil infusion as liniment for joint pains.
5.	*Aloe vera* (L.) Burm.f (Asphodelaceae)	Kwar, Ghritkumari	H	W, Cv	Lf and Gel	as such, cooked, pickle and local recipe	Oral	Leaf eaten fresh, cooked, pickle, as marmalade, '*halwa*' (a flour-based sweet pudding) or as gel in arthritis
6.	*Argyreia nervosa* (Burm. f.) Bojer (Convolvulaceae)	Vidhara, samudrasos	Cl	Cv	Rt	powder	Oral	Root powder is given to treat joint pains and rheumatism.
7.	*Artemisia scoparia* Waldst. & Kitam (Asteraceae)	Jhaun, jhaunfla	H	W	Wp	powder	Topical	Powdered plant (mixed with sesame or mustard oil, nutmeg, ginger and cloves) used as liniment for musculo-skeletal pains, swellings, stroke-affected limbs and postpartum massage
8.	*Azadirachta indica* A. Juss. (Meliaceae)	Neem	T	W, Cv	St, Lf, Ft and Oil	as such, infusion	Oral, topical, Fomentation	Leaf and fruit useful in treating joint pains; oil and oil infusion of leaves used as liniment for joint pains; hot-water infusion of twigs is used for fomentation of swellings.

9.	*Baccharoides anthelmintica* (L.) Moench. (Asteraceae)	Kali jiri	H	Mk	Ft	as such, powder	Oral	Fruit is given to treat swollen joints.
10.	*Barleria cristata* L. (Acanthaceae)	Jhinti	Sh	W	Rt and Lf	infusion	Fomentation	Hot water infusion of root and leaf used in fomentation of swellings.
11.	*Berberis aristata* DC. (Berberidaceae)	Kashmal, rasont, daruhaldi	Sh	Mk	Rt	extract	Oral	Root extract called '*rasaut*' is given in arthritis.
12.	*Boerhavia diffusa* L. (Nyctaginaceae)	Itsit, utshat, punarnava	H	W	Wp and Rt	As such, powder and poultice	Oral, topical	Root powder is used in rickets ; root pieces are tied in a thread (i) worn around neck in rickets and general weakness in children, (ii) on ankle to treat sciatica pain; plant paste applied as poultice on backache
13.	*Bombax ceiba* L. (Malvaceae)	Sembal, mochras, kapok	T	W	Rt and Bk	powder	Oral	Bark and root powder given in joint pains.
14.	*Brassica juncea* (L.) Czern. (Brassicaceae)	Peeli sarson, sarma	H	Cv	Oil	as such	Topical	Oil as liniment for all kinds of musculo-skeletal pains.
15.	*Brassica nigra* (L.) K.Koch (Brassicaceae)	Rai	H	Cv	Sd	powder	Oral	Seed powder given in general body swellings and arthritis.
16.	*Brassica rapa* L. (Brassicaceae)	Shaljam, toria	H	Cv	Tb	infusion	Fomentation	Hot water infusion of tuber used to foment swellings.
17.	*Bryophyllum pinnatum* (Lam.) Oken (Crassulaceae)	Patharchat, zakhm-e-hyat	H	Cv	Lf	as such, decoction, powder	Oral	Leaves are eaten fresh, as powder or taken as decoction in arthritis.
18.	*Butea monosperma* (Lam.) Taub. (Fabaceae)	Dhak, palash, kesu	T	W	Fl and Gum	poultice and local recipe	Oral, topical	Gum is used in making '*panjiri*' for backaches; flower as poultice for swollen abdomen and backaches.
19.	*Calotropis procera* (Aiton) Dryand. (Apocynaceae)	Ak, madar	Sh	W	Rt, Lf, Fl, Lx and Oil	as such, powder, infusion	Oral, topical	Tender leaf and root powder is used to treat arthritis; flower powder in joint pains; a teaspoonful of latex in a '*patasha*' (a puffed sugar biscuit) for rheumatism; oil or oil infusion of leaf as liniment for arthritis.
20.	*Cannabis sativa* L. (Cannabaceae)	Bhang	Sh	W, Cv	St and Lf	infusion, poultice	Topical and fomentation	Leaf paste tied as poultice on swellings; hot infusion of twigs for fomentation of local swellings and joints.
21.	*Carica papaya* L. (Caricaceae)	Papita, papaya	T	Cv	Ft	as such, cooked	Oral	Fruit taken ripe or as cooked vegetable in arthritis.
22.	*Casearia tomentosa* Roxb. (Salicaceae)	Chilla	T	W	Bk	poultice	Topical	Powdered fresh bark tied as poultice on arthritic joints.
23.	*Cassia fistula* L. (Fabaceae)	Amaltas, alis	T	W, Cv	Fl and Sd	powder and local recipe	Oral	Seed powder or flower (as '*gulkand*'- a sweet preserve of petals) useful in arthritis.
24.	*Catharanthus roseus* (L.) G.Don (Apocynaceae)	Sadabahar	H	Cv	Lf and Fl	as such	Oral	Fresh leaf and flowers are eaten in arthritis.
25.	*Celastrus paniculatus* Willd. (Celastraceae)	Malkanghni, sankhiru	Cl	W	Oil	as such	Topical	Oil is used for massage of swellings, arthritic joints and to relieve numbness of limbs.
26.	*Chamaecrista absus* (L.) H.S.Irwin & Barneby (Fabaceae)	Chaksu, bankulthi	H	W	Sd	as such	Oral	Seed is used in treating rheumatism.
27.	*Cicer arietinum* L. (Fabaceae)	Chana, chhole	H	Cv	Sd	cooked, roasted, sprouted and local recipe	Oral	Seed taken roasted, sprouted, as '*chutney*', soup or cooked '*dal*' for arthritis
28.	*Cinnamomum camphora* (L.) J.Presl (Lauraceae)	Kapur	T	Mk	Wd and Bk	extract	Oral	Wood and bark extract called 'camphor' is given in body pains (with mint and lemon juice).
29.	*Cissampelos pareira* L. (Menispermaceae)	Patindu	Cl	W	Bk and Lf	poultice	Topical	Bark and leaf paste as poultice on paining joints.

30.	*Citrus aurantiifolia* (Christm.) Swingle (Rutaceae)	Kaghzi nimbu, Nimbu	T	Cv	Ft	juice	Oral	Fruit juice used in treating body pains.
31.	*Citrus aurantium* L. (Rutaceae)	Malta	T	Cv	Lf and Ft	as such and juice	Oral, topical	Leaf tied on swollen joints and internal injuries; fruit juice used in treating body pains.
32.	*Cleistanthus collinus* (Roxb.) Benth. ex Hook.f. (Phyllanthaceae)	Korda	T	Mk	Bk	poultice	Topical	Crushed bark is poulticed on dislocated bones and fractures.
33.	*Colchicum luteum* Baker (Colchicaceae)	Suranjan, hirantutiya	H	Mk	Rz	powder	Oral	Rhizome powder is given in arthritis.
34.	*Commiphora mukul* (Hook. ex Stocks) Engl. (Burseraceae)	Guggal	T	Mk	Gum	as such, decoction and soaked	Oral	Gum taken as such, soaked or as decoction in treatment of rheumatism.
35.	*Crocus sativus* L. (Iridaceae)	Kesar, saffron	H	Mk	Sy and St	infusion	Topical	Dried style and stigma (*kesar)* used in making liniment oil for musculo-skeletal pains.
36.	*Croton tiglium* L. (Euphorbiaceae)	Jamalghota	Sh	Mk	Oil	as such	Topical	Oil used as a liniment for massaging arthritic joints.
37.	*Curcuma aromatica* Salisb. (Zingiberaceae)	Jangli haldi	H	Cv, Mk	Rz	as such, powder	Oral	Rhizome is useful in treating arthritis.
38.	*Curcuma caesia* Roxb. (Zingiberaceae)	Kali haldi	H	Mk	Rz	poultice	Topical	Paste (with bark powder of *Litsea glutinosa*) tied on aching joints and internal injuries.
39.	*Curcuma longa* L. (Zingiberaceae)	Haldi, baswar	H	Cv	Rz	as such, boiled, powder, pickle and local recipe	Oral	Rhizome as raw/powder/pickle, '*panjiri*', spice or boiled in milk for strengthening bones and in treatment of arthritis, internal injuries, swellings *etc*.
40.	*Cuscuta reflexa* Roxb. (Convolvulaceae)	Amarbel, akashbel	Cl	W	Wp	infusion	Fomentation	Hot-water infusion of fresh stems used for fomentation of aching joints and swellings, especially during pregnancy.
41.	*Cyperus rotundus* L. (Cyperaceae)	Deela, motha	H	W	Rt	as such	Oral	Fresh root is eaten to relieve joint pains.
42.	*Dalbergia sissoo* DC. (Fabaceae)	Tahli, sheesham	T	W, Cv	Lf	poultice	Topical	Poultice of leaf paste tied on the site of internal injuries and aching joints.
43.	*Datura innoxia* Mill. (Solanaceae)	Safed dhatura	Sh	W	Lf and Sd	as such, poultice, infusion	Oral, topical	Seeds, used in treating joint pains; leaf paste as poultice on aching joints and sprains; oil infusion of leaf as liniment for swellings and muscular pains.
44.	*Dodonaea viscosa* (L.) Jacq. (Sapindaceae)	Maindar	Sh	W, Cv	Bk	powder and poultice	Oral, topical	Bark powder given to heal internal injuries and fractures; paste tied on paining joints, dislocated bones and fractures.
45.	*Eclipta prostrata* (L.) L. (Asteraceae)	Bhringraj, bhangra	H	W	Wp	poultice	Topical	Paste tied on fractured bones.
46.	*Elettaria cardamomum* (L.) Maton (Zingiberaceae)	Chhoti elaichi	H	Mk	Ft	infusion	Topical	Oil infusion of fruit (with nutmeg, ginger, cloves and powdered plant of *Artemisia scoparia*) applied as liniment for musculo-skeletal pains and post-delivery massage.
47.	*Eucalyptus globulus* Labill. (Myrtaceae)	Safeda	T	Cv	Lf	infusion	Fomentation	Hot leaf infusion used to give fomentation for swellings and aching joints.
48.	*Euphorbia heterophylla* L. (Euphorbiaceae)	-	H	W	Lf and Lx	as such, decoction	Oral, topical	Fresh leaves as decoction in internal injuries and swellings; latex applied on arthritic joints.
49.	*Euryale ferox* Salisb. (Nymphaeaceae)	Makhana	H	Mk	Sd	as such, roasted and local recipe	Oral	Popped seeds called *makhana* eaten as such, roasted or added to '*panjiri*' in treating arthritis.
50.	*Flacourtia indica* (Burm.f.) Merr. (Salicaceae)	Kangu	T	W	Bk	infusion and poultice	Topical and fomentation	Bark is poulticed on arthritic joints, swellings and fractures; hot infusion used for fomentation of swellings and internal injuries.

51.	*Foeniculum vulgare* Mill. (Apiaceae)	Saunf	H	Cv	Ft	decoction, roasted and local recipe	Oral	Fruit taken in roasted or decoction form to treat internal swellings; as '*panjiri*' for joint pains, swellings and backache.
52.	*Gloriosa superba* L. (Colchicaceae)	Kalihari, Agnishikha	Cl	W	Bl	powder	Oral	Powdered bulb is taken in arthritis.
53.	*Gossypium arboreum* L. (Malvaceae)	Kapas	Sh	Cv	Oil	as such	Oral, topical	Used as cooking oil and for treating arthritis; applied as liniment for joint pains.
54.	*Holarrhena pubescens* Wall. ex G.Don (Apocynaceae)	Kutaja, Karva indrajau	T	W	Bk and Sd	powder	Oral	Powdered bark and seeds are given in arthritis.
55.	*Holoptelea integrifolia* Planch. (Ulmaceae)	Pardesi, Rajain	T	W	Lf	poultice	Topical	Leaf paste is tied as poultice to relieve muscular pains and aching joints.
56.	*Ipomoea carnea* Jacq. (Convolvulaceae)	Akra, Besharam	Sh	W	Lf	poultice	Topical	Mature leaves are coated with mustard oil and tied on paining joints.
57.	*Justicia adhatoda* L. (Acanthaceae)	Basuti, vasaka	Sh	W, Cv	Rt and Lf	decoction, infusion	Oral, fomentation	Root decoction given in arthritis; hot water infusion of leaves (with leaves of *Azadirachta indica*, *Murraya koenigii* and *Vitex negundo*), for fomentation of swellings.
58.	*Lagenaria siceraria* (Molina) Standl. (Cucurbitaceae)	Lauki, ghiya	Cl	Cv	Ft	cooked	Oral	Fruit eaten as cooked vegetable or soup during body pains.
59.	*Launaea nudicaulis* (L.) Hook.f. (Asteraceae)	Dudhkal, bhadrakali buti	H	W	Lf	paste	Topical	Leaf paste is applied on aching joints.
60.	*Lens culinaris* Medik. (Fabaceae)	Masur dal	Cl	Cv	Sd	cooked	Oral	Eating cooked '*dal*' is useful in healing internal injuries.
61.	*Linum usitatissimum* L. (Linaceae)	Alsi	H	Cv	Sd and Oil	as such and local recipe	Oral	Seed taken as '*laddoos*', '*panjiri*' and 'halwa' for arthritis and backache; oil given to treat backache.
62.	*Litsea glutinosa* (Lour.) C.B.Rob. (Lauraceae)	Rahain, maidalakri	T	W	Bk	powder, poultice and local recipe	Oral, topical	Bark powder or '*halwa*' is very effective in healing fractures and internal injuries; bark paste applied as poultice on arthritic joints and swellings.
63.	*Luffa cylindrica* (L.) M.Roem. (Cucurbitaceae)	Kali tori	Cl	Cv	Ft	cooked and juice	Oral	Fruit as cooked vegetable, soup or as juice in arthritis.
64.	*Macrotyloma uniflorum* (Lam.) Verdc. (Fabaceae)	Kulath	Cl	Cv	Sd	cooked, decoction	Oral	Seeds taken as cooked '*dal*' or decoction in joint pains.
65.	*Madhuca longifolia var. latifolia* (J.Koenig ex L.) J.F.Macbr. (Sapotaceae)	Mahua	T	Cv	Lf, Ft and Oil	as such, decoction and poultice	Oral, topical	Leaf poultice for joint pains; oil used for massaging joint pains and backache; decoction of fruit is given to heal internal injuries and fractures.
66.	*Melia azedarach* L. (Meliaceae)	Darek, bakain	T	W, Cv	Ft	powder	Oral	Fruit powder useful for treatment of rheumatism.
67.	*Mentha piperita* L. (Lamiaceae)	Pudina	H	Cv	Wp	as such, juice and local recipe	Oral	Whole plant taken fresh, as juice or '*chutney*' in body ache.
68.	*Mucuna pruriens* (L.) DC. (Fabaceae)	Gajali bel, kaunch	Cl	W, Cv	Sd	as such	Oral	Seed kernel eaten during fractures.
69.	*Murraya koenigii* (L.) Spreng. (Rutaceae)	Gandhila, kari patta, meetha neem	Sh	W	St, Lf and Ft	as such, poultice, infusion	Oral, topical, fomentation	Tender leaf and ripe fruit for joint pains, backache; leaf paste as poultice on joint pains; hot-water infusion of twigs for fomentation of swellings.
70.	*Musa* x *paradisiaca* L. (Musaceae)	Kela	H	Cv	Ft	As such, cooked	Oral	Fruit eaten as fresh or cooked vegetable for arthritis.
71.	*Myristica fragrans* Houtt. (Myristicaceae)	Jaiphal	T	Mk	Sd and Aril	as such, local recipe and powder	Oral, topical	Seed (nutmeg) and aril (mace) used in rheumatism, as ingredient in *laddoos*' and '*panjiri*' for backaches; seed powder used in making liniment oils for massage during swellings, arthritis and post-delivery care.

72.	*Myrsine africana L.* (Primulaceae)	Chhota mendhru	Sh	W	Lf	paste	Topical	Leaf paste is applied on arthritic joints and local swellings.
73.	*Narthex asafoetida* Falc. ex Lindl. (Apiaceae)	Hing	H	Mk	Gum	infusion	Fomentation	Hot-water infusion used for fomentation of swellings and body pains (during pregnancy).
74.	*Nerium oleander* L. (Apocynaceae)	Kaner, kaud gandhila	Sh	W, Cv	Lf	infusion	Fomentation	Hot water infusion of leaf used to foment swellings.
75.	*Nigella sativa* L. (Ranunculaceae)	Kalonji	H	Mk	Sd	infusion	Topical	Oil infusion of seed is applied on inflamed joints.
76.	*Ocimum tenuiflorum* L. (Lamiaceae)	Tulsi	H	Cv	Rt, Lf and Sd	as such, juice and powder	Oral	Leaf and seed taken in body ache; seed powder and root juice is given to treat general/local swellings.
77.	*Opuntia monacantha* (Willd.) Haw. (Cactaceae)	Chhitar chhun, naagphani	Sh	W, Cv	Ft	as such	Oral	Ripe fruit is eaten to relieve body aches.
78.	*Oroxylum indicum* (L.) Kurz (Bignoniaceae)	Tatpalanga	T	W	Rt and Bk	powder	Oral	Bark and root powder used in treating arthritis.
79.	*Physalis minima* L. (Solanaceae)	Rasbhari, bhambola	H	W	Wp	cooked	Oral	Whole plant cooked as vegetable is used to cure swellings and body aches.
80.	*Piper longum* L. (Piperaceae)	Pippali mul, magha	Cl	Mk	Ft	as such and powder	Oral	Fruit is given in arthritis.
81.	*Piper nigrum* L. (Piperaceae)	Kali mirch	Cl	Cv	Ft	as such, burnt, cooked, decoction, local recipe, paste, powder and roasted	Oral	Fruit is used variously to treat arthritis.
82.	*Plumbago zeylanica* L. (Plumbaginaceae)	Chitrak	Sh	W, Cv	Rt	as such	Oral	Root is used to treat arthritis.
83.	*Phyllanthus emblica* L. (Euphorbiaceae)	Amla	T	W, Cv	Ft	as such, juice, paste, powder, pickle and local recipe	Oral	Raw fruit or powder or '*triphala churan*' (fruit powder of *Phyllanthus emblica*, *Terminalia chebula* and *T. bellirica*) in arthritis.
84.	*Ricinus communis* L. (Euphorbiaceae)	Arind	Sh	W, Cv	Rt, Lf, Sd and Oil	as such, decoction, powder and poultice	Oral, topical	Decoction of root (with root of *Withania somnifera* and ginger) is given in joint pains; seed powder in rheumatism; leaf paste as poultice on swellings and joint pains; oil as liniment for joint pains
85.	*Saccharum officinarum* L. (Poaceae)	Ganna	H	Cv	St	juice, extract and local recipe	Oral, topical	Fresh stem juice or as jaggery or cooked as '*kheer*'in arthritis; poultices made from jaggery in musculo-skeletal ailments.
86.	*Salvadora persica* L. (Salvadoraceae)	Peelu	T	Mk	Oil	as such		Oil used in massaging joint pains.
87.	*Santalum album* L. (Santalaceae)	Chandan	T	Cv, Mk	Wd	decoction	Topical	Decoction of heartwood (called '*chandan*') is given to heal internal injuries and arthritis.
88.	*Sesamum indicum* L. (Pedaliaceae)	Til	H	Cv	Sd and Oil	as such, roasted and local recipe	Oral, topical	Seed eaten as such, roasted or added to local recipes for treating arthritis; oil as liniment in swellings and arthritis.
89.	*Solanum aculeatissimum* Jacq. (Solanaceae)	Chhoti kantkari	Sh	W	Ft	powder and paste	Oral, topical	Fruit powder in arthritis; paste is applied on swellings.
90.	*Solanum americanum* Mill. (Solanaceae)	Makoh	H	W	Wp and Ft	boiled, cooked	Oral	Whole plant taken as cooked vegetable to reduce swellings; ripe fruit boiled as 'tea' to get relief in arthritis.
91.	*Solanum virginianum* L. (Solanaceae)	Halindi, badi kantkari	H	W	Rt and Ft	powder	Oral	Powdered fruit and root is given in arthritis.
92.	*Spermadictyon suaveolens* Roxb. (Rubiaceae)	Padari	Sh	W	Rt	powder	Oral	Root powder useful in treatment of arthritis.
93.	*Sphaeranthus indicus* L. (Asteraceae)	Gorakhmundi	H	W	Rt	powder	Oral	Root powder is taken in arthritis.
94.	*Stephania elegans* Hook. f. & Thomson (Menispermaceae)	Biskhappar, sandoo	Cl	W	Tb	poultice	Topical	Paste of stem tuber is tied on paining joints.
95.	*Strychnos nux-vomica* L. (Loganiaceae)	Kuchla	T	Mk	Sd	powder	Oral	Seed powder is given in arthritis.

96.	*Swertia chirayita* (Roxb.) Buch.-Ham. ex C.B.Clarke (Gentianaceae)	Chirata, chirayata	H	W	Wp	as such, decoction and powder	Oral	Whole plant is used in treating rheumatism.
97.	*Syzygium aromaticum* (L.) Merr. & L.M.Perry (Myrtaceae)	Laung	T	Mk	Fl bud, Oil	as such and infusion	Topical	Flower bud ('clove') or its oil used in making liniment for swellings, arthritis and postpartum massage.
98.	*Tamarindus indica* L. (Fabaceae)	Imli	T	Cv	Ft and Sd	as such, decoction and paste	Oral, topical	Fresh fruit or as decoction in arthritis; seed paste applied externally on arthritic joints.
99.	*Terminalia arjuna* (Roxb. ex DC.) Wight & Arn. (Combretaceae)	Arjuna	T	W, Cv	Bk	decoction, infusion, powder	Oral	Bark powder, decoction or infusion in arthritis.
100.	*Terminalia bellirica* (Gaertn.) Roxb. (Combretaceae)	Baheda	T	W, Cv	Ft	powder	Oral	Fruit powder or as *'Triphala Churan"* is useful in arthritis.
101.	*Terminalia chebula* Retz. (Combretaceae)	Harar, haritaki	T	W, Cv	Ft and Oil	powder, pickle and local recipe	Oral, topical	Fruit is taken as powder, "*triphala churan", pickle* or as *morabba* in arthritis,; oil used as liniment for arthritis.
102.	*Terminalia tomentosa* Wight & Arn. (Combretaceae)	Asan, sain	T	W	Bk	poultice	Topical	Bark powder is made into poultice and tied on arthritic joints.
103.	*Tinospora sinensis* (Lour.) Merr. (Menispermaceae)	Glo, giloy, guduchi	Cl	W	St	as such, decoction, powder	Oral	Tender stem taken fresh, as powder or decoction in arthritis.
104.	*Trachyspermum ammi* (L.) Sprague (Apiaceae)	Ajwain	H	Mk	Ft	as such, cooked, decoction, infusion, local recipe/drink, powder, roasted	Oral and fomentation	Fruit as a spice, roasted, decoction, powder or added to local recipes and drinks to relieve swellings; hot-water infusion used for fomentation of local swellings.
105.	*Tribulus terrestris* L. (Zygophyllaceae)	Bhakra, gokhru	H	W	Rt and Ft	decoction, burnt, local recipe and powder	Oral, topical	Root powder given in arthritis; fruit decoction in swellings, arthritis, back ache; as '*panjiri*' for body ache; fruit ash mixed in sesame oil, used as liniment for joint pains.
106.	*Trigonella foenum-graecum* L. (Fabaceae)	Methi	H	Cv	Sd	as such, cooked and roasted	Oral	Seeds as such, roasted or spice in arthritis, backache, swellings.
107.	*Triticum aestivum* L. (Poaceae)	Gehun, kanak	H	Cv	Sd	poultice	Topical	Half-baked bread is poulticed on swollen joints and sites of internal injuries.
108.	*Verbascum thapsus* L. (Scrophulariaceae)	Ban tamakhu	H	W	Lf	poultice	Topical	leaf is tied on aching joints
109.	*Vigna mungo* (L.) Hepper (Fabaceae)	Urd dal	H	Cv	Sd	poultice	Topical	Seed paste is used as poultice on aching joints.
110.	*Vitex negundo* L. (Lamiaceae)	Banah, nirgundi	Sh	W	St, Lf and oil	as such, infusion, paste, poultice	Oral, topical and fomentation	Tender shoot and leaf is taken in body ache and back sprains; leaf paste is applied as poultice on dislocated bones and fractures; seed oil as liniment in arthritis; hot-water infusion of twigs is used for fomentation of swellings.
111.	*Withania somnifera* (L.) Dunal (Solanaceae)	Ashwagandha, asgandh	Sh	W, Cv	Rt and Lf	as such, decoction and powder	Oral	Root and leaf is useful in treating rheumatism.
112.	*Woodfordia fruticosa* (L.) Kurz (Lythraceae)	Dhau, dhami	Sh	W	Fl	infusion	Topical	Oil Infusion of flowers is used as liniment for body massage (before and after delivery).
113.	*Zingiber officinale* Roscoe (Zingiberaceae)	Adrak	H	Cv	Rz	As such, cooked, decoction, extract, pickle, juice, powder and local recipe/drink	Oral, topical	rhizome taken as such, juice, culinary spice or as ingredient of '*panjiri*' and local drinks to treat arthritis, body ache; extract ('*ark*') used in liniments for giving massage in swellings and arthritis.

GH= Growth Habit; AS=Availability status; H=Herb; Sh=Shrub; T=Tree; Cl=Climber; W= Wild; Cv=Cultivated; Mk=Market

Plant parts used: Rt= Root; Rz= Rhizome; Bl= Bulb; Tb= Tuber; Wp=Whole plant; St= Stem; Bk= Bark; Lf= Leaf; Fl= Flower; Fl bud=Flower bud; Ft= Fruit; Sd=Seed; Lx= Latex; Wd= Wood; Sy= Style; Sg= Stigma

Table 2: Number of species corresponding to different families

Families	No. of species	Families	No. of species
Acoraceae	1	Loganiaceae	1
Acanthaceae	2	Lythraceae	1
Amaranthaceae	1	Malvaceae	2
Amaryllidaceae	1	Meliaceae	2
Apiaceae	3	Menispermaceae	3
Apocynaceae	4	Musaceae	1
Asphodelaceae	1	Myristicaceae	1
Asteraceae	5	Myrtaceae	2
Berberidaceae	1	Nyctaginaceae	1
Bignoniaceae	1	Nymphaeaceae	1
Brassicaceae	3	Pedaliaceae	1
Burseraceae	1	Phyllanthaceae	1
Cactaceae	1	Piperaceae	2
Cannabaceae	1	Plumbaginaceae	1
Caricaceae	1	Poaceae	2
Celastraceae	1	Primulaceae	1
Colchicaceae	2	Ranunculaceae	1
Combretaceae	4	Rubiaceae	1
Convolvulaceae	3	Rutaceae	4
Crassulaceae	1	Salicaceae	2
Cucurbitaceae	2	Salvadoraceae	1
Cyperaceae	1	Santalaceae	1
Euphorbiaceae	4	Sapindaceae	1
Fabaceae	11	Sapotaceae	1
Gentianaceae	1	Scrophulariaceae	1
Iridaceae	1	Solanaceae	6
Lamiaceae	3	Ulmaceae	1
Lauraceae	2	Zingiberaceae	5
Linaceae	1	Zygophyllaceae	1

Herbs were predominant among the reported species (46) followed by 32 trees, 21 shrubs and 14 climbers (Fig. 1). Majority of the species, 60 were wild followed by 53 cultivated and 21 were purchased from the market for preparing herbal remedies either singly or in combination with other plant parts (Fig. 2). There were 62 plant species reported for arthritis followed by 37 for general / local body swellings, 35 for joint pains and 10 each for rheumatism and to heal fractures. Other ailments that were treated included body aches, muscular pains and body massages for relief and rejuvenation, especially in pre- and post-partum care (Fig. 3).

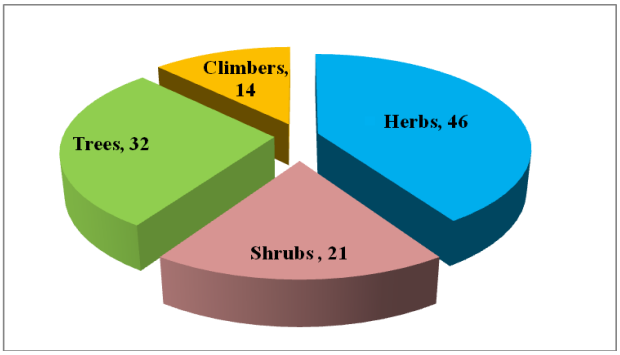

Figure 1: Growth habit of recorded plant species

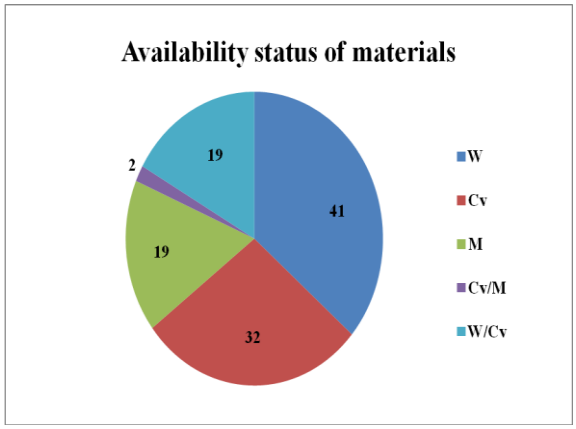

Figure 2: Availability of the plants species

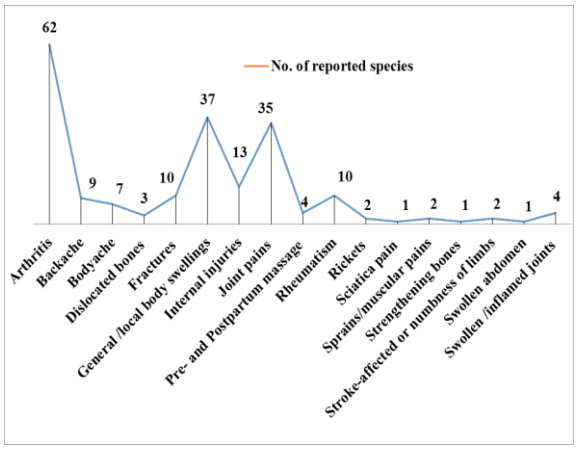

Figure 3: Number of species used for different ailments

The remedies were prepared either using an individual species or its parts and a mixture of two or more species. Most frequently species were used as fresh (48) or its powder (40) besides poultices (24), infusion (22), local recipes (21), decoction (19) or in cooked form (15). Others were used as juice, paste, roasted, sprouted, soaked, 'tea'or the 'ash'. The local recipes like *morabba, panjiri, kheer, halwa, gulkand, chutney, laddoos, shikanji/sherbat/tea*' *etc*. were consumed for strong bones and rejuvenation (Fig. 4). These remedies were administered orally (79), topical applications (51) as liniment or massage oil, poultices or as a fine paste. Fomentation of affected parts by the steam of plant extracts was also practiced (Fig. 5). Leaves were the most commonly used plant parts followed by fruits and seeds. It may be due to easy and frequent availability of the leaves (Fig. 6).

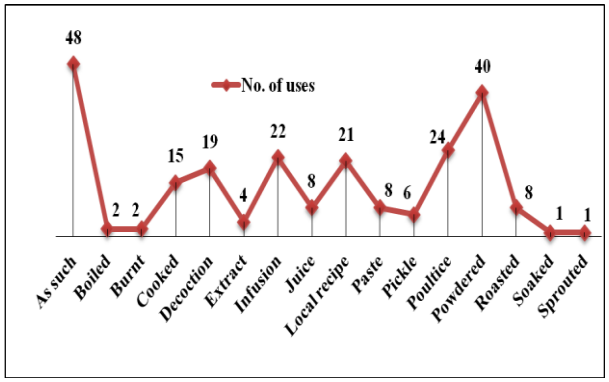

Figure 4: Different modes of remedial preparations.

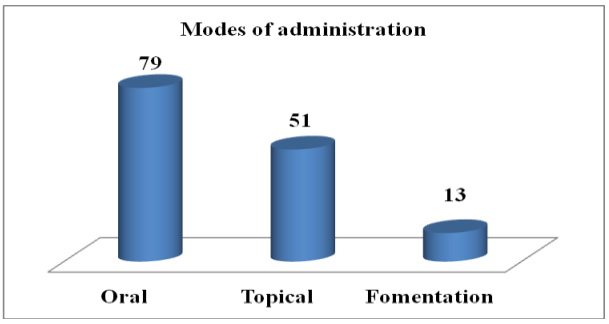

Figure 5: Modes of administration of different remedial preparations

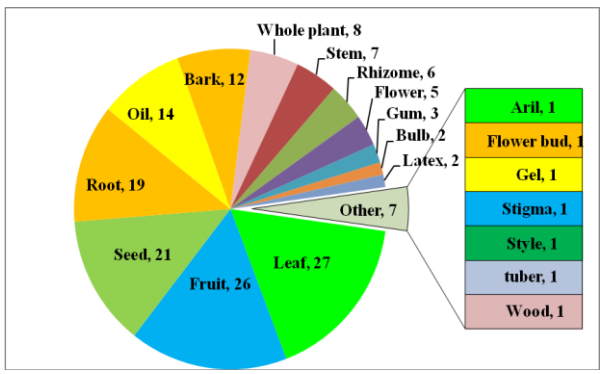

Figure 6: Plants, their parts or products used in various remedies

Cavero and Calvo (2015) reported the use of 38 plant species belonging to 24 families for the treatment of musculoskeletal disorders in Navarra, Spain. Aerial plant parts were most frequently used in medicinal preparations. Another study had reported the use of 142 plant species from 69 families treat musculoskeletal disorders. The herbaceous species were the most dominant and leaves were the commonly used plant part (Malik et al., 2018). According to Kantasrila et al. (2020) a total of 175 species were used by the Karen people in Thailand to treat Musculoskeletal System Disorders (MSDs). Leaves and roots were the most commonly used parts. The members of family Fabaceae (Leguminosae) had contributed the most in different preparations. The most common mode of administration was oral ingestion. These findings are in agreement to the present study. Rathi and Rathi (2020) reported that different tribal populations were using 23 plant species belonging to 20 families for the treatment of musculoskeletal disorders. They utilized 9 different plant parts and 5 types of medicinal preparations for external and internal applications. These studies have corroborated the information gathered during the present study.

CONCLUSION

Present study has revealed the use of plant based medicinal preparations of 113 species belonging to 57 families. The study has quantified the traditional knowledge of the natives to take care of their musculoskeletal ailments. The use of selected plant parts indicates the positive outlook towards the health and conservation of the plant species. These remedies are still practiced by the people because of their easy availability, affordability and known side effects, if there are any. Further studies can be planned for chemical characterization of such important and selected species for identification and isolation of chemical compounds of medicinal value.

ACKNOWLEDGEMENTS

Authors are thankful to the Chairperson Department of Botany, Panjab University, Chandigarh for providing the necessary facilities during this work.

REFERENCES

Cavero, R. Y. and M. I. Calvo (2015). Medicinal plants used for musculoskeletal disorders in Navarra and their pharmacological validation. *Journal of Ethnopharmacology*, 168: 255-259

Chowdhuri, S. K. (2000). Ethnobotany. In: *Studies in Botany* Vol. *2*. 7th edn. Mitra, D., Guha, J. and Chowdhuri, S. K. (Eds) Kolkata: Manasi Press. P. 855-867.

Foster, G. M. and B. G. Anderson (1978). *Medical Anthropology* John Wiley and Sons Ltd. New York.

Kantasrila, R., Pandith, H., Balslev, H., Wangpakapattanawong, P., Panyadee, P. and Inta, A. (2020). Medicinal Plants for Treating Musculoskeletal Disorders among Karen in Thailand. *Plants (Basel)*, doi: 10.3390/ plants9070811

Katewa, S. S., Chaudhary, B. L. and Jain, A. (2004). Folk herbal medicines from tribal area of Rajasthan, India. *Journal of Ethnopharmacology*, 92(1): 41-46.

Lange, D. (1997). Trade figures for botanical drugs world-wide. *Medicinal Plant Conservation Newsletter*, 3: 16-17.

Malik, K., Ahmad, M., Zhang, G., Rashid, N., Zafar, M., Sultana, S. and Shah, S. N. (2018). Traditional plant based medicines used to treat musculoskeletal disorders in Northern Pakistan. European Journal of Integrative Medicine, 19: 17-64.

Rathi, B. and R. Rathi (2020). Quantitative Analysis of Medicinal plants used by the Traditional healers of Karanja block of Wardha district for treating Musculoskeletal disorders. *International Journal of Ayurvedic Medicine*, 11(2), 175–183.

Seth, S. D. and B. Sharma (2004). Medicinal plants in India. *Indian Journal of Medical Research*, 120(1): 9-11.

Tilburt, J. C. and T. J. Kaptchuk (2008). Herbal medicine research and global health: an ethical analysis. *Bulletin of the World Health Organization*, 86(8): 594-599.

Timothy, W. C. and M. C. Craig (2007). Molecular understanding and modern application of traditional medicines: triumphs and trials. *Cell*, 130(5): 769-774.

Vishwakarma, A. P., Vishwe, A., Sahu, P. and Chaurasiya, A. (2013). Magical remedies of Terminalia arjuna (ROXB.). *International Journal of Pharmaceutical Archive*, 2(8): 189-201.

World Health Organization. (2013). In: World Health Organization (Ed.)., WHO Traditional Medicine Strategy: 2014-2023. W.H.O. Press, Geneva, Switzerland.

FORM IV
(See rule 8)

1.	Registration No.	:	ISSN-0555-7631
2.	Place of Publication	:	Room no.28-28, Old Correspondence Building Panjab University, Chandigarh – 160014 (India)
3.	Periodicity of Publication	:	Annual
4.	**Publisher's & Editors' Name**	:	
	Editor-in-Chief	:	Professor Devinder Mehta
	Nationality	:	Indian
	Editor	:	Professor Desh Deepak Singh
	Nationality	:	Indian
	Address	:	Research Journal (Science) Room No. 28-29, Old Correspondence Building, Panjab University, Chandigarh- 160014 (India)
5.	Printer's Name	:	Mr. Jatinder Moudgill
	Nationality	:	Indian
	Address	:	Manager Panjab University Printing Press Chandigarh – 160 014.
6.	Name and address of the Individuals who own the newspaper and partners or shareholders holding more than one percent of the total capital.	:	Panjab University, Chandigarh

Professor Devinder Mehta, hereby declare that the particulars given above are true to the best of my knowledge and belief.

Professor Devinder Mehta
Editor-in-Chief

PANJAB UNIVERSITY RESEARCH JOURNAL (SCIENCE)

LIFE MEMBERSHIP FORM

Name _____

Qualification _____

Area of Specialization _____

Present Designation _____

Address: (Tick the address on which you would like to receive the journal. Local members would receive the journal by hand)

i. Office _____
_____

ii. Residence _____
_____

Telephone (O) _____
(R) _____
(Mobile) _____
Fax _____
Email. _____

Payment Mode:

(Only local cheques are acceptable. Draft to be drawn in favour of **The Registrar, Panjab University, Chandigarh**

If by cheque/Draft:
Cheque/D.DNo. _____ Date _____ Amount_____
Name of the Bank: _____

Date _____
Place: _____

SIGNATURES

Subscription fee:

	Inland	**Foreign**
Life Membership:	Rs. 3000/-	US $ 250
Annual Subscription:	Rs. 400/-	US $ 50

Send to: The Editor-in-Chief
Research Journal (Science)
Room No. 28-29, Old Correspondence Building
Panjab University, Chandigarh-160014 (India)

Published by :
EDITOR-IN-CHIEF
Research Journal (Science)
Panjab University, Chandigarh-160 014
INDIA

www.puchd.ac.in

ISSN-0555-7631